Master Thesis

Analysis of real-time ESP data for detecting producer-injector interaction

Written by:
Kathrin Zlodnjak, BSc
m1135141

Advisor:
Univ.-Prof. Dipl.-Ing. Dr.mont. Herbert Hofstätter
Dipl.-Ing. Ilhami Giden

Leoben, 14/11/2016

Chair of Petroleum and Geothermal Energy Recovery

EIDESSTATTLICHE ERKLÄRUNG

Ich erkläre an Eides statt, dass ich diese Arbeit selbständig verfasst, andere als die angegebenen Quellen und Hilfsmittel nicht benutzt und mich auch sonst keiner unerlaubten Hilfsmittel bedient habe.

_____
Datum

_____
Unterschrift Verfasserin
Kathrin, Zlodnjak
Matrikelnummer: 1135141

AFFIDAVIT

I declare in lieu of oath, that I wrote this thesis and performed the associated research myself, using only literature cited in this volume.

_____	_____
Date	Signature of Authoress
	Kathrin, Zlodnjak
	Student number: 1135141

Kurzfassung

Aufgrund des Neuentwicklungsprojekts des 16. Tortons wurden traditionelle Gestänge-tiefpumpen durch Tauchkreiselpumpen ersetzt. Die neu installierten Pumpen sind mit Untertagesensoren ausgestattet, die den Eingangsdruck an der Pumpe messen und aufzeichnen. Basierend auf dieser Datenlage und durch die dichte Anordnung der Sensoren im Feld entstand die Idee, diese Druckreaktionen zu untersuchen, um Gruppen von sich gegenseitig beeinflussenden Produzenten und Injektoren zu identifizieren.

Insgesamt wurden 30 Produzenten mit Tauchkreiselpumpen und 15 Wasserinjektoren in die Analyse miteinbezogen. Das primäre Ziel wurde durch die Erfassung von insgesamt vier Sondengruppen erreicht. Anhand von täglichen Durchschnittswerten der Druckdaten am Pumpeneinlass war es möglich Verbindungen zwischen Injektionsausfällen und Druckanstiegen herzustellen. Zusätzlich gelang es, eine Beeinflussung einer produzierenden Horizontalbohrung auf umliegende Sonden festzustellen. Nach der Aufbereitung der Druckdaten wurde mit einer analytischen Kalkulation die Dauer einer Druckwelle von einer injizierenden Sonde zu einer produzierenden nachgerechnet. Das Ergebnis variiert, in Abhängigkeit der Distanz, zwischen zwei und 113 Stunden, die eine Druckwelle benötigt, damit sie am Produktionssensor erkennbar ist. Des Weiteren wurde die Zeit, die eine Wasserfront bis zum Durchbruch am Produzenten braucht, bestimmt. Da mit sehr hohen Wasseranteilen produziert wird, wurde eine Wasserkegelberechnung durchgeführt, die eine bereits stattfindende Wasserkegelaktivität nachweist. Ein Interferenztest wurde konfiguriert, um den Druckabbau am Produzenten, im Falle eines Injektionsausfalls, nachzustellen. Das Projekt wurde um eine weitere Herangehensweise erweitert, indem ein Stromlinienmodell anhand historischer Produktions- und Injektionsdaten aufgesetzt wurde. Hierbei wurden Injektions- und Produktionsoptimierungsstrategien vom verwendeten Programm vorgeschlagen. Diese wurden am Ende mit ihrer Anwendbarkeit abgeglichen. Die meisten Vorschläge sind von dem jetzigen technischen und wirtschaftlichen Betrachtungszeitpunkt aus nicht anwendbar. In Zukunft können diese Empfehlungen jedoch in die weitere Vorgehensweise miteinbezogen werden.

Abstract

Due to the redevelopment of the 16th Torton reservoir, traditional sucker rod pumps were replaced by high volumetric electrical submersible pumps (ESPs). The newly installed pumps got equipped with downhole sensors, measuring the pump intake pressure. For this reason, and as result of the dense distribution of sensors over the field, the idea arose to investigate in the pressure responses of producing wells in order to identify clusters of injectors and producers that are interconnected.

Basically, 30 ESP-producers and 15 injectors were considered in the analysis. The first target was accomplished by the detection of four clusters using the downhole sensors' pressure data on a daily average basis. Furthermore, one horizontal producer was observed, whose turn-off would cause a huge impact on surrounding producer wells. In addition to the hard-fact research approach, analytical methods were used to calculate the time span a pressure wave would need to travel from an injection well to a producer. The results, depending on the distance, vary from two hours to 113 hours for a pressure wave to response at a producer's sensor. Together with the amount of time a water front requires for flooding a certain area, water coning investigations were conducted. Those investigations showed an already prevalent coning activity. An interference test was performed to investigate in the pressure "build-up" after an injection break-down. As a last analysing method, a streamline surveillance model was set up, in order to illustrate the injected water distribution based on historical production and injection data. It was also possible to perform optimization recommendations on the field's injection and production strategy. At the end, these options, suggested by the applied software, were squared with their feasibility in real life. Several technical and economical limitations led to inapplicability for most of the proposed ideas at this point in time. In the future, recourse to some of the suggested strategies can be taken into consideration.

List of Tables

List of Figures

Abbreviations

OMV	Österreichische Mineralölverwaltung
SRP	Sucker rod pump
ESP	Electrical submersible pump
STB	Stock tank barrel
bbl	Barrel
AOI	Area of interest
TH	Tortonian horizon
SS	Subsurface
OIIP	Oil initially in place
GIIP	Free gas initially in place
OWC	Oil-water contact
ft³	Cubic feet
kh	Permeability x height
LÖSST	Lebendölsammelstation (gathering station)
cm	Centimeters
HSSE	Health, safety, security, environment

Table of content

1 Introduction

In the course of the 16th Tortonian reservoir's surveillance program in the Matzen Field, operated by OMV in Lower Austria, already installed sucker rod pumps (SRP) were replaced by electrical submersible pump (ESP) systems. The goal targeted was a doubling of the gross production rate, which was expected to create an oil rate increase, too. Basically, this was achieved by flooding the formation with injected water and thus, due to the high energy applied, reach a higher oil production. As a result of limited production rate achieved by using SRP, electrical submersible pumps got installed that are able to handle these high amounts of fluid.

For observation purposes and the reduction of operating costs, a downhole sensor was installed below every ESP unit's motor. Benefits derived from the installation of these downhole sensors include the knowledge of real-time data involving pressure, temperature and vibrations. Considering the high amount of sensors, compared to the reservoir size, it appeared possible for OMV to investigate the flow behaviour of the reservoir's western part, called Bockfließ area.

Due to the increased water flooding activity, some pathways between certain injector-producer pairs can be washed out, which may result in the formation of highways leading to a poorer displacement of oil. These highways can get bypassed, if production and injection rates are adapted in a way that other pathways are more attractive for the injected fluid to take. This reorientation in flowing direction conduces to more oil that gets recovered.

Firstly, information about the reservoir of interest was gathered in order to get an idea about its structure and production history. Subsequently, this data was used to relate the project to others with the intention of comparing investigation and optimization strategies. The quality of the processed data as well as its sources was described briefly. Furthermore, a description of programs used for data analysis and result representation is given.

The next step dealt with the sensor data gathering and processing in that way that clusters of injectors and producers were observable and defined. This was achieved by looking at the pressure changes of producers, when variations in the field's injection behaviour occurred. An illustration of the injection behaviour is given by the software OFM[TM] in the way that the water cut and its distribution over a certain area is pictured. Additionally, analytical calculations were executed dealing with the evaluation of a pressure wave's duration and fractional flow, to name a few.

The last step was accomplished by the suggestion of optimization opportunities, including a streamline simulation of the area of interest using the simulator 3DSL. A recommendation was made for improving the injection strategy including an optimization of injection- as well as production rates.

2 Literature research

In the literature research chapter the area of interest is described by its location and reservoir parameters. In addition, the most important features related to the reservoir region (f.e. fractional flow and water coning) are described on a general basis.

2.1 16th Tortonian

The 16th Torton (TH) is the key reservoir in the Matzen field, which is situated in the northeast of Vienna. The Matzen field is the core element in the Vienna Basin, Austria. The described constellation is geographically illustrated in Figure 1.
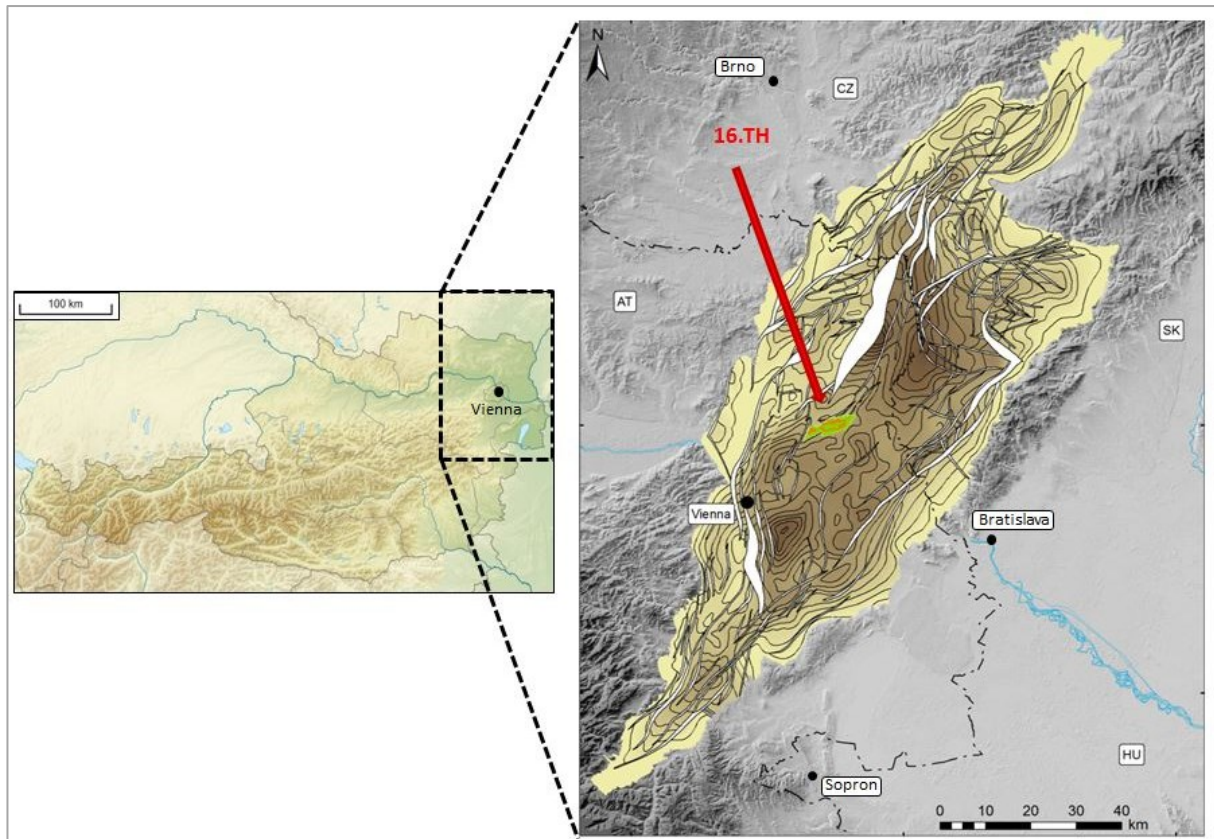
Figure 1: 16th TH indicated on the Vienna Basin depth structure map [36], [38]

The 16th TH was explored in the year 1949 with oil initially in place (OIIP) of 87 million m³ and a gas initially in place (GIIP) of 2.7 billion m³. The reservoir is characterised by a current average water cut between 97 % and a mean porosity of 27 %. The reason why it is very hard to give detailed information regarding the permeability is that the values occupy a large range, starting with a minimum value of 18 millidarcy (mD) and ending up in a maximum of 10 darcy (D), according to core analysis. In order to obtain data concerning the average depth of the oil-water contact (OWC), electrical measurements were applied that result, together with production tests, in an OWC depth of -1490 meters subsea (SS). Geologically, it is very important to mention that the reservoir is composed of rather homogeneous sandstone with a pay thickness of up to 70 meters. The vertical permeability is limited by so called "hard layers", composed of shallow marine limestone that acts as flow obstruction in

vertical pathways and is responsible for the formation of thief zones. As a consequence, circulating fluids can get lost. The reservoir's temperature is at a value of 60 °C.

A schematic of the 16th TH is shown in Figure 2, which indicates the breakdown of the reservoir into the areas Hauptscholle and Bockfließ that are separated by a saddle, marked in yellow.
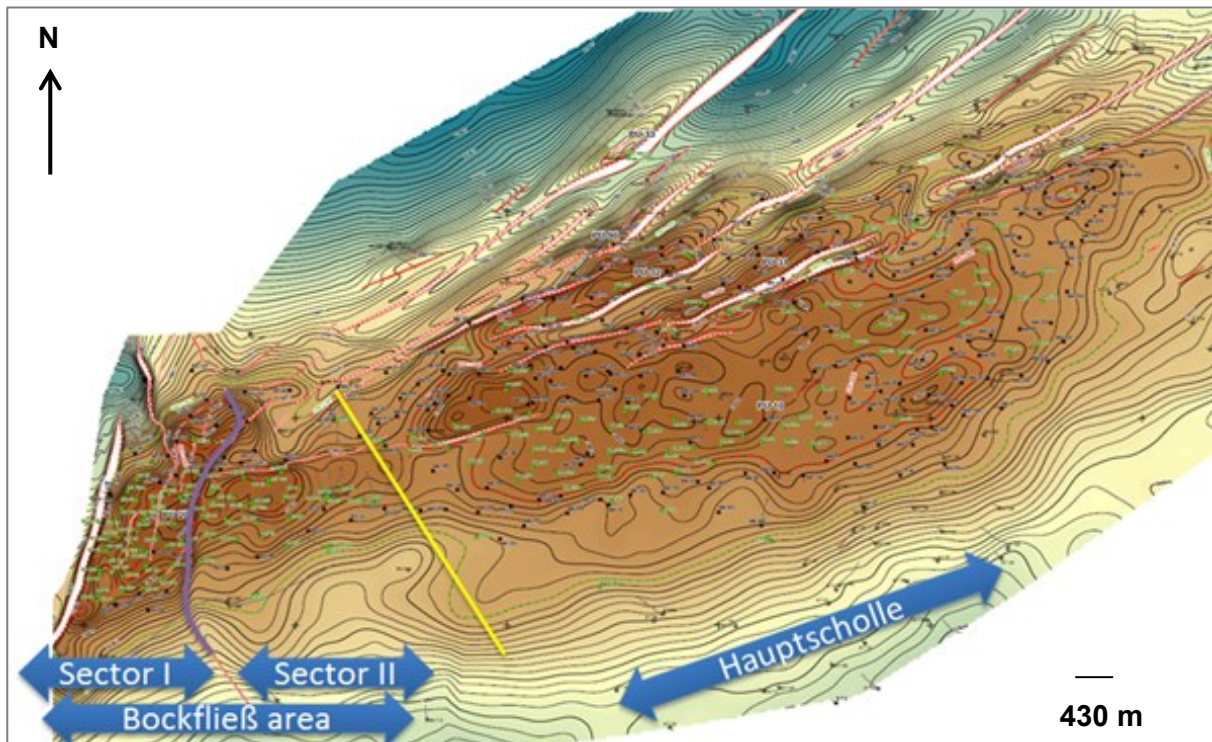
Figure 2: Illustration of the constructive elements making up the 16th TH

The area of interest (AOI) is represented by the Bockfließ area, which is further divided into two sectors. Sector I, with an OIIP of 13.7 million m³, is isolated from sector II, containing 13.6 million m³ oil initially in place, by a sealing fault, which is indicated by a violet line. A small gas cap, which was initially in place, is acting in sector I with an initial gas volume of 51 million m³ [1].

At the start of production, the 16th TH was in saturated state, which means that the bubble point matches the initial reservoir pressure of 160 bar and thus makes the presence of a gas cap possible. Having a look at the properties of the oil produced from this pool, it shows a specific gravity of 0.905 kg/m³, which corresponds to 25° API and an initial viscosity of 5.8 centipoise. The solution gas to oil ratio (GOR) corresponds to 44.8 m³(Vn)/m³. Important to mention is the force responsible for lifting the oil up to the surface, which is, in the case of the 16th TH, based on the driving mechanisms illustrated, together with the magnitude of their influence, in Table 1.

Table 1: Driving mechanisms influencing the energy support

Driving mechanism	Magnitude, %
Water drive	81
Gas cap drive	9.4
Solution gas drive	9.6

The water drive is compounded of a natural water drive and the injection of conditioned formation water [2]. In general, when looking at the production history of the reservoir, it is already declared as mature field [3]. As a result of the mentioned field maturity of the 16th TH, injection of water into the existing aquifer should improve the field's production behaviour.

Despite the field's maturity, reservoir studies and production analysis led to the conclusion that there is still a potential for production improvements. Therefore, with the start in the year 2013, a third of the installed SRP installations was replaced by high-volumetric ESPs. Each of them was prepared with a downhole sensor in order to provide an optimization of the pumping operation. Accompanied with the renewed downhole structure, the surface facilities got redesigned, allowing remote real-time monitoring of the pumps [4]. Principally, the AOI consists of 15 injectors and 32 ESP producers, where the injectors are primarily located at the edge and the producers in the centre of the AOI.

In the past, the water produced from the 16th TH was sent to the water treatment plant located in Schönkirchen. Though the facility got renewed in the year 2015, the plan did not include a doubling of the 16th TH reservoir's produced gross rate, which should be reached with the already mentioned redevelopment project. In order to be able to handle such high amounts of water, a water treatment facility in Auersthal was established. For a better understanding of the following explanation, the basic construction of the plant is illustrated in Figure 3. At first, the slug composed of water, oil and gas is produced via different pumps and transported over flow lines from the gathering station (LÖSST) to a slug catcher. The slug catcher (1) is switched in between the upstream flow lines and the processing unit to prevent from overloading the system and compensate variations in production.

Furthermore, a first phase separation is achieved in the slug catcher, splitting up the gaseous and liquid phase. The water in the slug catcher has a hydrocarbon content of 50.000 ppm.
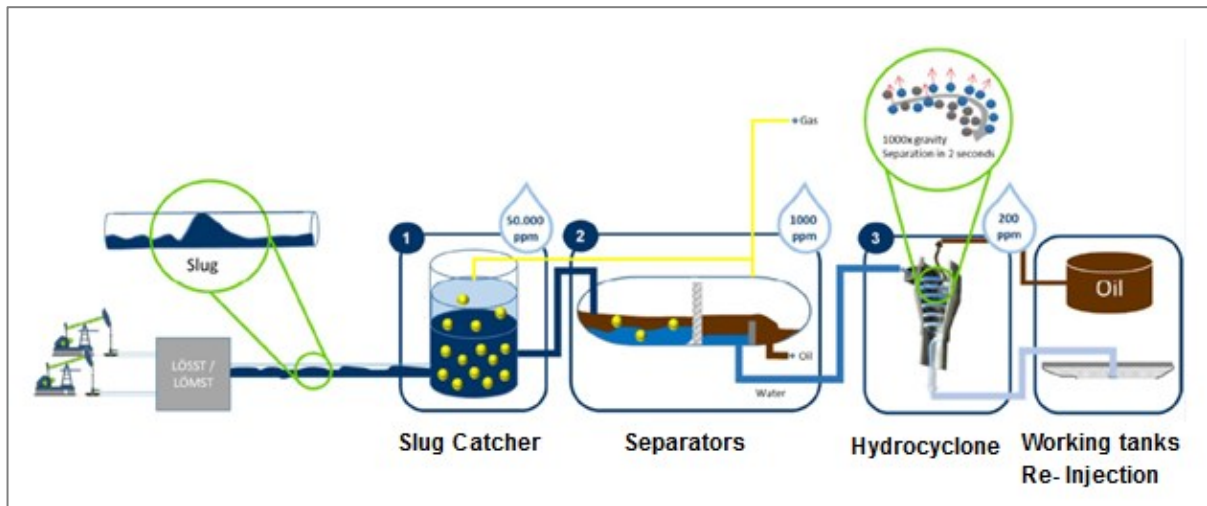
Figure 3: Basic setup of the extraction station Auersthal [41]

In the second step the fluid flows into seven separators (2) including one serving as a backup. These separators split up the fluid mixture into its individual phases due to gravity. Oil and Gas are directed out of the treatment system into designated vessels. The remaining water has a hydrocarbon content of approximately 1.000 ppm and is forwarded to the hydrocyclone units (3), demonstrated in Figure 4 [5].
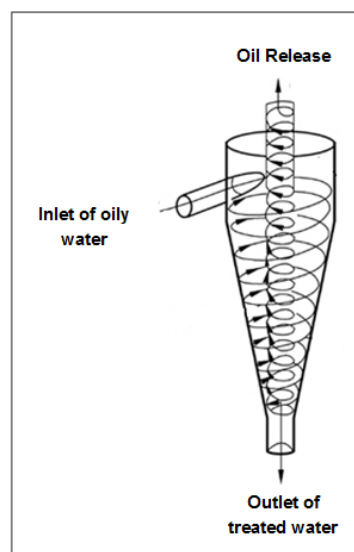
Figure 4: Sketch of a single hydrocyclone [37]

The hydrocyclone's working principle is based on the rotation of the fluid stream, which is fed into the cyclone. The denser water is collected at the outside wall and moves downwards against its outlet, whereas the less dense oil rotates upwards and is released at the facility's top. Reaching the unit's tail, the water has an overall hydrocarbon content of approximately 200 ppm. The working principle refers to one single hydrocyclone. However, the facility consists of three hydrocyclone batteries, where two batches are actually in service. The third battery serves as a backup tool in cleaning or failure situations. The principled setup of one battery is illustrated in Figure 5.
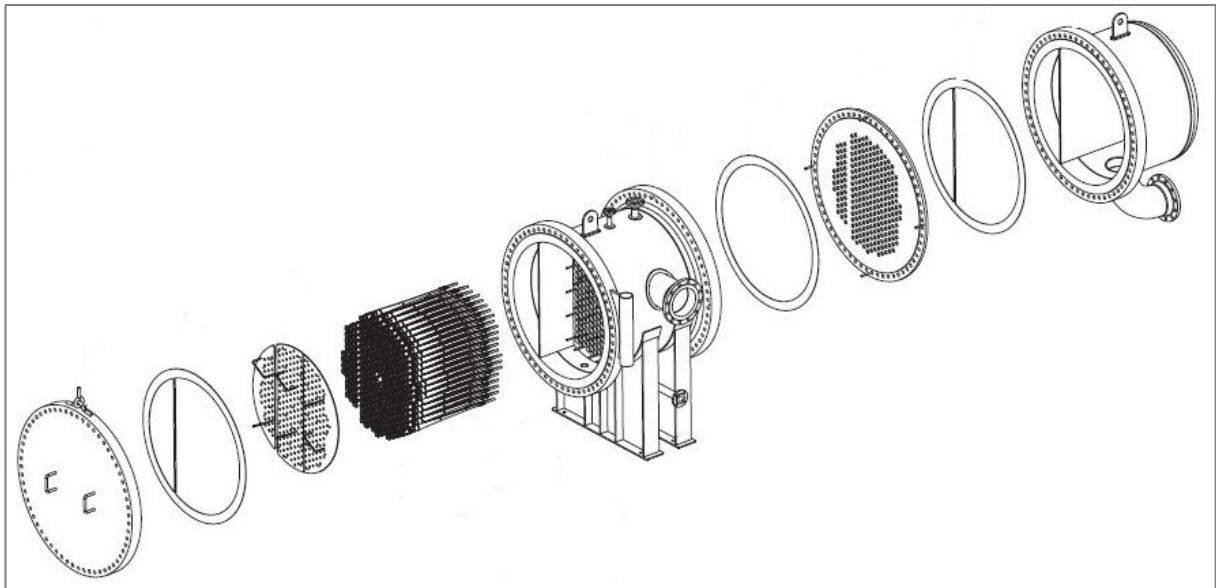
Figure 5: Schematic illustration of one hydrocyclone unit [5]

As displayed in Figure 5, one unit consists of 270 hydrocyclones, where the batch itself is split up into two chambers. This breaking up of the hydrocyclone units is justified in the alternating need of different capacities that have to go through. For cleaning purposes, each single hydrocyclone is disassembled from the battery and gets washed with water in order that accumulated sediments are removed from the system

Once the water treatment process with hydrocyclones is accomplished, the water flow is guided into the 16th TH reservoir via injection lines. The amount of water that is unable to be reinjected, is fed into the flow line, which guides the excess water to the central water treatment facility in Schönkirchen. The oil gathered by the separation scheme is stored in four storage tanks. The oil has to have a water cut of lower than one percent to be allowed to flow to the refinery for further treatment operations. In total, the extraction station Auersthal has a storage capacity of 28 000 m³. Table 2 shows the approximate production split up into the different fluids per hour.

Table 2: Production at extraction station Auersthal

Medium	Quantity
Asphaltic oil	30 t/h
Formation water	700 m³/h
Gas	3.500 Nm³/h

2.2 Injectivity index

As the water, which is treated in Auersthal, is reinjected into the 16th Tortonian reservoir, a considerable objective is the validation of the well's injection behaviour. For this reason, equation 2.2.1 was applied on data, which is known from injector BO 36, in order to determine the injectivity index (II). Explained in the very homogeneous behaviour of this specific reservoir and the similar treatment of injection wells' water, one well was chosen to represent the field's injection performance.

$$II = \frac{Q}{p_{bhi} - p_e} = \frac{k_w \times h_i}{141.2 \times \mu_w \times B_w \times \ln(\frac{r_e}{r_w} + S)} \qquad \textbf{2.2.1}$$

Q	injection rate [STB/d]
p_{bhi}	bottomhole injection pressure [psia]
p_e	far-field reservoir pressure [psia]
k_w	water effective permeability [mD]
h_i	injection height [ft]
μ_w	water viscosity [cp]
B_w	water formation volume factor [res vol/STC vol]
r_e	drainage radius [ft]
r_w	wellbore radius [ft]
S	skin [1]

Two approaches are described by equation 2.2.1 [6], that often lead to inconsistencies when compared with each other.

On the basis of a nodal strategy, illustrated in Figure 6, the left side of the equation results in an injectivity index being premised on exclusively directly measured values.
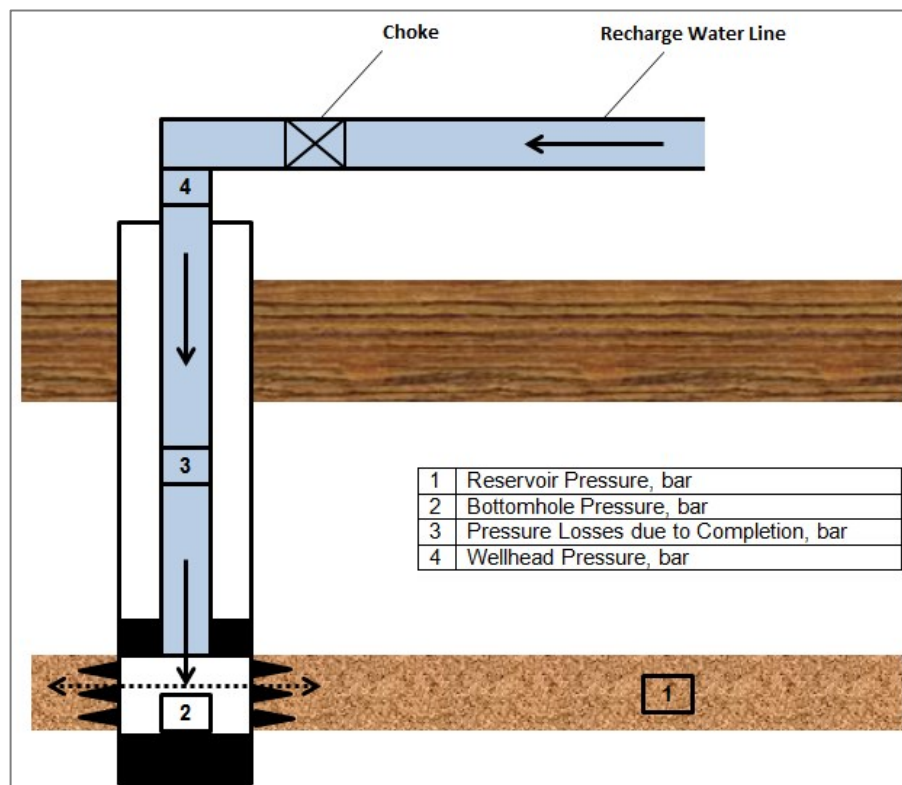
Figure 6: Explanation of the injectivity index calculation's nodal approach [39]

As observable in Figure 6, the well's bottomhole pressure must be higher than the reservoir pressure in order to achieve an injection of water into the formation. The amount of water that should find its way through the perforations into the reservoir in a distinct time is related to the pressure difference between the bottomhole and reservoir pressure.

A description for the bottomhole injection pressure was found by the application of equation 2.2.2 [6]. The used quantities and their origin are described in Appendix A.1.

$$p_{bhi} = p_{wh} + p_h - p_f \qquad\qquad \textbf{2.2.2}$$

p_h hydrostatic pressure [bar]
p_{wh} wellhead pressure [bar]
p_f friction pressure losses due to completion [bar]

Inserting the pressure quantities into equation 2.2.2 leads to a bottomhole injection pressure of 188.27 bars. With an injection rate of 800 m³/day and a reservoir pressure of 123 bars, equation 2.2.1 results in an injectivity index of 12.26 m³/d*bar.

Addressing now Darcy's approach, located at the right side of equation 2.2.1, a slightly different outcome is recorded. The applied values and their sources are illustrated in Appendix A.2. However, the usage of the right side of equation 2.2.1 implicates an injectivity index of 17 m³/d*bar. Consequently, another bottomhole injection pressure results from rearranging equation 2.2.1.

Comparing the above discussed two strategies with each other, Darcy's method results in a considerably lower pressure difference needed, between wellbore and reservoir, in order to inject water into the formation with a specific rate.

Various reasons can act as perpetrator for mismatches in the outcomes. The two most influencing factors were figured out by going through different calculation scenarios. On the one hand, the water's relative permeability is derived from special core analysis (SCAL) experiments. Although the SCAL methodology provides an approximate reproduction of the two-phase flow behavior inside the reservoir's pore space, it must be considered that the core being observed is only a locally restricted snapshot. In other words, the fluid's flow behavior, gathered by those laboratory measurements, is not necessarily completely employable for the whole reservoir area.

On the other hand, as a second element of uncertainty, the skin factor, is considered to be zero in this setup. Currently, no inflow issues are observable at the producing wells, which is an explanation for not considering any wellbore damages or other issues that can eventuate in a skin development.

If those two factors are brought into consideration, a match is very likely to be found between the two discussed approaches.

2.3 Pseudosteady-state flow regime

At the beginning of this paragraph, it is very important to briefly describe the three possible flow regimes in which a reservoir can act. After that the flow regime applied in the AOI will be explained in detail.

Principally, the fluid flow activity can be described by three options illustrated in Figure 7.
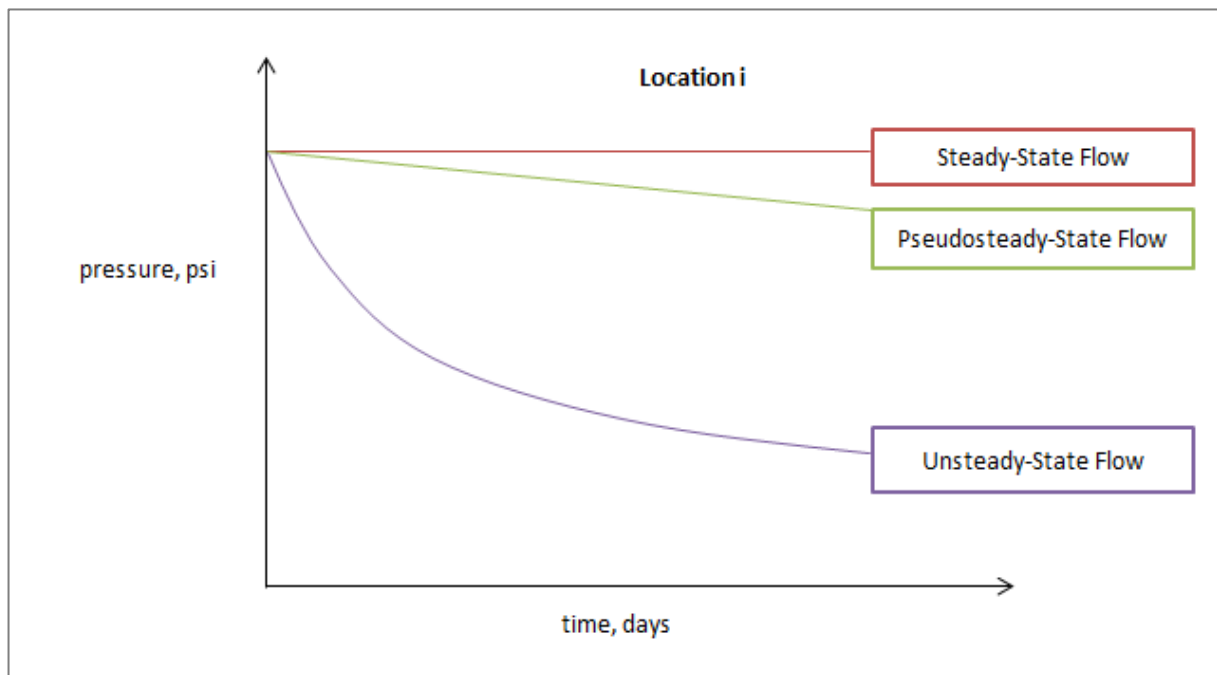
Figure 7: Flow regimes [6]

In steady-state flow conditions the pressure is not exposed to any variations with time. Thus, the pressure at every single position in the reservoir stays constant meaning that the amounts of fluid withdrawn from the system must enter the structure in equal amounts. In order to be able to apply a steady-state fluid flow behaviour, the reservoir has to get refilled entirely (e.g. strong aquifer).

The second system is described by an unsteady-state flow, which is also known as transient flow. In this case, the pressure change with time is dependent on location and time and is neither constant nor zero. The reservoir is assumed infinite in size so that the pressure disturbance, produced by the well's flowing action, moves through the reservoir without being affected by the reservoir boundaries [6]. Compared with the steady-state case, the results gathered from the transient flow regime's conditions are much more representative. The problem that comes along with the better applicability is the accompanied complexity of the outcomes [7].

The next section deals with the pseudosteady-state flow regime, which is used in the investigated area. In the short period of time, when the flow is transient, the well's pressure behaviour is not influenced by the reservoir boundaries. Once all boundaries are reached by

the produced pressure wave, the pseudosteady-state flow regime is applied instead of the unsteady-state one. In Figure 7 it is observable that a linear pressure versus time behaviour shows up, indicating a constant pressure variation with time on a specific location.

Mathematically, the above stated circumstances can be illustrated with equation 2.3.1 [6].

$$\left(\frac{\partial p}{\partial t}\right)_r = constant \qquad \textbf{2.3.1}$$

p   pressure [psi]
t   time [s]
r   location/radius [cm]

The usage of pseudosteady-state flow regimes was rare until the detection of a constant variation of well- and reservoir pressure with time was made in the case that the well produces at constant rates for a particular period of time.

Although the well's flow rate and pressure gradient are kept constant with time, which would indicate a steady-state flow regime, the absolute pressure is not, which makes the flow unsteady-state. This combination of the property pools of the two flow regimes led to the pseudosteady-state definition [7].

The constant term in equation 2.3.1 has to be defined using a material balance approach, starting with the compressibility of a fluid without free gas production, illustrated in equation 2.3.2.

$$c = \frac{-1}{V}\frac{dV}{dp} \qquad \textbf{2.3.2}$$

Rearranging equation 2.3.2 and extending it by the time derivative lead to the equation 2.3.3.

$$\frac{dp}{dt} = -\frac{q}{cV} \qquad \textbf{2.3.3}$$

In equation 2.3.4 the unit of the pressure decline rate is illustrated in psi/hr and the flow rate given in barrels per day is replaced by the flow rate expressed in STB per day with the introduction of the formation volume factor B_o.

$$\frac{dp}{dt} = -\frac{q}{24cV} = -\frac{Q_oB_o}{24cV} \qquad \textbf{2.3.4}$$

c   compressibility [1/psi]
V   pore volume [bbl]
q   flow rate [bbl/day]
Q_o flow rate [STB/day]
dp/dt   pressure decline rate [psi/hr]
B_o formation volume factor [bbl/STB]

The pore volume in the case of assuming a radial drainage arrangement is given by equation 2.3.5 converting the volume from barrel to ft³.

$$V = \frac{\pi r_e^2 h \phi}{5.615} = \frac{Ah\phi}{5.615}$$

2.3.5

A   drainage area [ft²]

The combination of equations 2.3.4 and 2.3.5 leads to equation 2.3.6 for expressing the constant.

$$\frac{dp}{dt} = -\frac{0.23396q}{c_t(\pi r_e^2)h\phi}$$

2.3.6

In order to describe the pseudosteady-state flow condition in the case of a radial flow geometry in the presence of slightly compressible fluids, equation 2.3.7 shows the diffusivity equation for transient flow.

$$\frac{\partial^2 p}{\partial r^2} + \frac{1}{r}\frac{\partial p}{\partial r} = \left(\frac{\phi \mu c_t}{0.000264k}\right)\frac{\partial p}{\partial t}$$

2.3.7

The expression $\partial p/\partial r$ is constant as described in equation 2.3.1 and can be replaced by the term illustrated in equation 2.3.6. Exerting integration on the combined result, leads to equation 2.3.8.

$$r\frac{dp}{dr} = -\frac{887.22q\mu}{(\pi r_e^2)hk}\left(\frac{r^2}{2}\right) + c_1$$

2.3.8

The integration constant c_1 can be calculated by the introduction of boundary conditions like $(\partial p/\partial r)_{re} = 0$. Equation 2.3.9 gives the expression for the integration constant c_1.

$$c_1 = \frac{141.2q\mu}{hk}$$

2.3.9

Inserting the integration constant c_1 into equation 2.3.8 and again performing an integration process, the final result is gathered shown in equation 2.3.10.

$$(p_i - p_{wf}) = \frac{141.2q\mu}{kh}\left[\ln\frac{r_e}{r_w} - \frac{1}{2}\right]$$

2.3.10

In the last step, the flow rate is calculated in STB per day, which gives the equation 2.3.11 [6].

$$Q = \frac{0.00708kh(p_i - p_{wf})}{\mu B[\ln\left(\frac{re}{rw}\right) - 0.5]}$$

2.3.11

2.4 Interference test

Firstly, the main purposes of interference tests are discussed followed by a further explanation of these kinds of tests.

Basically, interference tests are multiple-well tests, which means that communication between an active source well and one or more observation wells is generated. A certain response is achieved by changing the rate at the source well and thus creating a pressure disturbance that is recognized at the observation wells situated in the distance r from the active one [8]. A sketch of this set-up is represented by Figure 8. This change in the pressure behaviour with respect to time, when the flow rate is changed, can be seen as an indication of reservoir characteristics (f.e. no communication between two wells in a reservoir).
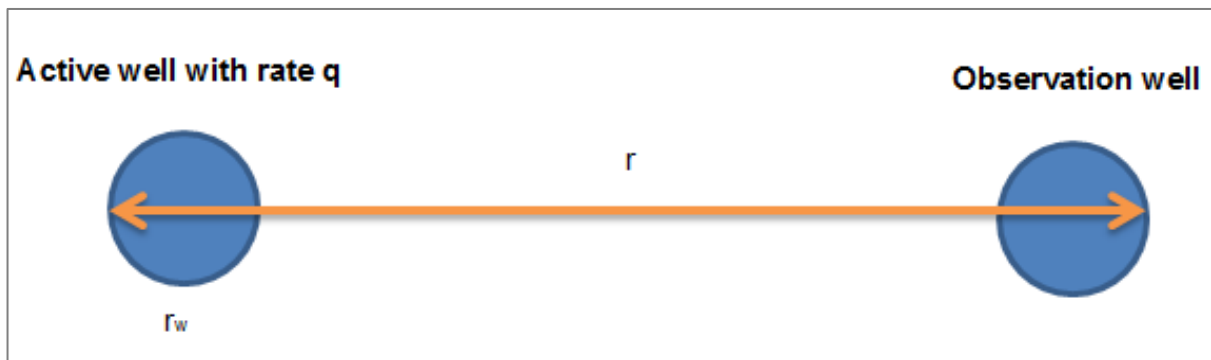
Figure 8: Constellation of an interference test

The time and magnitude of the pressure variation recorded at the observation well is dependent on the reservoir properties (i.e. transmissibility, equation 2.4.1, and storage, equation 2.4.2) of the surveyed region. The longer the time span in which the test is conducted, the more accurate the results for transmissibility and storage will be.

$$transmissibility = \frac{kh}{\mu} \qquad\qquad \textbf{2.4.1}$$

k   permeability [mD]
h   formation thickness [ft]
μ   fluid's viscosity [cP]
k/μ   fluid's mobility [mD/cP]

$$storage = \phi h c_t \qquad\qquad \textbf{2.4.2}$$

ɸ   porosity [1]
h   formation thickness [ft]
c_t total compressibility [psi^{-1}]

Therefore, interference tests give the possibility to decide whether wells are located in the same pool or not [9].

The easiest method for the interpretation of interference tests is type-curve matching. Creating a type curve is managed by plotting the theoretical variation in pressure monitored at one observation well versus the time difference on a log-log plot. In order to provide adaptability, dimensionless variables are used for the type-curve. The same plot is created with field data on a so called tracing paper, and subsequently matched by positioning the tracing paper above the type-curve. The axes of the two graphs should be kept parallel, while the best fit between the two curves is achieved. Consequently, reservoir properties as skin and kh-product can be determined.

In the case of the 16th TH the time for the pressure to be recognized at the observation well and the distance r between source well and observation well are known. With this information it is possible to get a better understanding about the reservoir's conductivity and thus take some steps to prevent from generating high permeable flow pathways.

At the end of chapter 2.4 it should be mentioned that wellbore storage and skin can falsify the result leading to an overestimation of formation storage and an underestimation of transmissibility. Wellbore storage effects are longer lasting, if damages of the wellbore are encountered [10].

2.5 Water cut and water coning

This chapter explains two main reasons for the abandonment of an oil well in the early production lifetime and the resulting reduction of ultimate recovery.

2.5.1 Water cut

In the first time of production, the water cut of oil wells is relatively low. Depending on the formation properties and production concept, the production of water with oil increases more or less rapidly. This might be caused by injection of water due to improved oil recovery (IOR) efforts or water coning, which will be discussed in 2.5.2. Not only does a high water cut indicate less production of oil, so that more oil is left downhole, but also increases the risk of sand production. Water weakens the perforation's strength and thus enhances the danger of producing sand [11].

Consequently, it is of great importance to control the production of water in an oil well. For this purpose, two main mechanisms can be distinguished:

   I.   Mechanical solutions
   II.   Chemical solutions

The usage of packer and plugs are considered as mechanical methods to manage the flow of water. Alternatively, chemical solutions deal with the injection chemicals into the formation. The idea behind that is the expansion or solidification of these materials in the pore space and thus achieving a lower permeability of the formation [12].

2.5.2 Water coning

Principally, water coning is the mechanism that describes water moving up to the perforations of a producer well. Complications triggered by water coning involve negative impacts on the productivity and efficiency. Furthermore water has corrosive properties and has to be disposed, which might have huge effects on costs. In the worst case, coning of water can lead to a premature abandonment of the producing well.

Producing from a well always causes pressure changes. Those pressure gradients are responsible for the downward movement of the gas-oil contact and the upward movement of the water-oil contact near the wellbore. Due to gravity forces, a counterforce is acting against the tendency of the fluid to move the path of least resistance, which leads to bell shaped schematics of the contacts shown in Figure 9.
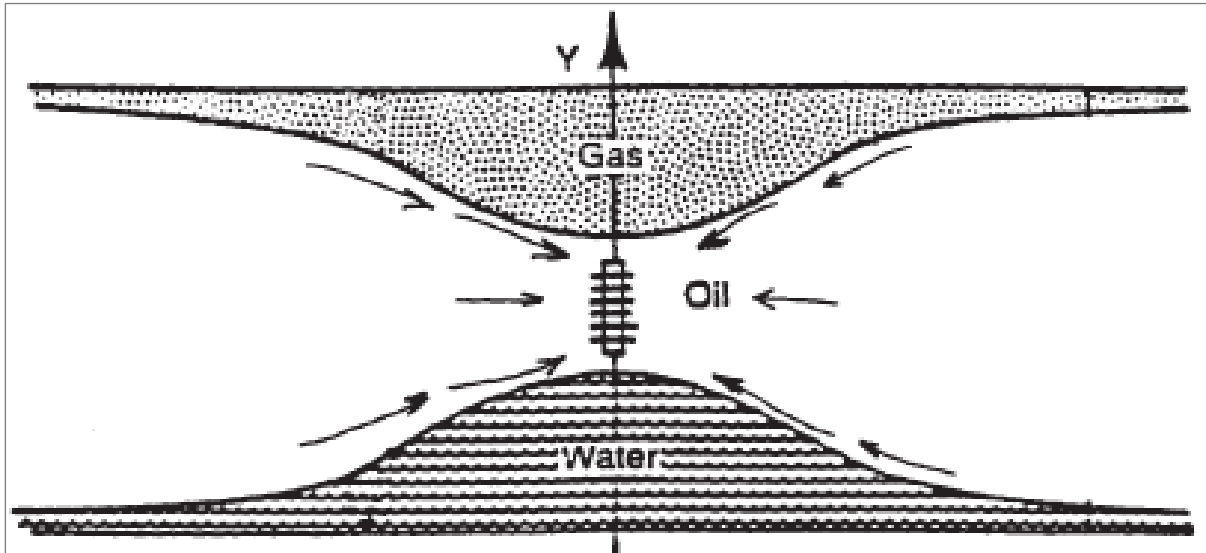
Figure 9: Contacts demonstrated with coning effect [6]

Basically, the bell shape of Figure 9 can be explained by the presence of three major forces, responsible for the fluid's flow behaviour. The first one is the capillary force, which is only mentioned here for the sake of completeness, because of its minor effect on the coning action. Secondly, gravity segregation causes a vertical upward- or downward force depending on the fluids' densities. The pressure difference caused by the production is classified under the term viscous forces. Together with gravity forces, viscous forces tend to generate equilibrium. This statement explains the existence of cones, when the viscous forces, due to fluid flow, go beyond gravity forces.

Related to the force balance, mentioned in the previous paragraph, two different types of cones can be distinguished. The first one is defined as stable cone, which indicates a coning action that neither leads to a growing nor to a shrinking cone. Stable cones are occurring, if the production rate is kept constant and thus the pressure gradients are maintained at the same values too. A steady-state environment is generated and leads to a cone that is not reaching the wellbore. In contrast, the existence of an unstable cone is accelerated by unsteady-state flow conditions until the point of steady-state flow is reached. In the meanwhile the pressure gradient can increase in that extent that the viscous forces are higher than the gravity forces and this leads to a growth of the unstable cone which affects the well after some time. The limiting factor for the development of each system is the critical production rate of the well. It describes the maximum oil production rate without coning of water into the wellbore. At this rate the cone is just at the edge between a stable and an unstable cone.

However, the reduction of coning tendencies is of importance. One way to do that is to improve the horizontal permeability by acidizing the formation. This does not lead to a decreased vertical permeability at all, but causes a greater ratio of horizontal to vertical permeability, which, at the end, arranges a much more even increase in water level. A shut-in can manage a restabilization of the contacts, which only solves the problem temporarily [6].

2.6 Fractional flow

This section deals with fractional flow, which is a very important topic in reservoir engineering, when water floods are applied for achieving a greater oil recovery.

In order to achieve a higher oil displacement, the reservoir is sometimes flooded with water. Consequently, the effectiveness of the displacement has to be controlled using parameters like volume of displaced oil, oil production rate and volume of water produced per volume of oil [13].

One approach of predicting the displacement performance is provided by Leverett's (1941) fractional flow equation.

2.6.1 Fractional flow equation

The fractional flow of water, f_w, is illustrated in equation 2.6.1 by assuming a system consisting of the two immiscible phases, oil and water.

$$f_w = \frac{q_w}{q_t} = \frac{q_w}{q_w + q_o} \qquad \textbf{2.6.1}$$

f_w	fractional flow of water [bbl/bbl]
q_w	water flow rate [bbl/day]
q_o	oil flow rate [bbl/day]
q_t	total flow rate [bbl/day]

Darcy's equation for both, oil and water flow, is shown in equations 2.6.2 and 2.6.3.

$$q_o = \frac{-k_o A}{\mu_o}\left[\frac{\partial P_o}{\partial x} + g\rho_o \sin(\theta)\right] \qquad \textbf{2.6.2}$$

$$q_w = \frac{-k_w A}{\mu_w}\left[\frac{\partial P_w}{\partial x} + g\rho_w \sin(\theta)\right] \qquad \textbf{2.6.3}$$

k_o	effective permeability oil [mD]
k_w	effective permeability water [mD]
μ_o	viscosity of oil [cP]
μ_w	viscosity of water [cP]
p_o	pressure of oil [psi]
p_w	pressure of water [psi]
ρ_o	oil density [lbm/ft³]
ρ_w	water density [lbm/ft³]
A	cross section [ft²]
x	distance [ft]
θ	dip angle
$\sin(\theta)$	positive for updip flow and negative for downdip flow

It is possible to use Darcy's approach, because the formation is assumed homogeneous [6]. Figure 10 demonstrates the situation of a 1-D displacement of a tilted system.
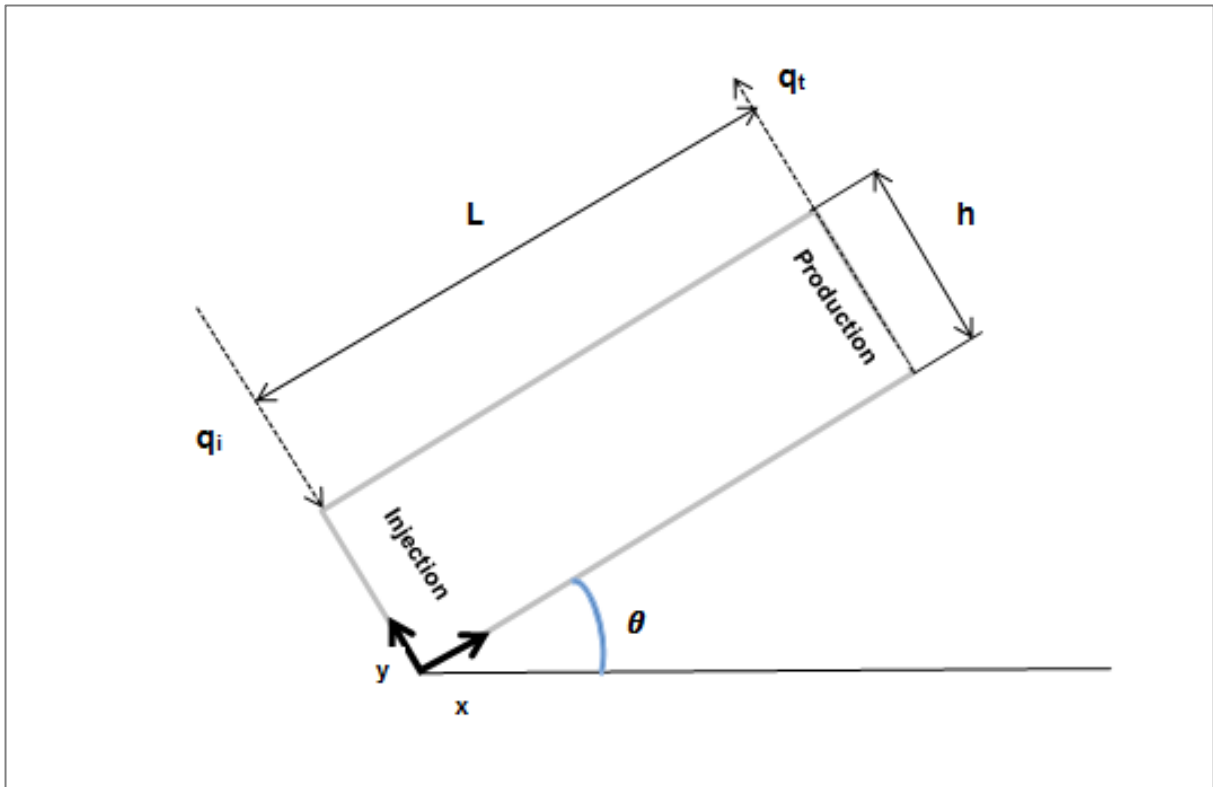
Figure 10: Prototype of a 1-D displacement system [13]

The combination of the equations 2.6.2 and 2.6.3 under consideration of equation 2.6.4 for capillary pressure, leads to the final result for the fractional flow of water illustrated in equation 2.6.5.

$$P_c = p_o - p_w \qquad\qquad \textbf{2.6.4}$$

$$f_w = \frac{1+\left(\frac{0.001127(kk_{ro})A}{\mu_o i_w}\right)\left[\frac{\partial p_c}{\partial x}-0.433\Delta\rho\sin(\theta)\right]}{1+\frac{k_{ro}}{k_{rw}}\frac{\mu_w}{\mu_o}} \qquad\qquad \textbf{2.6.5}$$

k_{ro}	relative permeability oil [1]
k_{rw}	relative permeability water [1]
i_w	injection rate water [bbl/day]
f_w	water cut [bbl/bbl]
k	absolute permeability [mD]

Due to the fact that capillary pressure gradients are typically very small, they can be neglected. As a consequence, the fractional flow equation can be written as shown in equation 2.6.6.

$$f_w = \frac{1-\left(\frac{0.001127(kk_{ro})A}{\mu_o i_w}\right)\left[0.433(\rho_w-\rho_o)\sin(\theta)\right]}{1+\frac{k_{ro}}{k_{rw}}\frac{\mu_w}{\mu_o}} \qquad\qquad \textbf{2.6.6}$$

Having a look at equation 2.6.1 it is observable that the lowest value of f_w is zero percent and the uppermost one hundred percent. Is the connate water saturation reached, no water flow occurs and the value of f_w becomes zero. Contrarily, if the residual oil saturation is met, no oil is flowing, which indicates a water cut of 100%. These statements are illustrated in Figure 11.
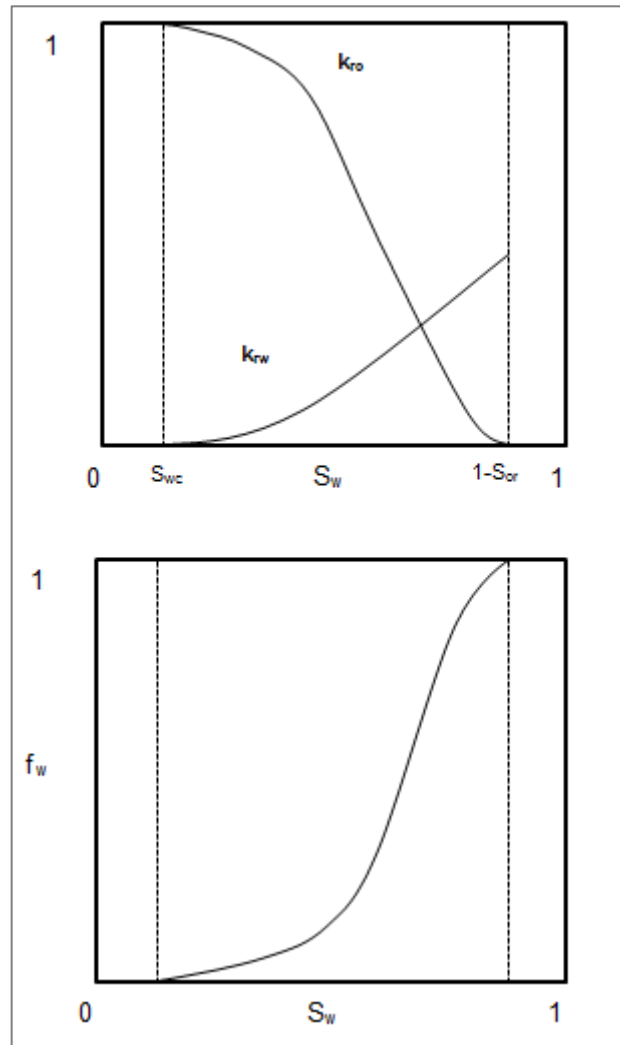
Figure 11: Relative permeability curve (top) and fractional flow curve of water (bottom) as function of water saturation [6]

Furthermore, if the water cut rises, a proportional decline in oil fractional flow and oil mobility is caused. Knowing that, an injection method should be chosen, which leads to a decrease in water fractional flow [6].

2.7 Voidage replacement ratio

In order to be able to illustrate the portion of reservoir volumes injected compared to reservoir volumes produced, the voidage replacement ratio (VRR) was introduced and is shown in equation 2.7.1.

$$VRR = \frac{injected\ reservoir\ volumes}{produced\ reservoir\ volumes} = \frac{B_{w,inj}I_{w,inj} + B_{g,inj}I_{g,inj}}{B_oQ_o + B_wQ_w + B_g(GOR - R_s)Q_o} \qquad \textbf{2.7.1}$$

B_x formation volume factor of fluid x
I_x injected volume of fluid x
Q_x produced volume of fluid x
GOR   produced Gas Oil Ratio
R_S solution Gas Oil Ratio

Principally, there are two ways the VRR can be obtained. On the one hand, an instantaneous VRR can be calculated by looking at injected and produced reservoir volumes on a daily or monthly basis. On the other hand, the VRR can be gained over a cumulative approach, which typically uses the beginning of the injections for calculations.

Unfortunately, it is possible that some of the injected fluid gets lost into the formation as a result of, for example, leaking faults or poor cement casing bonds.

Having a look at the instantaneous approach, a value for VRR equal or greater than 1.0 means that the same or more volumes are injected than produced, which necessarily causes the reservoir pressure to be increased or at least maintained. Contrary, a reduction of reservoir pressure is indicated by a VRR less than 1.0.

At the start of production, the pressure will drop. If the reference date for the VRR calculations is represented by the production start and the value of VRR goes up to 1.0 again, the reservoir pressure would have reached a value in the vicinity of the original one. [14].

2.8 Wellbore integrity

Wellbore integrity is an important division of HSSE. Primarily, it deals with controlling the fluid flow in a wellbore and the annular flow from the well to the surface. A standardized definition is given by NORSOK D-010 (2004) where wellbore integrity is declared as an: "application of technical, operational and organizational solutions to reduce risk of uncontrolled release of formation fluids throughout the life cycle of a well" [15]. Once a well is in mature state the risk concerning material failure, caused by corrosion activities and the influence of stresses, is increasing. An explanation for the degradation of materials with time and in case of CO_2 influence lies in the chemical composition of those materials. Principally, two main wellbore integrity defects trigger categories can be distinguished, which are shown in Figure 12.
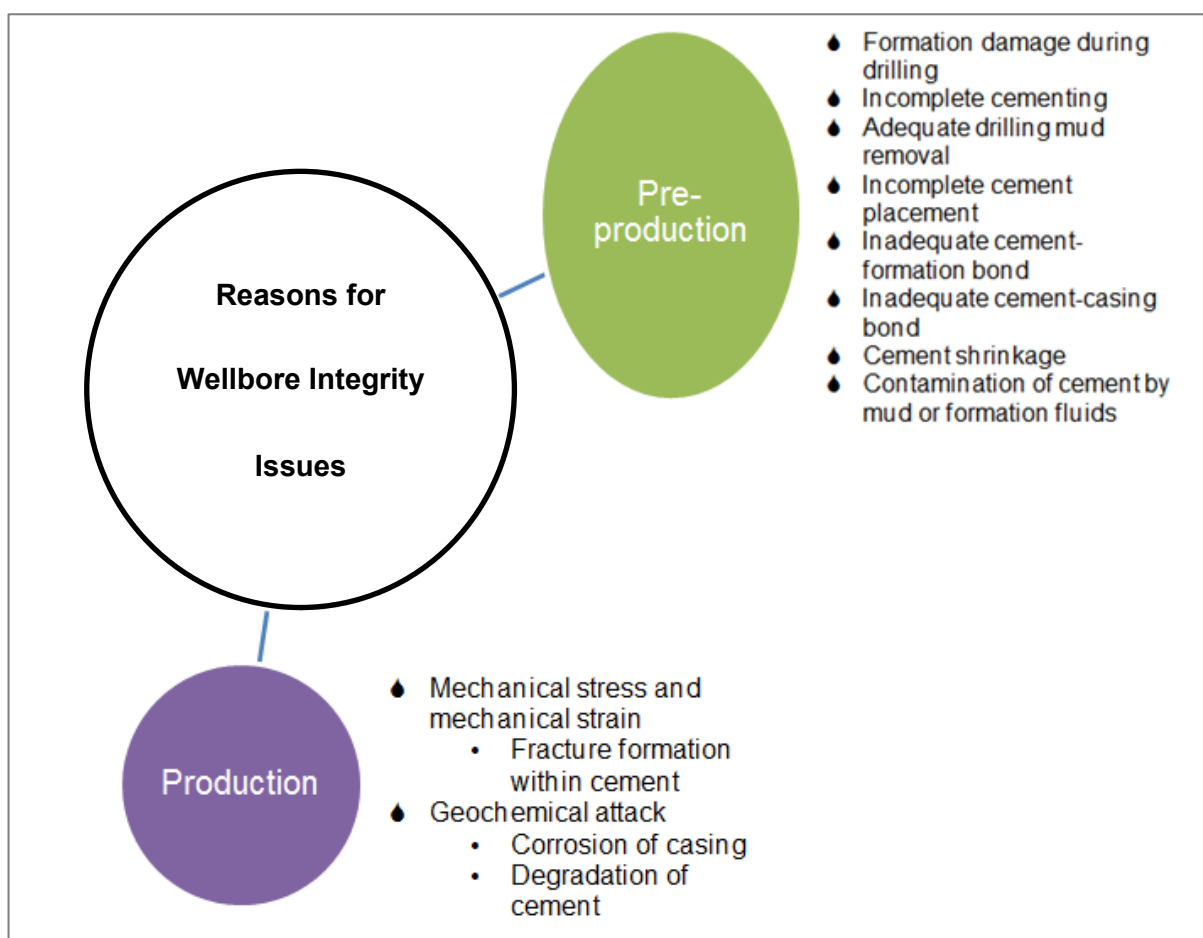
Figure 12: Possible causes for wellbore integrity failures [16]

As a consequence of poor wellbore integrity, leakages and, what is dicier, blowouts can develop [16]. Critical ramifications, if well leakage gets an issue, are material damage, human injuries, production losses, environmental impacts and a bad reputation for the company, to name but a few. In order to prevent those situations, companies should be able to act proactively, which is achieved by knowing the well's integrity status at every point in time [15].

Due to the high water cut in the 16th TH's gross production, casing leak evolution should be brought into focus. The Bockfließ area consists of 108 wells with an average water cut of 92.7 percent. Averaging the years of existence until a casing leak was observed leads to approximately 50 years runtime per well. From the mentioned 108 wells, 23 were affected by casing leaks and two wells even got plugged and abandoned.

An additional finding, derived from the analysis performed by OMV's production department in Gänserndorf in the year 2015, concerns the fact that 70 percent of the casing leaks were found subsequent to corrosion inhibitor injection. Considering that, prevention of casing leaks using corrosion inhibitors cannot be guaranteed. This condition is explained by the fact that most of OMV's wellbores were installed 50 to 60 years ago and inhibitor injection started in 1968 at the earliest. So, maybe already affected wellbores only experienced a deceleration of corrosion rate, but were already damaged in the sense of a thinned casing wall.

Another theory establishes an involvement of the installed ESP configurations. In order to achieve an appropriate explanation of this approach, OMV's internal corrosion workflow and basic setup of a corrosion inhibitor are explained subsequently.

Out of experiments, the partial pressure of CO_2 is determined. Table 3 describes the conclusions made out of the measured partial pressure data.

Table 3: Partial pressure of CO_2 and its correlated likelihood to corrode

Partial pressure of CO_2, bar	Chance to corrode
< 0.2	No corrosion
0.2 – 0.5	Very low corrosion
0.5 – 1.0	Low corrosion
1.0 – 3.0	High corrosion
> 3.0	Very high corrosion

In consequence of the increase in gross production and by analysing eight wells, a rise in average partial pressure of CO_2 was observable in the extent of 0.02 bars. Combined with the better temperature conservation of the system, which was achieved by the new flood circle's installation, a higher corrosion rate, measured in millimetres per year, can be concluded. Furthermore, an increase in the flow velocities leads to a removal of the established protective iron carbonate layer, which also occasions an enhanced corrosive behaviour under the pretext of erosional corrosion.

2.9 Reference reservoirs

In order to be able to draw some parallels to other reservoirs in the Matzen field and gain some benefits and information from previous activities, the 8th and 9th Tortonian horizons get examined in the next two subchapters.

2.9.1 9th Tortonian

In the 9th TH reservoir an aquifer is acting from southern and eastern direction. In order to be able to sweep also the oil from the northern side of the horizon, water injection was initiated in the north. Consequently, a case of washed out pathways, so called "highways", between injector and producer could be observed.

The occurrence is described by an injection through well Schönkirchen 313 (S 313) and a production by the wells S 263 and S 255. After producing for almost nine years, well S 263 got uneconomic in layers five and six. Reasons included a high water cut. The distance between the two producers, from the injector's point of view, is about 280 m. A hydraulic connection between the injector well and producer S 255 could be detected. Having a look at Figure 13 it is observable that if the eruptive producing S 255 is hydraulically connected to the injector in layers five and six, S 263 is prone to get watered out. As a consequence, the producer S 263 was uplifted to the layer 9_3, where more potential was recognizable.
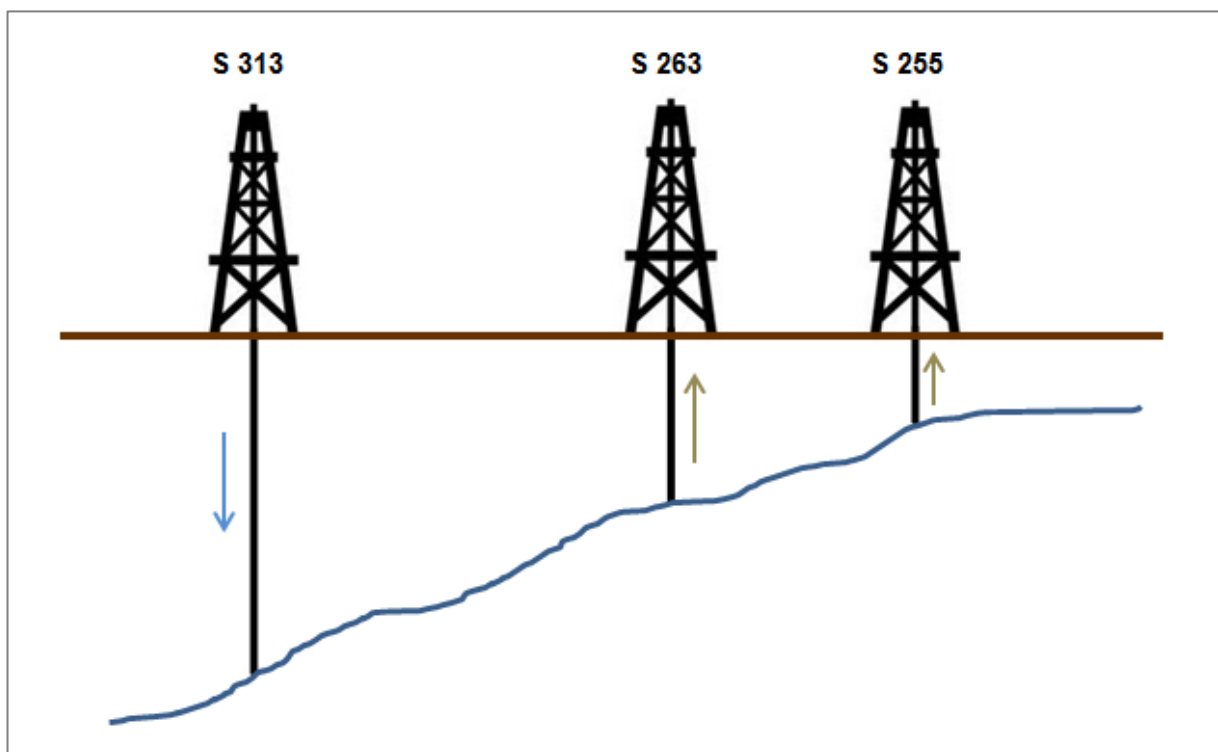

Figure 13: Basic sketch of the injection scenario between one injector and two producers

2.9.2 8th Tortonian

As distinguished from the 9th Tortonian's behaviour, the 8th TH has little to no aquifer support. The first ten years of production were driven by solution-gas, where a pressure drop from 112 bar to 85 bar occurred. Water injection was initiated below the OWC in the year 1960, which led to a pressure increase because of performing at a VRR, which was explained in chapter 2.7., above one. In the year 2004, pressure was again at a value of 102 bar.

Generally, the reservoir is composed of sandstone that shows vertical and lateral heterogeneities. The porosity varies between 20 and 32 percent and the permeability was observed to be about 300 mD with some small-sized exceptions that show a permeability of 1 Darcy. From the 340 initially producing wells, 90 are still in production. All of them are operating with an artificial-lift system, dominated by sucker-rod pumps. Only 10 percent of the production wells are working with gas lift methodology. The main reason for investigations in the 8th Tortonian reservoir was the fact that the production of the whole Matzen field is gathered in a central separation station with a limited capacity for fluid handling. In 2005 a redevelopment in the 16th TH reservoir led to an increase in gross production, which implicated that the other reservoirs had to lower their gross rate.

For economic reasons and simplicity for on-field engineers a streamline surveillance model was used in order to investigate the flow behaviour and thus come up with a strategy to enhance oil production by understanding the interaction between injector and producer. The northeast section of the 8th TH production is mainly driven by water injection, which represents a good property for an accurate modelling result. For the model itself a so called "shoe box" was used, which represents a single-layer model that includes all wells and perforations. The sandstone was assumed to be homogeneous with an incompressible fluid occupying the pore space managed by implementing constant-pressure boundary conditions on both sides of the shoe box. It should be pointed out that geological features on a larger scale, like any kind of flow barrier, are having a bigger influence on the applicability of the model than local permeability or local porosity.

In the end it was possible to filter out interconnected well pairs. This result allows a more detailed view on how the injected water is behaving downhole and which pathways are popular for the fluid to take. Figure 14 represents an outcome of the 3DSL simulator. Injector and producer pairs are indicated by different colours, giving an appropriate view on the downhole injection pattern.

Nevertheless, a plausibility check was necessary to prove the model outcome. As the injected water shows less salinity [ppm], than the formation water, it was possible to use the concentration of chloride ions as natural tracer. Still, there are some uncertainties regarding the actual origin of the water, because using a salinity approach, it is not detectable from which injector a certain producer is influenced.
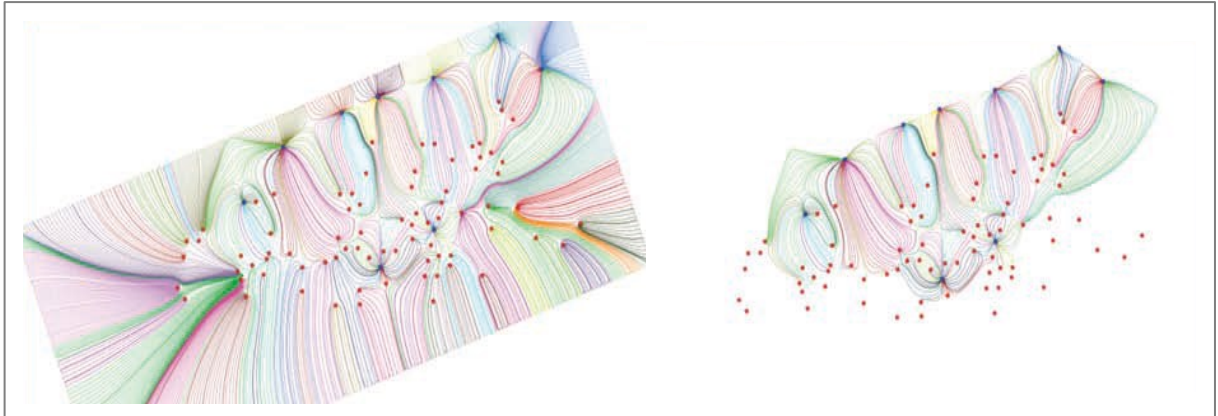
Figure 14: Streamline illustration of injectors influencing certain producers in the 8th TH [18]

Summing up the two methodologies, it was found out that each injector/producer constellation has different oil cuts. It is important, for providing a proper flood management, to prize connections with higher oil cuts above wells with lower oil cuts by adjusting the rate. An algorithm from Thiele and Batycky [17] was then used to determine the target rates. In the example of the 8th TH, the result, gathered from the algorithm, was not used to full extent, but only for finding out, if it is necessary to decrease or to increase the rate. The rate itself was subsequently defined qualitatively, because of restrictions concerning the artificial lift configuration.

In the end it was possible to adjust the well rates in that extent that untouched oil got displaced towards producers and new flood patterns ensued [18].

3 Data applicability and processing

The third chapter deals with the usability of gathered data and, as a second subchapter, with the description of data sources and data processing programs.

3.1 Data

Based on measuring inaccuracies and different sources of data, some predefined intentions could not be realized, which are described in the next paragraphs.

3.1.1 Chloride ion concentration

Additionally to the pressure analysis approach, the difference between the chloride ion concentration of water injected and water produced should have been examined. The evaluation should give information about the produced water's origin with the chloride ion concentration serving as naturally acting tracer.

Seen from a historical perspective, the chloride ion concentration in this specific area was a useful indicator for whether the produced water arose from an aquifer or an injection well. With the aim of comparing the chloride ion concentrations from different wells, a normalization mechanism was established. For this reason, the chloride ion concentration was divided by a quantity called alkalinity, also referred to as m-value.

Principally, a gathered water sample is characterized by a particular pH-value. The alkalinity is determined by the amount of acid, represented on the base of hydrogen ions, needed to be fed into the medium to lower the pH-value to a value of 4.3. This feeding procedure is accomplished by titration [19]. Generally, the injection water has an m-value of approximately 20 mmol per liter, whereas the 16th TH formation water is characterized by an m-value of 30-40 mmol per liter. As the quotient between chloride ion concentration and m-value results in a smaller digit, the well was assumed to be rather unaffected from injection water, while a high ratio led to the conclusion that injection water already influences the well's production to a greater extent.

Unfortunately, this strategy was no longer applicable for this reservoir. Due to the fact that the formation has been flooded by injection water over years, the fluid properties have experienced a change insofar as the produced water cannot be distinguished from injected water anymore, when observing the chloride ion concentration. This unfavorable circumstance can be recognized by watching the chloride ion concentration at the extraction station in Auersthal. The already mentioned separators are filled by different flow lines, gathering the production from different parts of the field. While the produced fluid is treated as illustrated in chapter 2.1, it does not change the fluid's chloride ion concentration directly.

As a matter of principle, the different flow lines, containing fluid with dissimilar salinity, run together in a later point of the process eventuating in a weighted average chloride ion concentration depending on the fluid's rate and salinity per flow line. Due to the fact that the chloride ion's concentration received at the production flow lines is nearly the same as it is

for the fluid injected, it is impossible to indicate an influence of one specific injector on distinct producers. Exact values of the salinity with reference to the corresponding flow lines are illustrated in Table 4.

Table 4: Chloride ion concentration allocated to flow lines

Flow line	Chloride ion concentration, ppm
F9200 LÖMST MA 15, MA 16	11 836
F9300 BO 204	11 504
F9500 MA 8, MA 9, MA 9A, MA 9C	11 905
F9700 HL, PIR, BO 208	9 764
Hydrocyclone Exit: Injection Water	11 405

*MA: Matzen; BO: Bockfließ; HL: Hochleiten; PIR: Pirawarth

As observable in Table 4, the injection water has a chloride ion concentration of approximately 11 400 mg/l and an m-value of 20 mmol per liter, as already mentioned. Consequently, the ratio results in a value of 570 g/mol. Referring to the quotient of the data measured at the producing well BO 80 this year, which gives a magnitude of about 530 g/mol, a definite distinction cannot be achieved anymore.

Suggestions concerning the further investigations into chloride ion concentrations are discussed in chapter 5.2.2.

3.1.2 Sensor data

The daily average pressure and pump frequency data was extracted from the software LOWIS^{TM} into Microsoft Excel for further processing. Though BO 208 should initially be taken into account in the analysis, it appeared more reasonable not to consider the well with regard to pressure manipulation at the inlet into the wellbore induced by the type of completion.

Referred to the already mentioned completion, AICDs, Autonomous Inflow Control Devices, were installed on the horizontal section of the well BO 208 to ensure a continuous inflow.

In general, inflow control devices are used in horizontal wells. The installation of horizontal wells is explained by an increase of continuance in the zone of interest in order to maximize production out of this zone and delay a breakthrough of water or gas. Unfortunately, horizontal wells suffer from a heel-toe effect, which is explained in a subsequent section. As a consequence, the sweep efficiency can be lowered dramatically, which results in a disadvantageous impact on the ultimate oil recovery.

The primary goal, which should be achieved by installing ICDs, is to avoid the risk of water cone generation, which is referred to as a crest, when speaking of horizontal wells.

A second circumstance deals with the friction pressure drop in the tubing, which is of greater extent in horizontal wells than in vertical ones. Considering that a lower pressure drawdown in the horizontal section might be a result, more production is achieved from the heel than from the toe. In order to provide an illustration of the previous explained situation, Figure 15 shows four graphs that explain typical flux profiles, if no control device is applied [20].
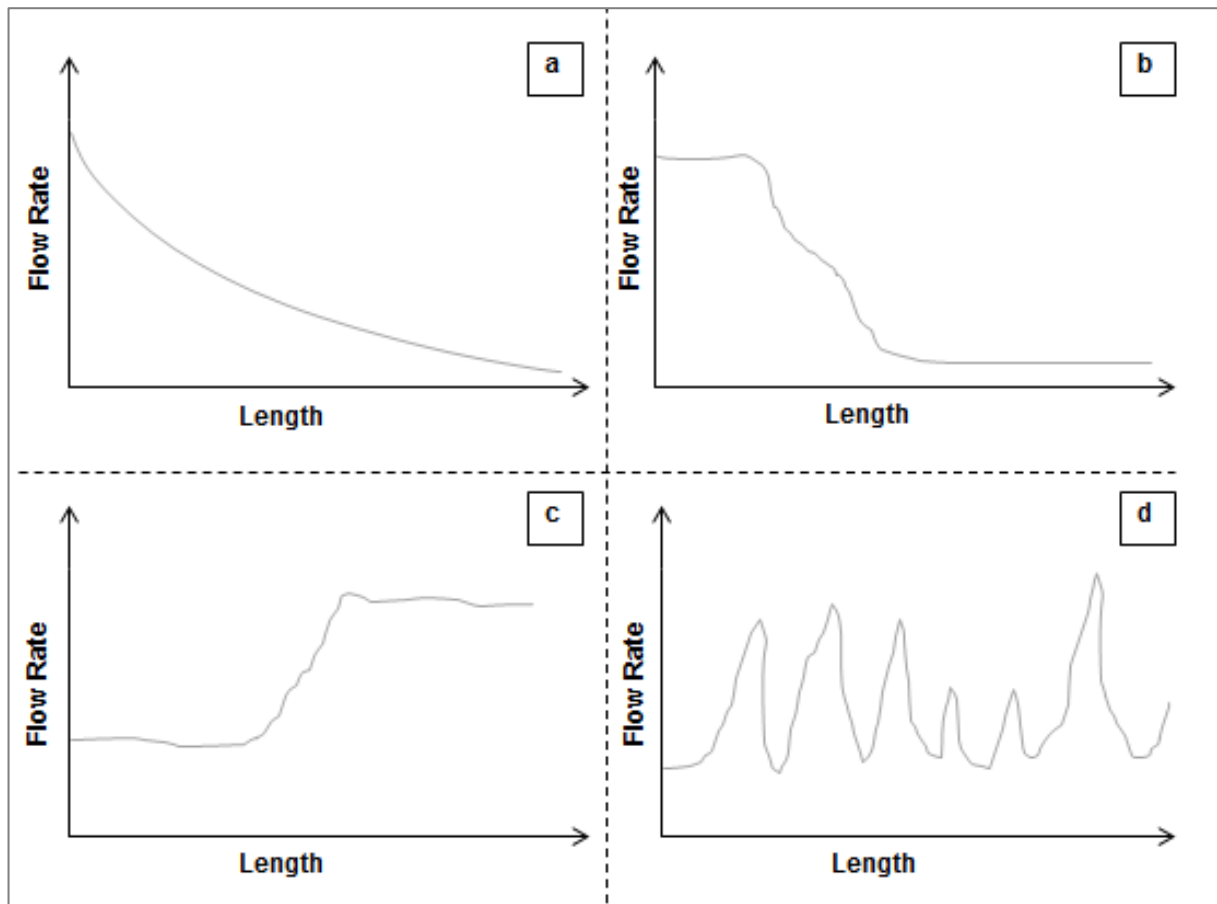
Figure 15: Horizontal wells' flowing profile at different reservoir conditions (a: homogeneous formation, b: high permeability at heel; c: high permeability at toe; d: varying permeability [20]

Two completion techniques can be distinguished for providing an inflow's control, where an Interval Control Valve (ICV) acts actively and an Inflow Control Device (ICD) operates passively [21].

After applying ICDs a more evenly inflow behavior is guaranteed by creating a supplementary pressure drop at the well's inflow spots. Having a look at the completion sketch of BO 208 it is observable that the inflow points are assigned to different inflow compartments that are separated by packers [22]. This specific completion device acts as balancing tool to automatically adjust the inflow in an appropriate manner.

Different types of ICDs are currently available on the market, where the applied one is using the fluid's viscosity to choke back those fluids that obtain low viscosities. If one specific section was producing with a high gas or water cut, the flow would be constrained.

Therefore, a floating disk is installed between the valve's in- and outlet, where the floating disk can position itself up- or downstream depending on the produced fluid's viscosity. Because of the low viscosity of water, compared to oil, the floating disk would choke back the fluid stream by moving in the direction of the valve's upstream [20].

The operating principle is based on Bernoulli's law. Figure 16 shows a real life example of an AICD completion on the left side and an explanation of the underlying technique on the right side.
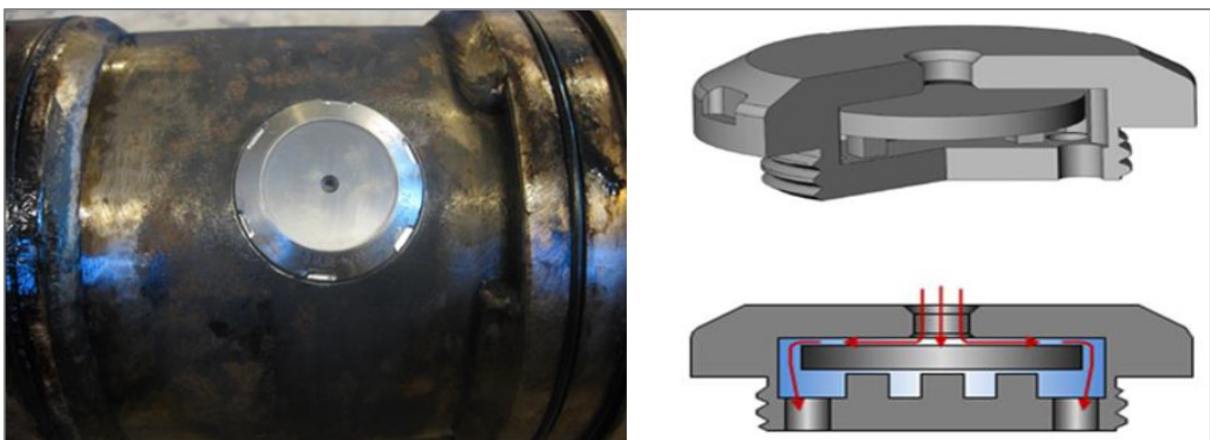
Figure 16: FloSure AICDs of the company Tendeka [22] with functional principle on the right side [23]

Lower viscosity fluids are prone to flow under higher velocities. Having Bernoulli's principle in mind, the pressure on the top of the disk has to decrease, as velocity increases. Along with a lower pressure region on the disk's upper side comes an increase in pressure on the disk's bottom part. As the red arrows in the right image of Figure 16 indicate, the floating disk restricts the flow of fluids with a low viscosity into the wellbore [23].

Considering the above described procedure, it seems clear that the recorded pressure experienced a manipulation. Due to this tremendous influence on the pump intake pressure, the data was no longer reliable for accomplishing an analysis approach.

3.2 Electrical submersible pump

This chapter is divided into the first part, which gives an overview of the operating principle of electrical submersible pumps (ESPs), a second subchapter describing the installed pump setup and the third section, dealing with the mounted downhole sensor.

3.2.1 General

The core element of an ESP is the centrifugal pump in multistage version, composed of a rotating impeller and a stationary diffuser. The fluid enters the impeller section and is moved by the centrifugal force to the outside wall and accesses the diffuser part. Consequently, as the fluid is accelerated by the impeller, the fluid's velocity and thus its kinetic energy is increased, leading to a decrease in pressure. Due to this pressure loss, more fluid is sucked into the impeller. As the fluid arrives in the diffuser part with greater cross section, the kinetic energy is lowered again and the pressure rises. Like already mentioned, multiple stages are in use generating a high enough head to lift the fluid from downhole to the surface at a desired rate. Figure 17 illustrates the explained system showing a two stage centrifugal pump.
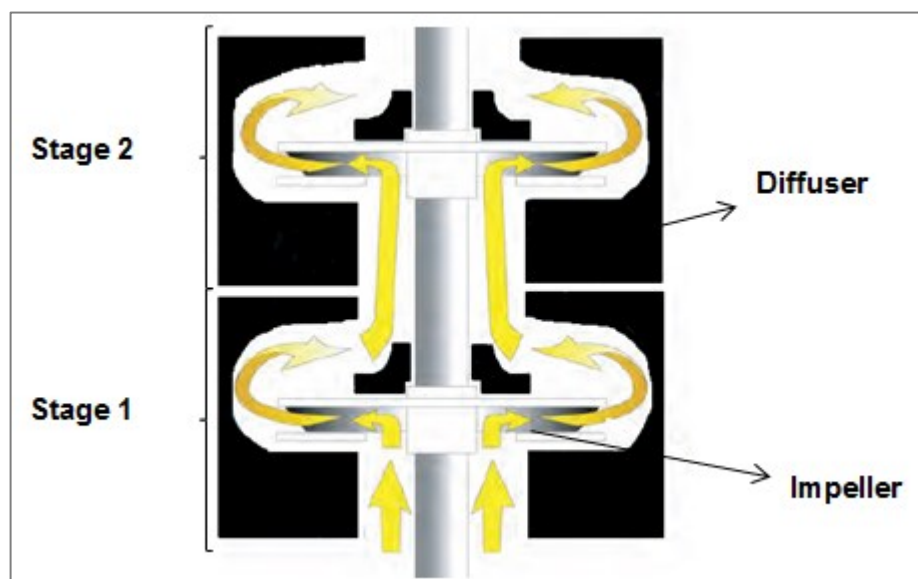
Figure 17: Diffuser and impeller illustrated in a two stage centrifugal pump [24]

In order to drive the pump, a shaft is transmitting the rotational motion from the motor to the impellers. Another very important constituent is represented by the sealing-chamber, which is located above the motor. One important task accomplished by the sealing-chamber is the separation of the wellbore fluid from the motor oil in order to prevent mechanical and electrical breakdown of the motor. Due to the fact that only the power cable, driving the motor downhole, and the surface controls are visible on surface, the footprint is relatively small, compared to sucker rod pumping systems [24].

3.2.2 Installed assembly

Different ESP-setups got implemented, varying in their number of protectors, motors and pumps. In Figure 18 a pump installation is pictured schematically.

Figure 18: Schematic sample of an installed pump configuration [30]

The pump curve of an installed pump type is illustrated in Appendix B.1.

3.2.3 Applied downhole sensor

In order to improve the cost efficiency factor and for providing an increased potential in reservoir management, all installed ESPs are equipped with a downhole sensor, which is located directly below the motor. These downhole sensors got installed for gathering data like pressure, temperature, leakage current and vibrations. Meeting the predefined requirem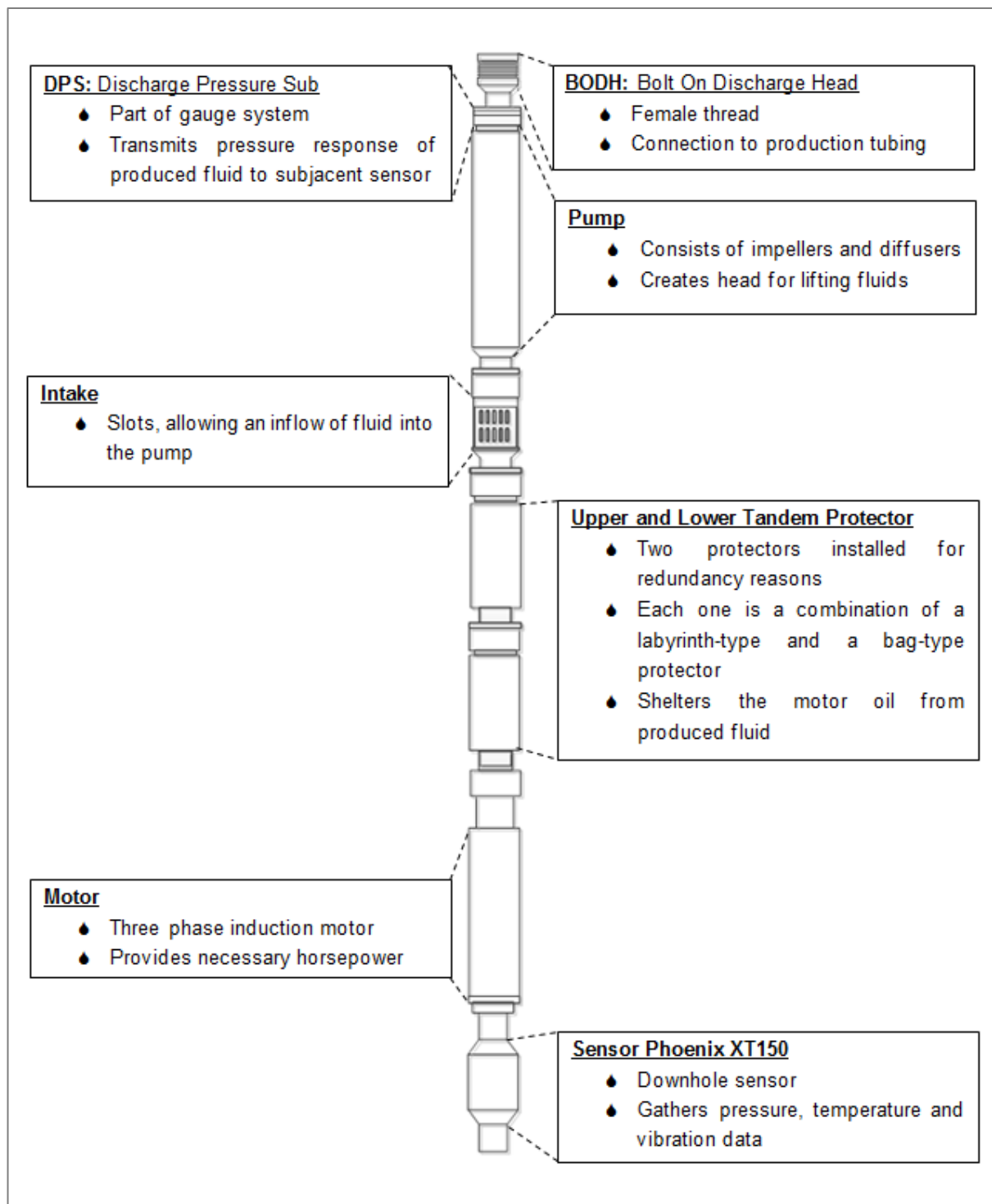ents best, the decision fell on the Phoenix XT150 sensor designed by the company Schlumberger, illustrated in Figure 19.
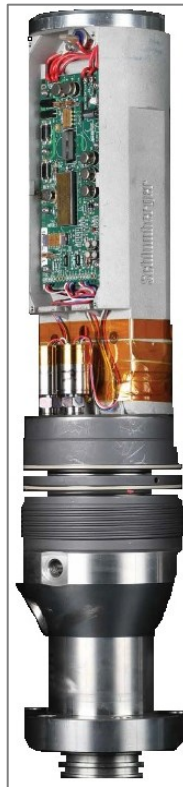
Figure 19: Downhole sensor Phoenix XT150 from Schlumberger [25]

Principally, the gauge is available in two different arrangements, which are labelled as Type 0 and Type 1. The difference between the two constellations is the additionally measured pump discharge pressure in the case of sensor Type 1. Type 0 gives information about the intake temperature and pressure, motor oil or motor winding temperature, vibrations and current leakage. Being able to investigate the pump performance if the discharge pressure is known, Type 1 was selected [4]. With the aim of improving the ESP's run life by appropriate monitoring, alarms can get configured for all gathered parameters, if a certain threshold gets undershot or exceeded.   The communication between the sensor and the surface is managed via ESP cable. The device is 57 centimetres long and has an outer diameter of 11.4 cm. The material is composed of 13% chromium steel. In respect of the temperature, a limitation of applicability is set to a value of 175°C at an operating duration of 24 hours. The sensor's accuracy is quantified by $\pm$ 0.35 bars. As one last note it should be mentioned that also a storing of historical data is possible [25].

3.3 Software

Different databases and applications are used to achieve the following three interactive targets:
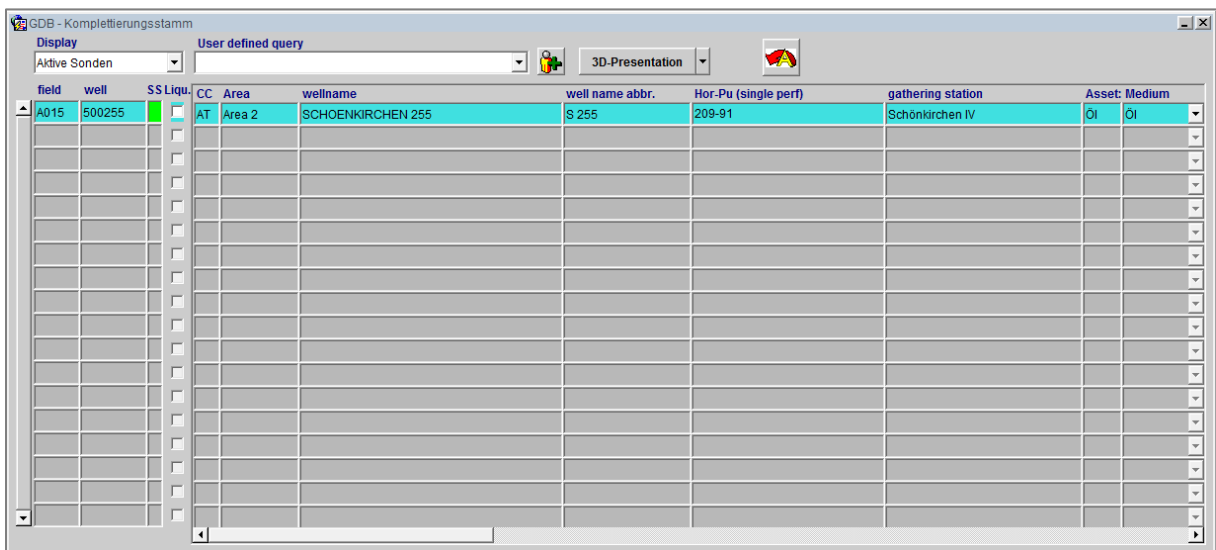
- ♦ Data gathering
- ♦ Proper demonstration of information
- ♦ Outcome illustration and analysis

The requisite programs are discussed in the subsequent paragraphs.

3.3.1 GDB

The shortcut GDB stands for "Gewinnungsdatenbank", which is OMV Austria's internal database based on Oracle. It serves as storage for treatment and production data for instance. On basis of the GDB, it is possible to search for a well's complete treatment history to find out complications a certain well probably had to deal with in the past. Furthermore production and injection reports including rates, water content and related pressure measurements are available.

Additionally, a data filtering can easily be applied by entering the desired conditions into the screen, demonstrated in Figure 20.

Figure 20: GDB filtering screen

As observable in Figure 20, different filtering conditions can be applied, including for example:

- ♦ Field
- ♦ Area
- ♦ Well Name
- ♦ Horizon and Production Unit
- ♦ Gathering station

♦ Asset

♦ Medium

♦ Pump Type

Important for the data gathering process is the "Daily production technical" window, illustrated in Figure 21 on the basis of an injector well. This window allows the user to have access to dynamic tubing pressure data and other parameters of a certain injection or production well at a defined date.

Date	TR H2O Inj. [m3]	H2O total [m3]	Liftgas [m3]	dyn. tub-pr.	dyn. cas-pr.	st. tub-pr.	st. cas-pr.	choke	ty.	FS
24.05.2016	600	600,0	0	41	0	0	0			24
17.05.2016	600	600,0	0	59	0	0	0			24
10.05.2016	600	599,7	0	59	0	0	0			24
03.05.2016	600	575,0	0	56	0	0	0			24
26.04.2016	600	575,0	0	56	0	0	0			24
19.04.2016	600	515,1	0	58	0	0	0			24
12.04.2016	600	504,0	0	53	0	0	0			24
05.04.2016	600	546,6	0	53	0	0	0			24
29.03.2016	600	572,0	0	53	0	0	0			24
22.03.2016	600	592,8	0	56	0	0	0			24
15.03.2016	600	513,5	0	53	0	0	0			24
09.03.2016	600	485,1	0	41	0	0	0			24
08.03.2016	600	424,5	0	41	0	0	0			21
01.03.2016	600	599,4	0	53	0	0	0			24
23.02.2016	600	532,2	0	52	0	0	0			24
17.02.2016	600	519,4	0	37	0	0	0			24
16.02.2016	600	432,8	0	37	0	0	0			20
09.02.2016	600	520,0	0	50	0	0	0			24
07.02.2016	600	644,4	0	39	0	0	0			24

Figure 21: Window of daily production technical in GDB

The GDB was developed in the year 1998 to improve the data storage and catalyse the internal searching and learning processes.

3.3.2 RMDB

The Reservoir Management Database (RMDB) pursues principally a quite similar approach compared to the GDB, explained in the previous chapter 3.3.1. As the name indicates the stored information deals with reservoir properties. A clear summary of the reservoir related data includes initial reservoir pressure, reservoir temperature, formation volume factor and density of the reservoir's inherent fluids, to name a few.

In addition the database provides reports concerning volumes and reserves of a specific production unit. The produced amount can be illustrated over time using a plotting feature.

With both, the GDB and RMDB, data can be exported into a word or excel file, which makes it easier to proceed in subsequent tasks, when it comes to data processing.

3.3.3 LOWIS^{TM}

LOWIS^{TM} stands for "Life of Well Information Software" and its basic target is to offer a more efficient approach in the area of well management. In order to achieve this goal, the web-based software provides an alarming system based on real-time data. Furthermore it is possible to analyse the gathered real-time data for improving the artificial lift strategy and to identify other complications, which may arise in the production sector. The overall goals of the feature are maintaining an optimum production of wells and thus improve the company's financial performance. The client's side is based on the ActiveX technology, responsible for the functionality and smooth data transfer.

Figure 22 shows, how the production engineer sees the properties of an observed well. On the one hand the dark blue rectangle shows the fluid related attributes and, on the other hand, the light blue rectangle illustrates the mechanical features measured with the downhole sensor, described in chapter 3.2.3.
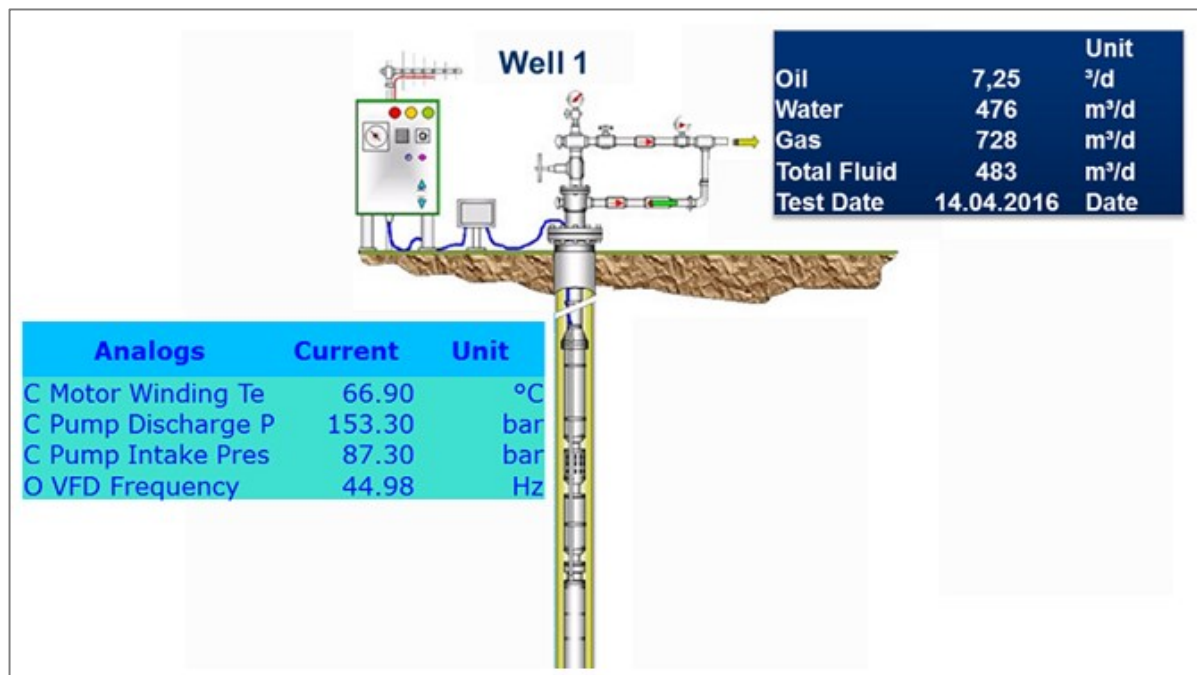
Figure 22: User Interface of LOWIS^{TM} [44]

Further analysis methods are provided by different investigation tools within the software package. To take a single example, it is possible to investigate in trends concerning production or ESP performance. Additionally, a plot involving a well's achieved production per year can be established, which allows a comparison with the performance of injectors that are placed near a producer. The latter point is very important for the accurate analysis of injector-to-producer interaction. Moreover, it is possible to export datasets to the Microsoft program Excel for ongoing research [26].

3.3.4 OFM^(TM)

OFM^(TM) means OilField Manager and is a software tool provided by the company Schlumberger. Principally, it is an analysis software for investigations in well and reservoir performance composed of three basic applications:

- Monitoring of a certain reservoir
- Observing the associated production of this reservoir
- Forecasting of production

OFM^(TM) establishes a connection to the database (GDB) and utilizes this information to generate wellbore diagrams and cross sections illustrating, for instance, the water cut distribution across a certain area. Furthermore, it gives the opportunity for examining aquifer influx directions and magnitudes for identifying the prevalent flow direction. As a result, an investigation in well-to-well communication is possible [27].

An important feature of the software, which has been already mentioned in the previous paragraph, is the illustration of the water cut (Figure 23).
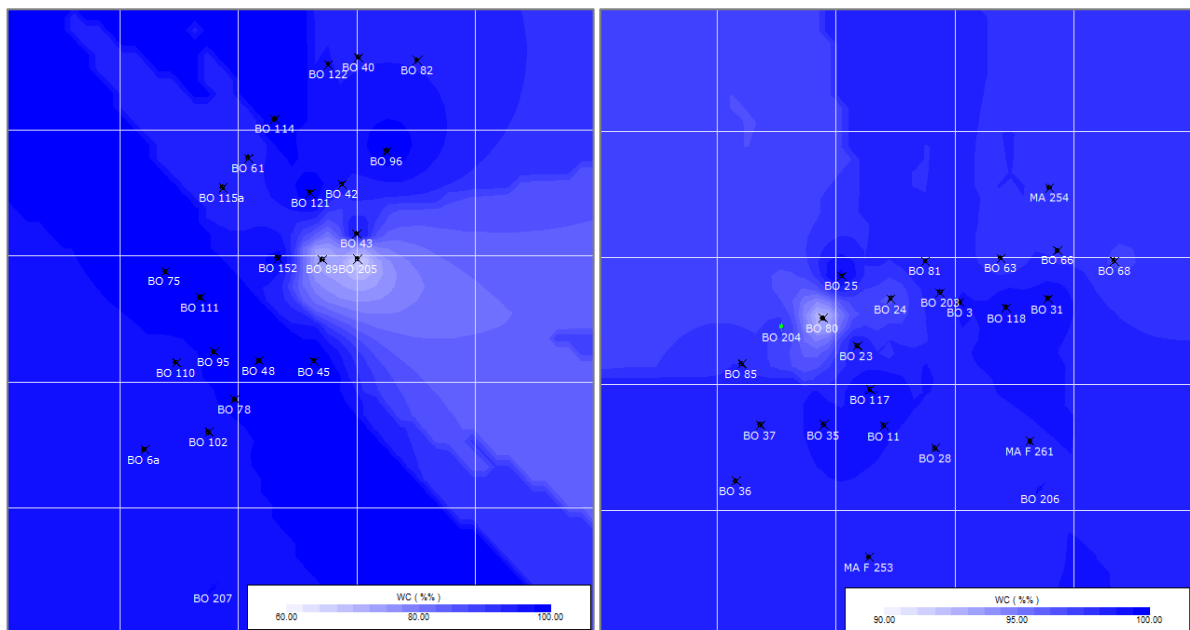
Figure 23: Water cut illustration of sector I (left) and sector II (right) [43]

The two representations of the water cut are based on different scales, where the left picture shows the water cut of sector I with a minimum value of 60 percent and the right picture reproduces the water cut of sector II based on a minimum value of 90 percent. As it can be seen, the majority of the area is already characterized by a water cut of nearly 100 percent.

Principally, the presentation is based on water cut values assigned to a well, recorded in the GDB, whereas the domain in-between multiple wells is approximated on the basis of those allocated values.

3.3.5 Streamline

Based on the reservoir flow simulator 3DSL it is possible to illustrate and, more importantly, quantify the flow behaviour between an injection well and a producer. Considering that a streamline acts as a joint between a source and a sink, the number of streamlines indicates the flow intensity between those two wells at any instant in time. Consequently, target rates can be optimized in order to achieve an improved flood pattern [28]. Basically, the streamline approach changes the previously prevalent static injector-producer constellation to a dynamic method of improving flood management based on a centred injector and circumjacent producers influenced by this particular injector. For quantification purposes of well-pair interactions, so called well-allocation factors (WAFs) are estimated. WAFs get valued by the usage of well locations, geological models and historical fluid rates and are applied for representing the relation between injected water and produced oil. Thus, they give an indication of the displacement efficiency.

Alternatively to streamlines, Flux Pattern (FP) maps can be used for the demonstration of interacting wells. FP maps consist of straight lines summarizing the various streamlines that act as connection between wells. Different features are describing the connection properties using different colours, labels and line thicknesses. Additionally the analysis of WAFs can be based on one injector, illustrated in Figure 24 (left), or on the producers, described in Figure 24 (right).
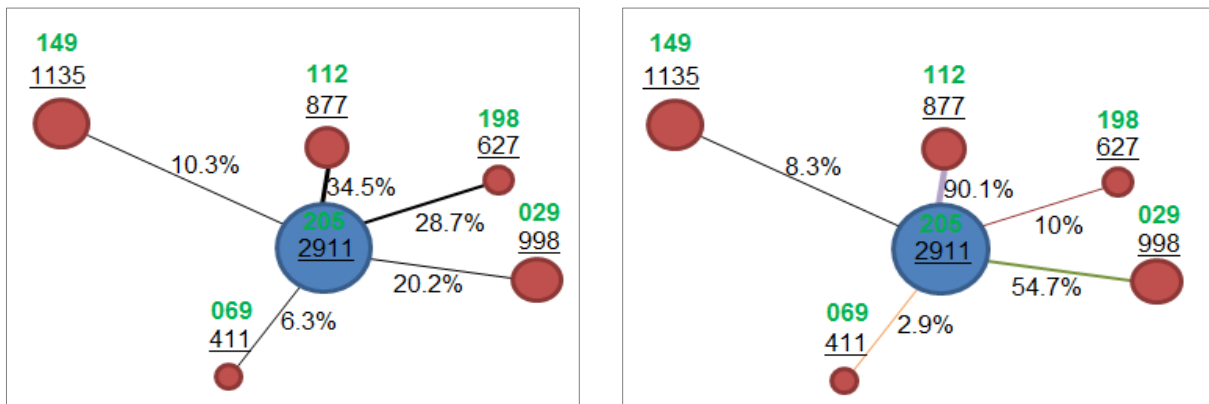
Figure 24: FP maps based on injector (left) and on producers (right) [18]

The blue spot in both pictures represents the injector and the red bubbles are defined as producers. A green number is observable above each well, which indicates the well identification. Looking at the underlined number, the volumes of fluid injected or produced are shown. A changing line thickness points to a difference in the influence magnitudes, whereas the various line colours in the right sketch refer to a particular producer. Furthermore, percentages are noticeable next to the connection lines. These numbers provide information about the contribution of the injector on the production of a certain producer or how much of the injection water makes the way to a specific producer [18].

4   Results

The results section is divided into a general information part about the two sectors, describing what the prevalent situation is like, and what should be achieved with the investigations, described in a second subdivision.

4.1 Status quo

On the one hand, the flooding approach leads to a higher gross production and, as a consequence thereof, to more oil recovered. On the other hand, the oil is replaced much faster, than under conventional producing conditions, which may results in leaving oil spots untouched. When the oil production was increased, the WOR experienced a dramatic growth.

Every year, predictions concerning reserves' estimations have to be met. The excessive production and injection in the course of the field's redevelopment project led to a deviation from this predefined production trend. In order to avoid a further movement in the direction of increasing WOR, the production strategy of the field needs to get improved. Otherwise a premature abandonment of the area would be the consequence.

4.2 Injector and producer interaction

First of all, it was important to condition and interpret the available ESP sensor data and correlate it with the daily production, the pump's frequency and, most importantly, with the injection rate of a certain injector. Subsequently, producer-injector pairs could be established, leading to the definition of cluster. A cluster is defined as a unit of interrelated producers and injectors. The time needed for the pressure disturbance, generated by the injected water, to reach a certain producer, was evaluated by three methods:

- Comparing the producer's pressure response with injection breaks based on plotting data gathered from downhole sensors
- Analytical calculation based on hydraulic diffusivity
- Evaluation, using a well testing approach

4.2.1 Fault transmissibility

A core element, which was observed at the very beginning of the analysis, was the transmissibility of the two major faults in the field of interest.
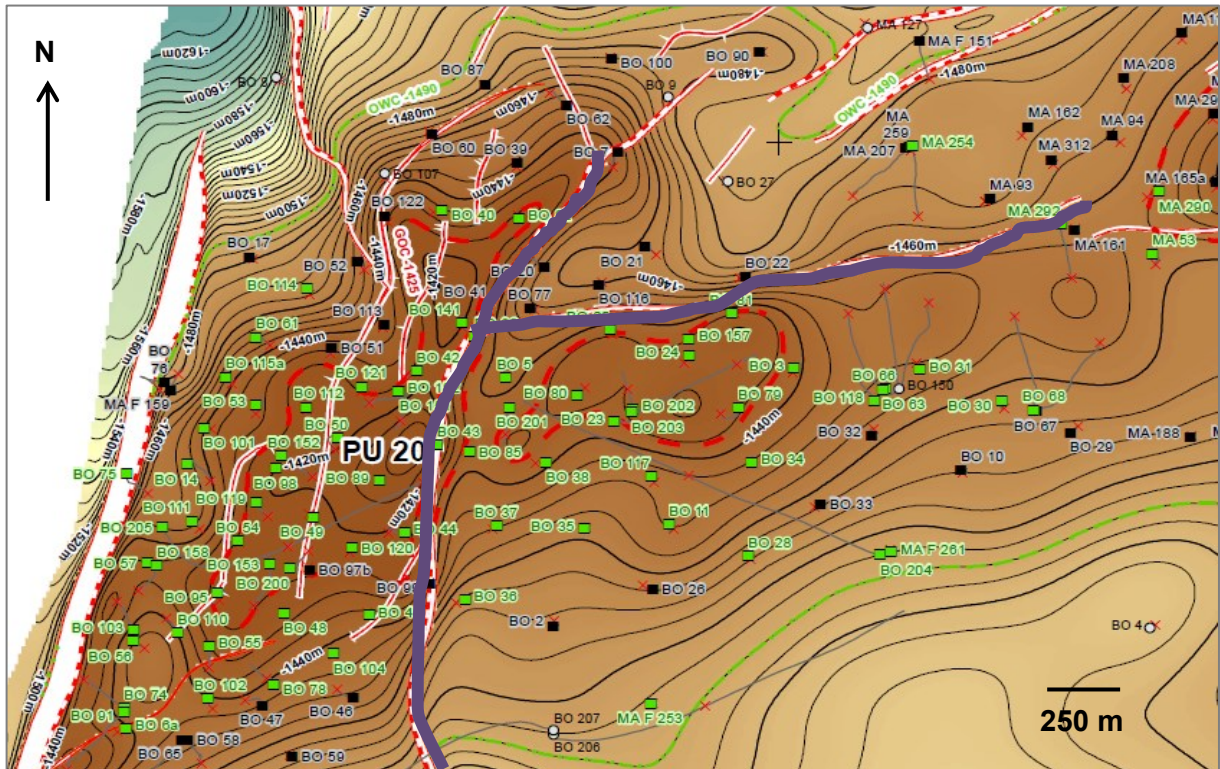
Figure 25: AOI with indicated faults

As Figure 25 shows, two major faults, marked in violet, are present in the investigated area. In order to prove the assumed transmissibility of zero in case of the fault in N-S direction, two constellations were examined, where BO 36 serves as injector:

1. Production via BO 45
2. Production via BO 43

Figure 26 and Figure 27 confirm that the two selected producers are actually not responding to the three major injection breaks of BO 36.

Figure 26: Interaction between BO 36 and BO 45

Figure 27: Interaction between BO 36 and BO 43

In relation to the second fault, extending in E-W direction, the injection is represented by MA 254 and the production by BO 81 and BO 66.

Figure 28: Interaction between MA 254 and BO 81

Figure 29: Interaction between MA 254 and BO 66

Consequently, when looking at Figure 28 and Figure 29 an influence of MA F 254 on the producers BO 81 and BO 66 cannot totally be excluded and further investigations should follow up.

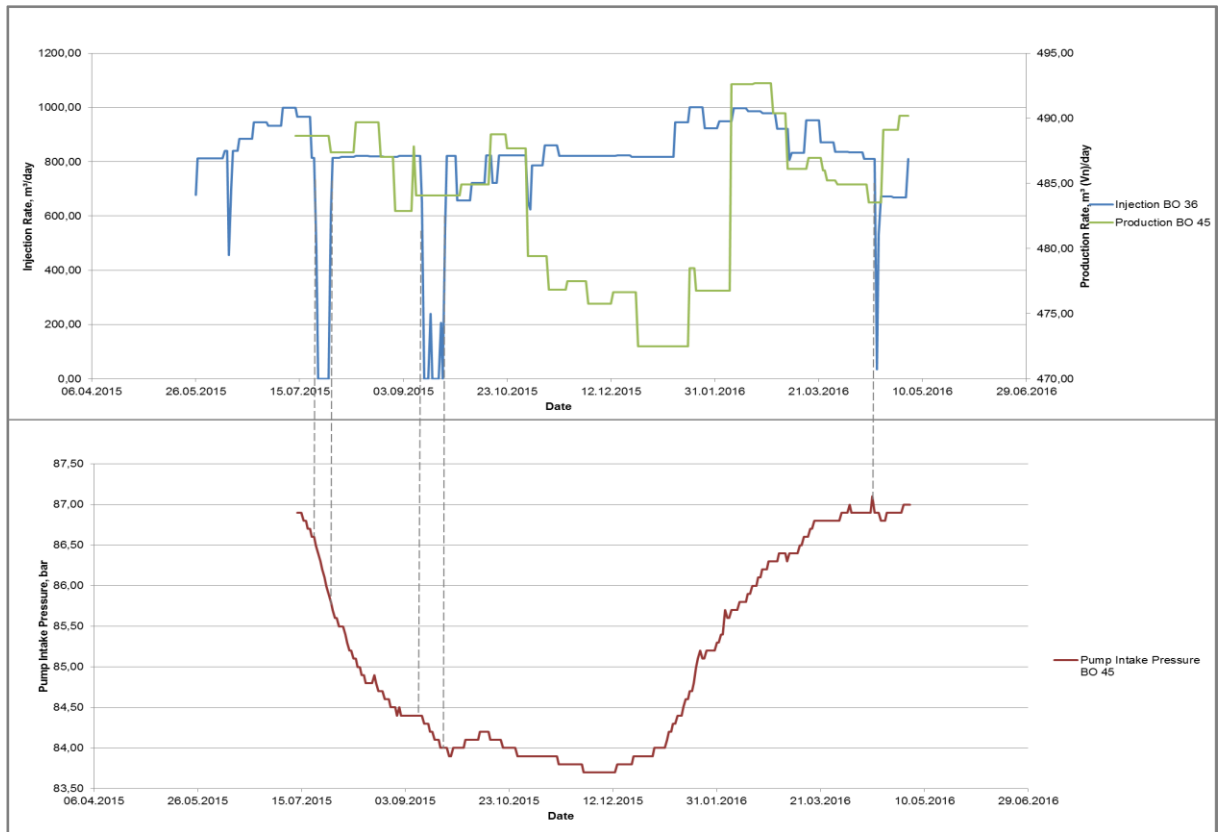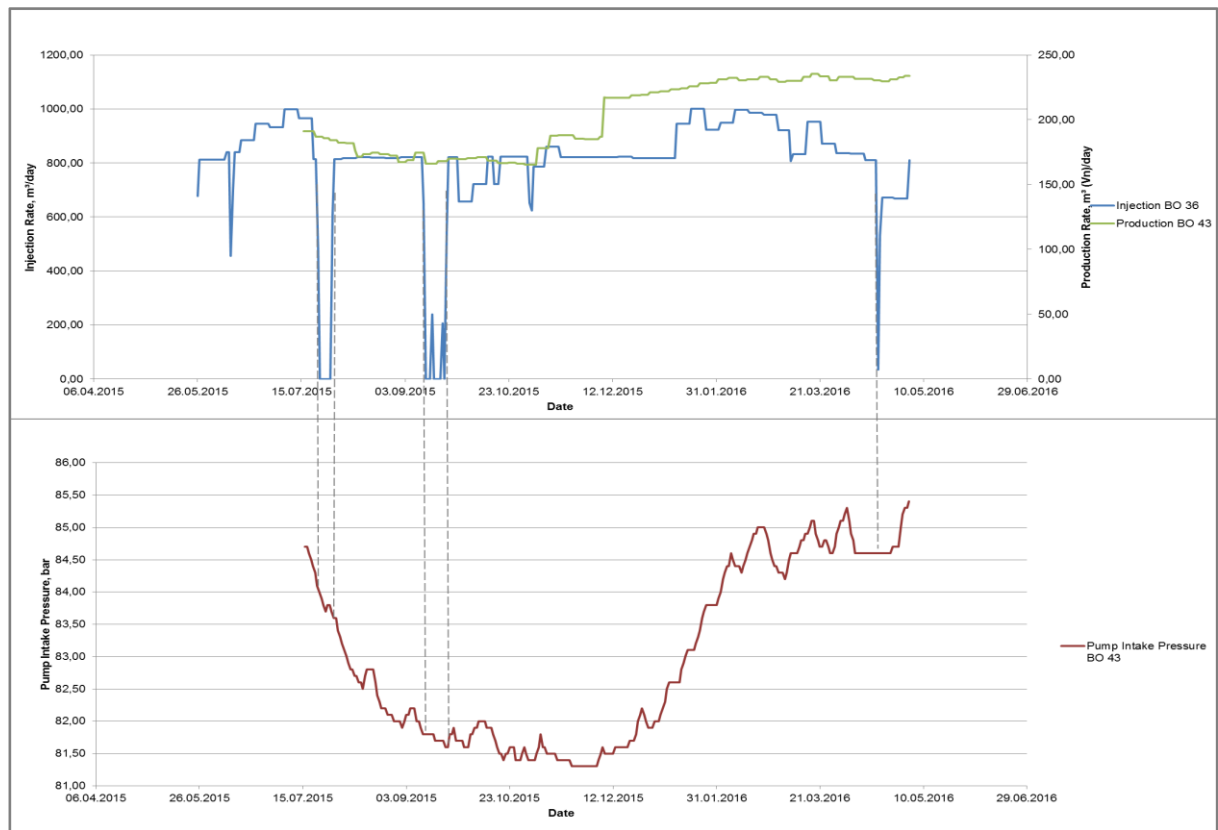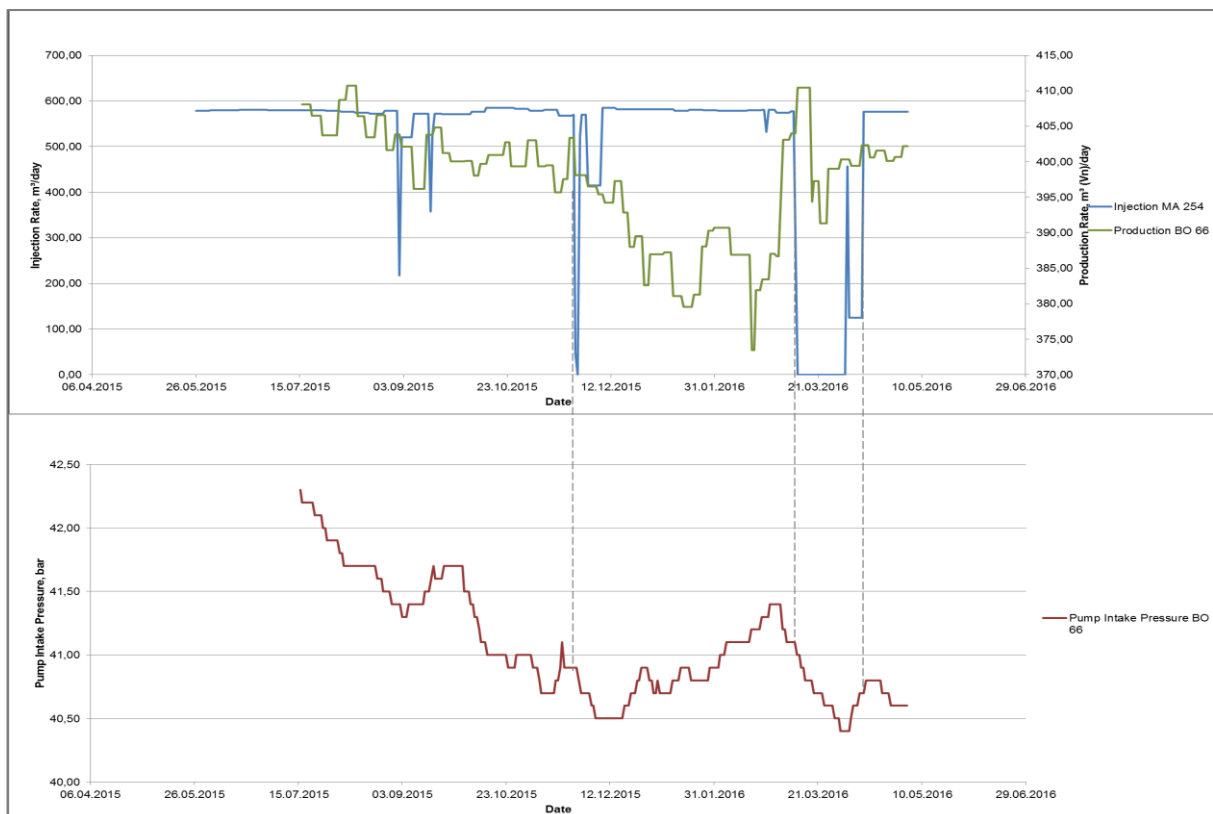Concerning the faults observable in sector one, it was not possible to derive any argumentation, characterized by means of pressure data, for the actual sealing behavior. This is related to the fact that too many injectors are flushing the region, so that no interaction through faults can be clearly identified. Based on geological observations all faults located on the area's left side are assigned with a transmissibility of zero.

4.2.2 Cluster establishment

In consequence of the 16th TH's high permeable behaviour, the categorization of individual clusters was very difficult to achieve. Nevertheless, this section deals with the description of identified connections between injectors and producing wells. Generally, four clusters could be figured out, where two ones share a great similarity, in the time frame and circumstances the investigation was focused on. This is why these two clusters are explained together in one subchapter. The numbering of clusters was chosen from the eastern side to the area's western part.

4.2.2.1 Cluster I and cluster II

Due to the area's homogeneity it seems obvious that a perfect match between producer and injector actions cannot be clearly recognized. Related to this statement, the first two clusters are discussed.

In principle, the first cluster is located at the area's very eastern section and consists of three injectors and four producers, as shown in Figure 30. In the south of cluster III, injector BO 206 is operated at a water injection rate of approximately 3000 cubic meters a day. This enormous amount of water is managed to get injected by a horizontal setting of the injection well in combination with a slotted liner completion.

Another aquifer supporting injector in the south is represented by MA F 261, which is located slightly above the horizontal section of BO 206. MA F 261 is composed of a slightly deviated pathway and contributes to the injection with about a third of BO 206's injection volume.

MA 254, as a third injector, acts on the very northern cardinal direction. Since this injector is located above a fault extending from eastern to western side, it probably is falsely assumed to not have any contact with wells situated below this mentioned fault. Nevertheless, interference between MA 254 and producing wells, located next to the fault, has already been suggested in chapter 4.2.1.
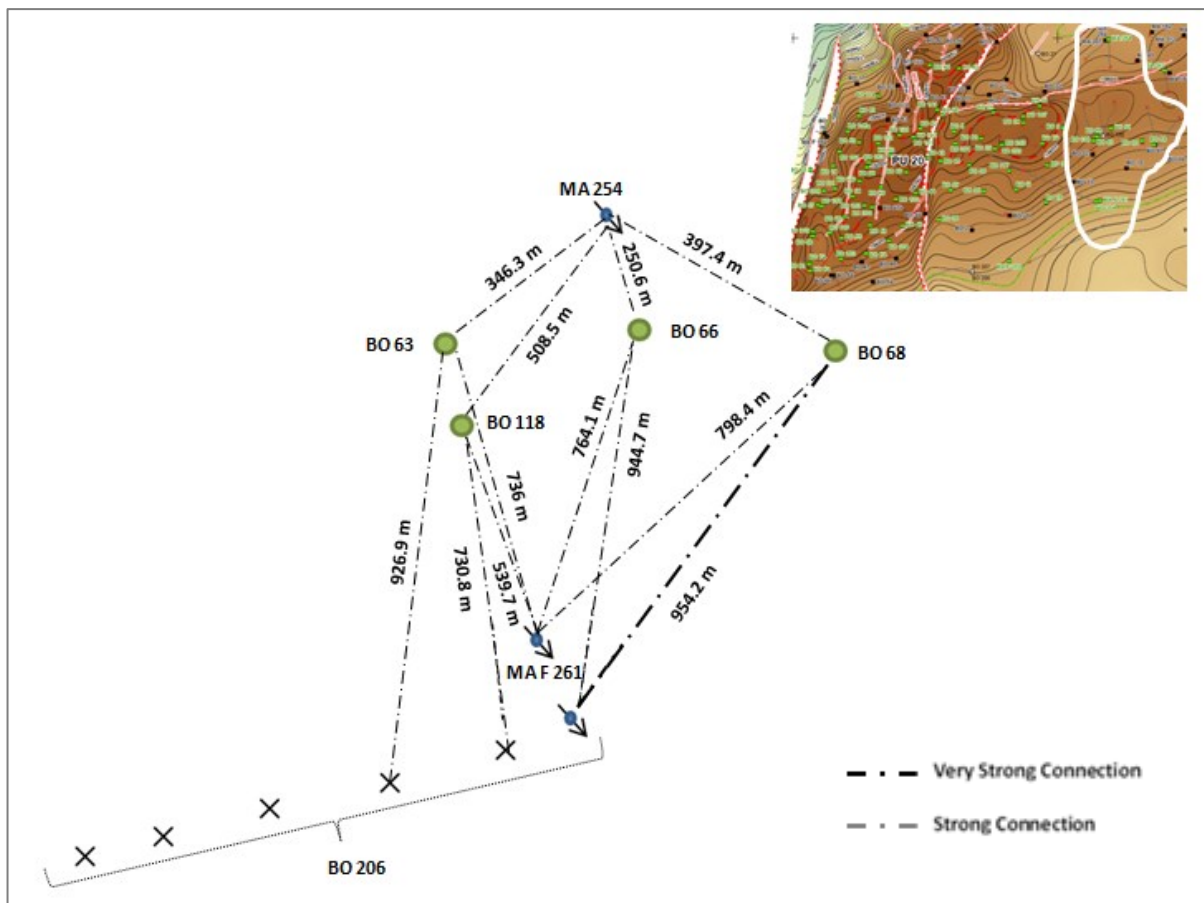
Figure 30: Interaction between injectors and producers in cluster I

Although the wells' interconnections seem confusing and random at first glance, their explanation is demonstrated via Figure 31. The latter provides an overview of the correlations between the wells by showing the pump intake pressure response of the producing wells in relation to events observed on the three surrounding injectors. In order to achieve an appropriate setting for the wells' pressure to be compared, a normalization of the data was carried out.

The normalization is focused on the pressure difference from one day to the subsequent one with its basis predefined at 100 bars.

As it is easily recognizable by observing the lower plot of Figure 31, the four producers are interrelated and share a common influence by certain events taking place in their surroundings.

With the intention of achieving a proper illustration of the injection water's amount per well, the injection rate of BO 206 is presented separately on the diagram's secondary y-axis.
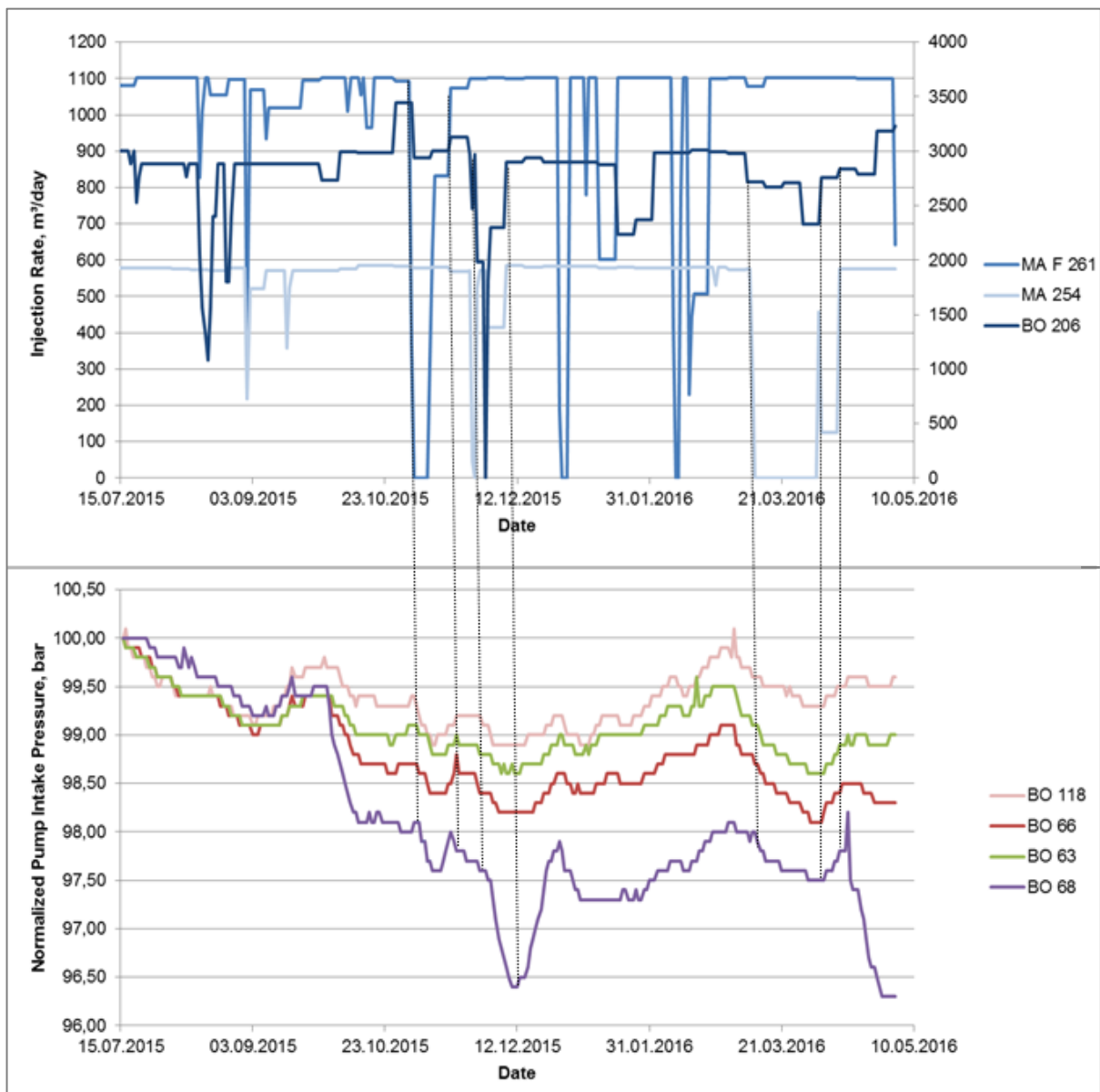
Figure 31: Connection from injectors to producers in cluster I with BO 206 on a secondary y-axis

Although a clear pattern between the four producer wells is observable, an allocation to one distinct influencing injector is not possible. It was therefore decided to select clearly recognizable connections between injectors and producers, illustrated by dotted lines, for demonstrating a relationship.

Principally, significant events from all three injectors are noticeable at the producer's pressure sensor. The first one happened as a combination of the injectors MA F 261 and BO 206 in November 2015. An injection break-down at BO 206 was responsible for the pressure valley visible in December 2015. At the end of the examined data range, a pressure decrease, followed by an increase, is observable as a consequence of a combined injection drop at the injector wells BO 206 and MA 254.

As already mentioned, the first and second clusters are considered to share a common behaviour. This is the reason why the second configuration is discussed immediately after the first one.

Basically, the second cluster consists of six producers and three injectors, whose configuration is shown in Figure 32.
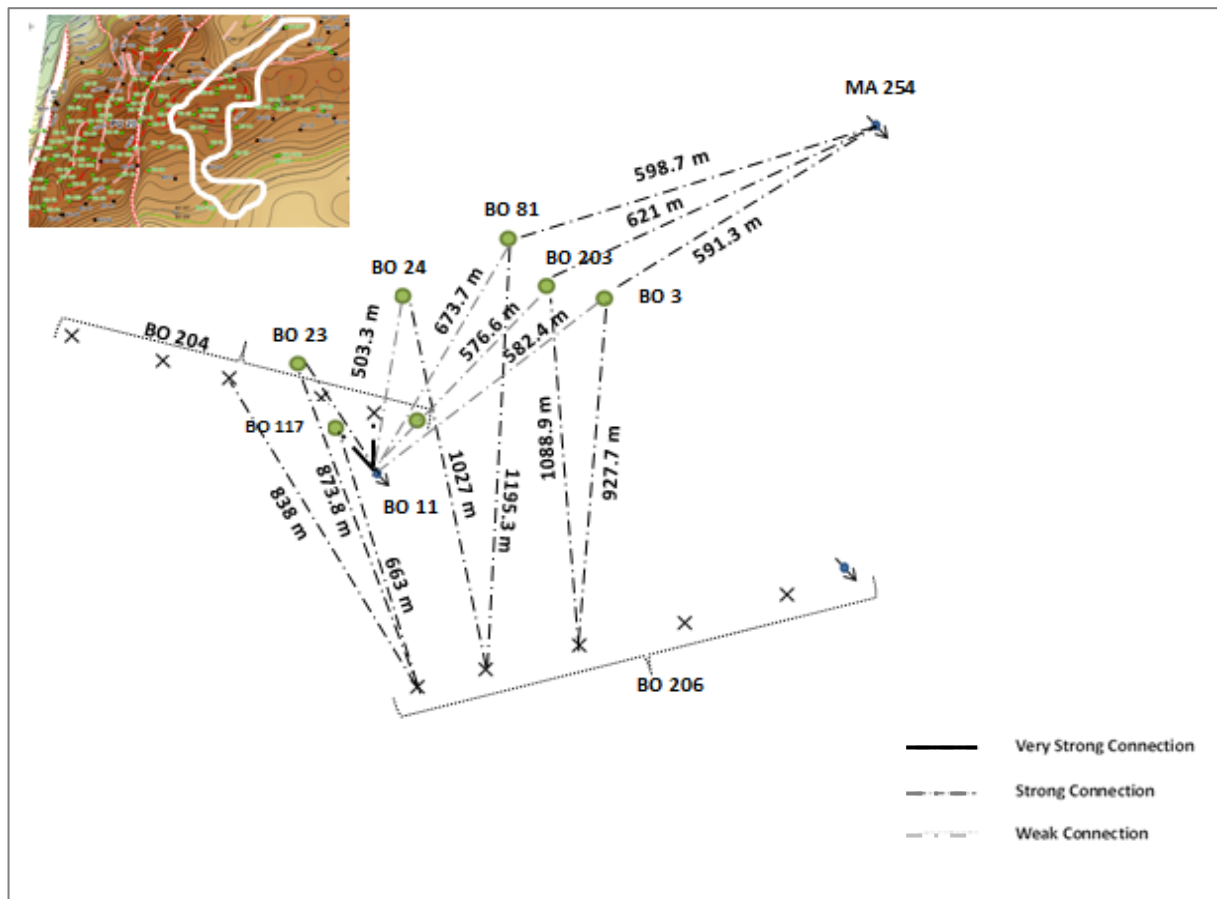
Figure 32: Interaction between injectors and producers in cluster II

The only two lines that are provided with a very strong connection can be found at injection well BO 11. They are connecting the former mentioned well with the adjacent production wells BO 117 and BO 204. For reasons of clarity, the distances in this part of the sketched map are not listed. The distance between BO 11 and BO 117 is considered to be around 154 meters, whereas producer BO 23 and injector BO 11 are about 336 meters away from each other. The two horizontal wells are indicated with black crosses, representing their open route. At their end, depending on their operating nature, a producer sign or an injector marking is pictured.

Like already carried out for the wells of cluster one, the producers' pump intake pressure responses were compared with injection break-downs of injectors in their surroundings.

For reasons of clarity, the analysis plots were divided into two charts, where Figure 33 shows two producers that experienced a production shut-down and Figure 34 illustrates consistently operated production wells.
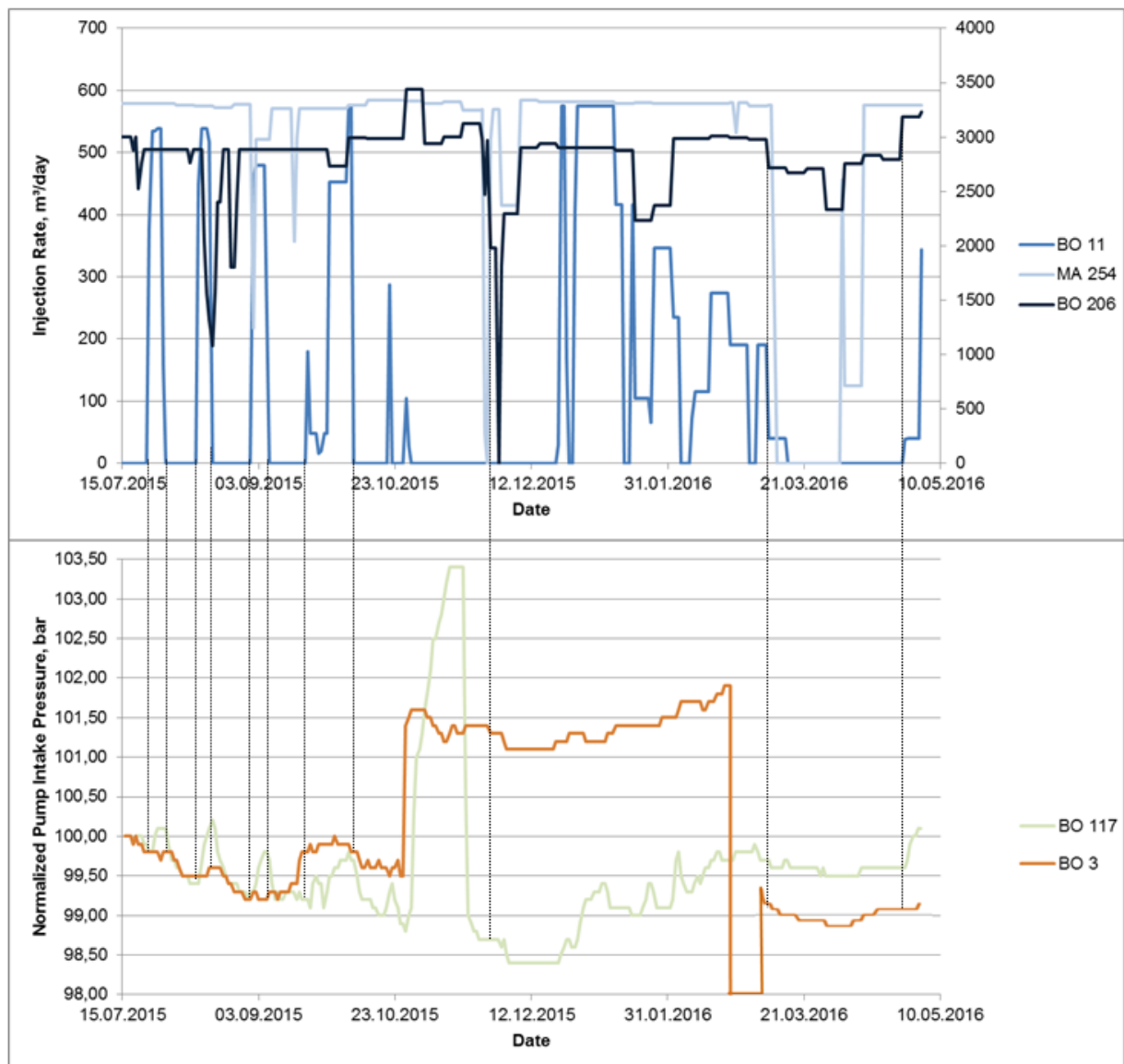
Figure 33: Connection from injectors to two producers with shut-down behavior in cluster I with BO 206 on a secondary y-axis

As it can be observed in the sketch above, a significant pressure build-up is recognizable at both producing wells, which leads to a uselessness of the measured pressure data in this time period due to a temporary well shut-off.

In principle, BO 117 is very much prone to be influenced by injection well BO 11, whereas producer BO 3 is more likely to be assigned to the wells of the first cluster.
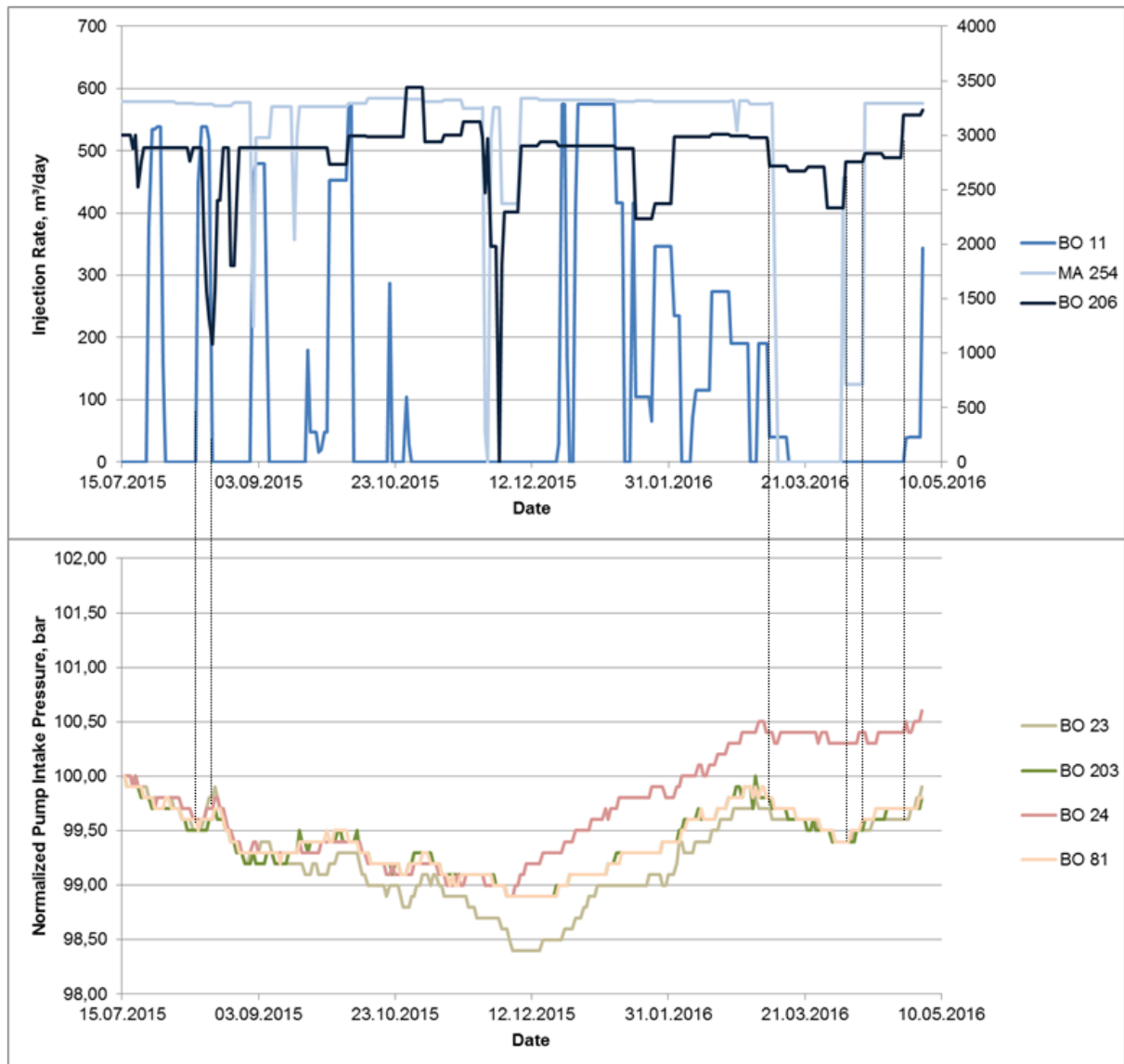
Figure 34: Connection from injectors to producers in cluster II with BO 206 on a secondary y-axis

By basing the analysis exclusively on obtained pressure data might allow a conclusion that those illustrated wells receive support from BO 11. However, having a glance on the injection rate of BO 11, a maximum value of around 600 cubic meter per day is achieved. Due to the fact that Figure 33 shows a direct and almost immediate response of producer BO 117 to events happening at BO 11, it is not far to seek that the water, injected at BO 11, travels to BO 117 and the horizontal well BO 204 straightaway. Those two wells are sharing the injection volume of BO 11.

A further argument for this statement is represented by a shut-in of the horizontal production well BO 204 in July 2016, which is illustrated in Figure 35. As indicated in green colour, an abnormal high pressure increase is observable at BO 204 due to the already mentioned shut-in. All wells from the second sector, except of the third cluster wells that are explained in chapter 4.2.2.2, had responded to the deactivated horizontal well by a pressure increase.

Subsequently, this allows the statement that other wells receive the pressure support that is normally predestined to be consumed by BO 204.
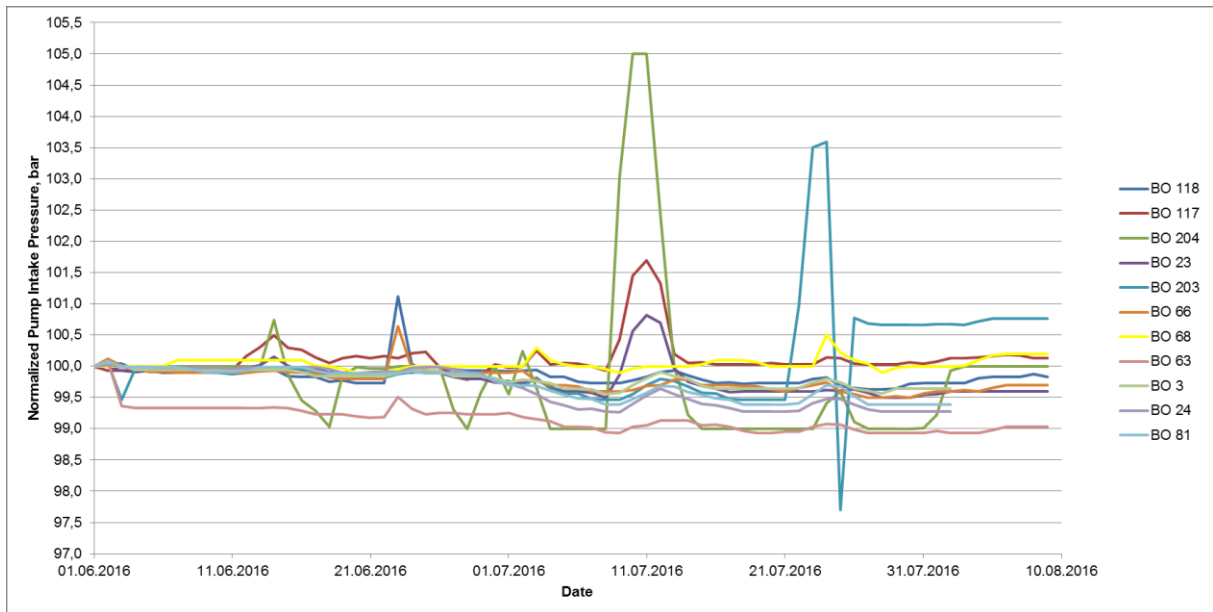
Figure 35: Reactions on the shut-in of horizontal producer BO 204

In order to obtain a clearer view on the reaction in the immediate vicinity of BO 204, only adjacent producers and their pressure responses are illustrated in Figure 36. It appears that the most dominant signal is noticeable at producers BO 117 and BO 23. Nevertheless, small indications are also observable at the producers of cluster one. As a consequence, all wells that are producing in sector two and are not allocated to the third cluster are considered to be assigned in a single cluster that sums up cluster one and cluster two.
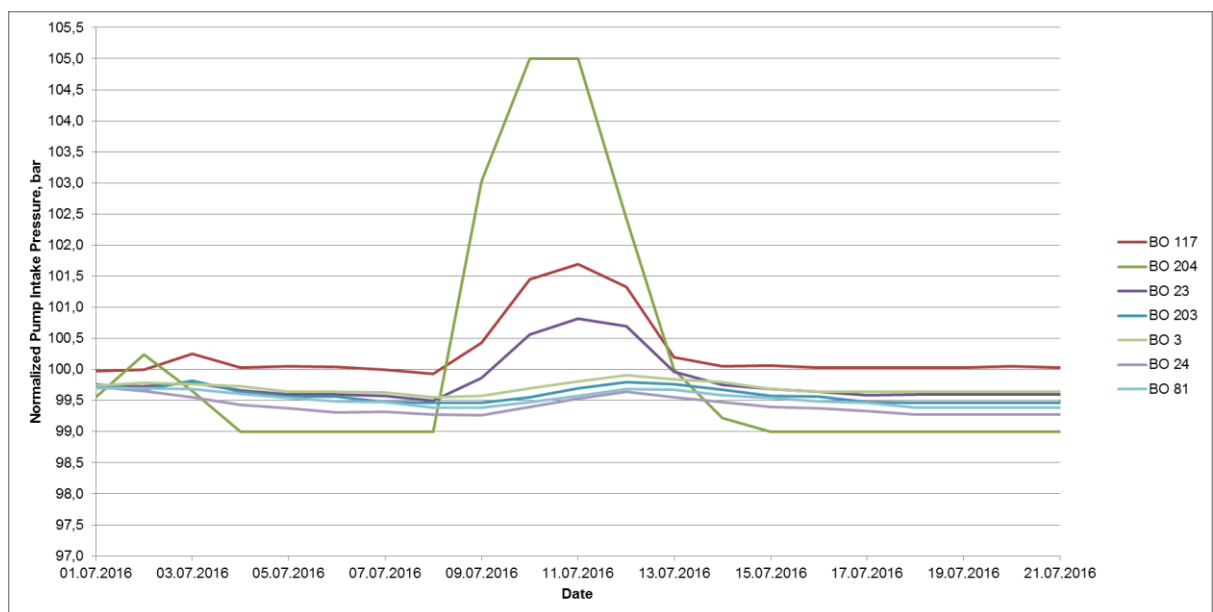
Figure 36: Reaction on the shut-in of BO 204 in a zoomed-in configuration for adjacent wells

4.2.2.2 Cluster III

The third cluster consists of two injectors and three producers. As observable in Figure 37, producers BO 85 and BO 37 mainly get supported by the water injected at the northern situated well BO 36. In relation to these two producers, BO 35 is more or less equally supported by BO 36 and MA F 253. Furthermore, impacts of the latter one are noticeable to a minor extend at the other two producers of the third cluster.
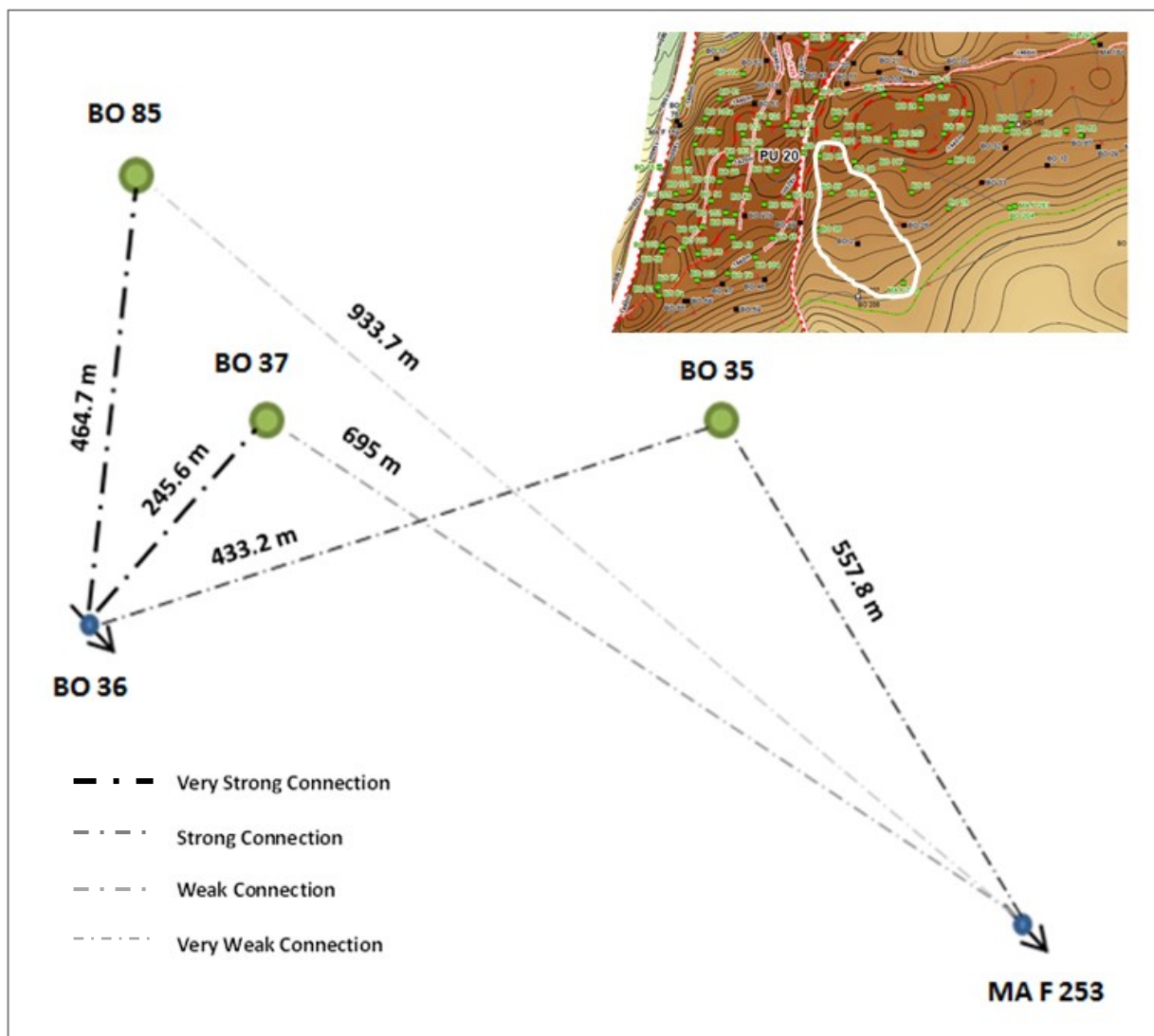
Figure 37: Connection from injectors to producers in cluster III

The above illustrated connections are proven by the pressure responses gathered at the ESP pump intake shown in Figure 38. In August 2015 it is obvious that the injection loss of BO 36 is observable at the location of all three producing wells. The second interaction is also clearly shown for BO 37 and BO 85. Responses, justified in the injection loss of MA F 253, are the reason for an unclear signal on BO 35. The influence of MA F 253 on the other two producers can also be assumed when considering the fact that the pressure builds up to a much higher extend in the second break-down, because MA F 253 got increased in injection volume again.
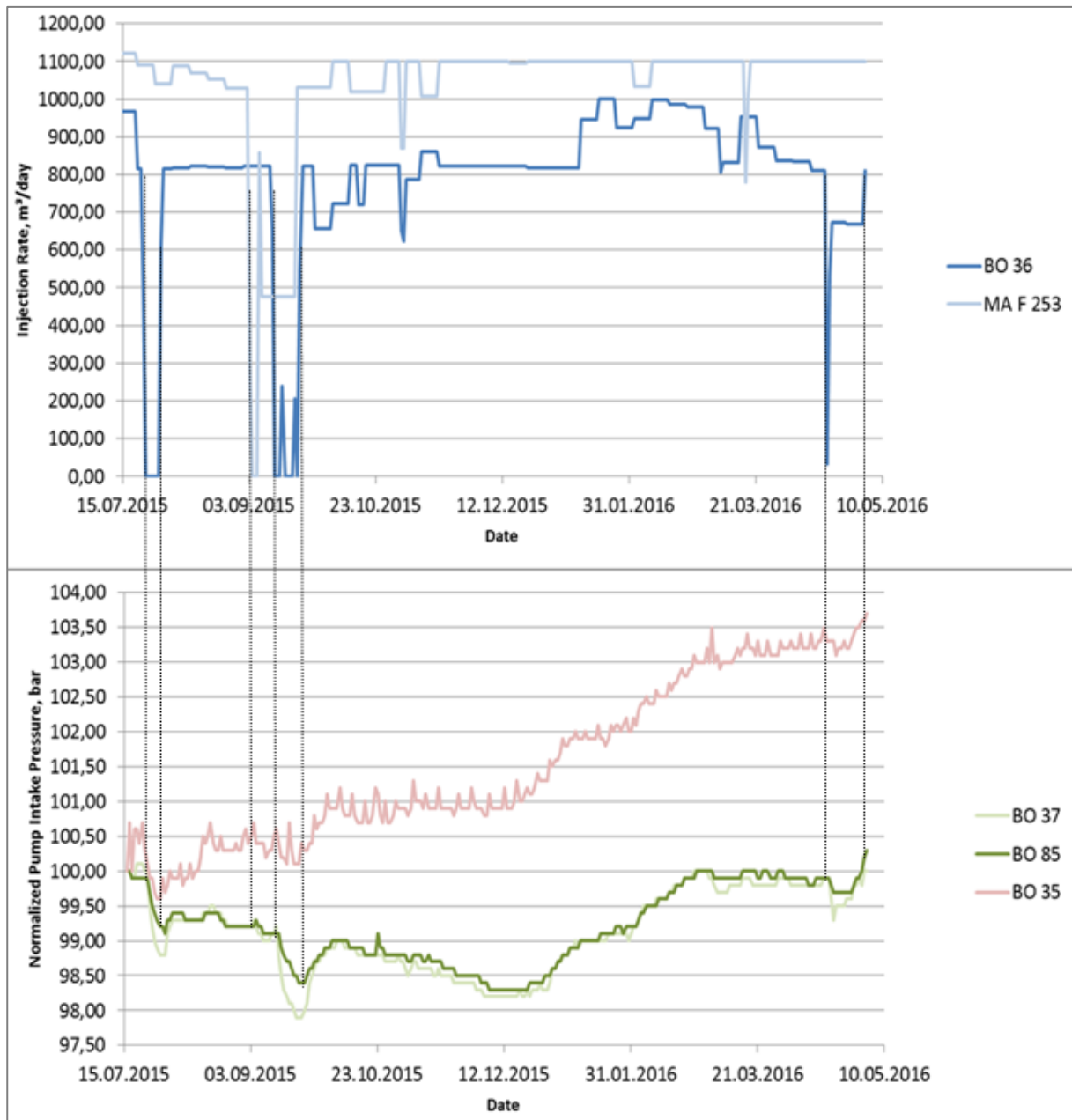
Figure 38: Pressure response to turned off injectors in cluster III

In this regard, also the last injection breakdown explicitly indicates a relationship of the wells summed up to cluster 3.

4.2.2.3 Cluster IV

As distinguished from former explained clusters, the fourth accumulation of similarly behaving wells is located in the first sector.

For the reason of better understanding, the explanation plot for the conclusion to sum up the producing wells to one single cluster was separated into two time dependent charts.

Figure 39 illustrates the influencing nature of injectors, located on the most northern part of sector one, on certain producers. The production well BO 96 is increasing in pump intake pressure in an abnormal way, which can be explained by a production shut-down of this well during the observed time space. It is demonstrated that the five selected producers share a great similarity in their pump intake pressure behaviour. Though it was impossible to allocate a certain producer to one single injector, it can be clearly seen that the influence is characterized by an interaction between different injectors.
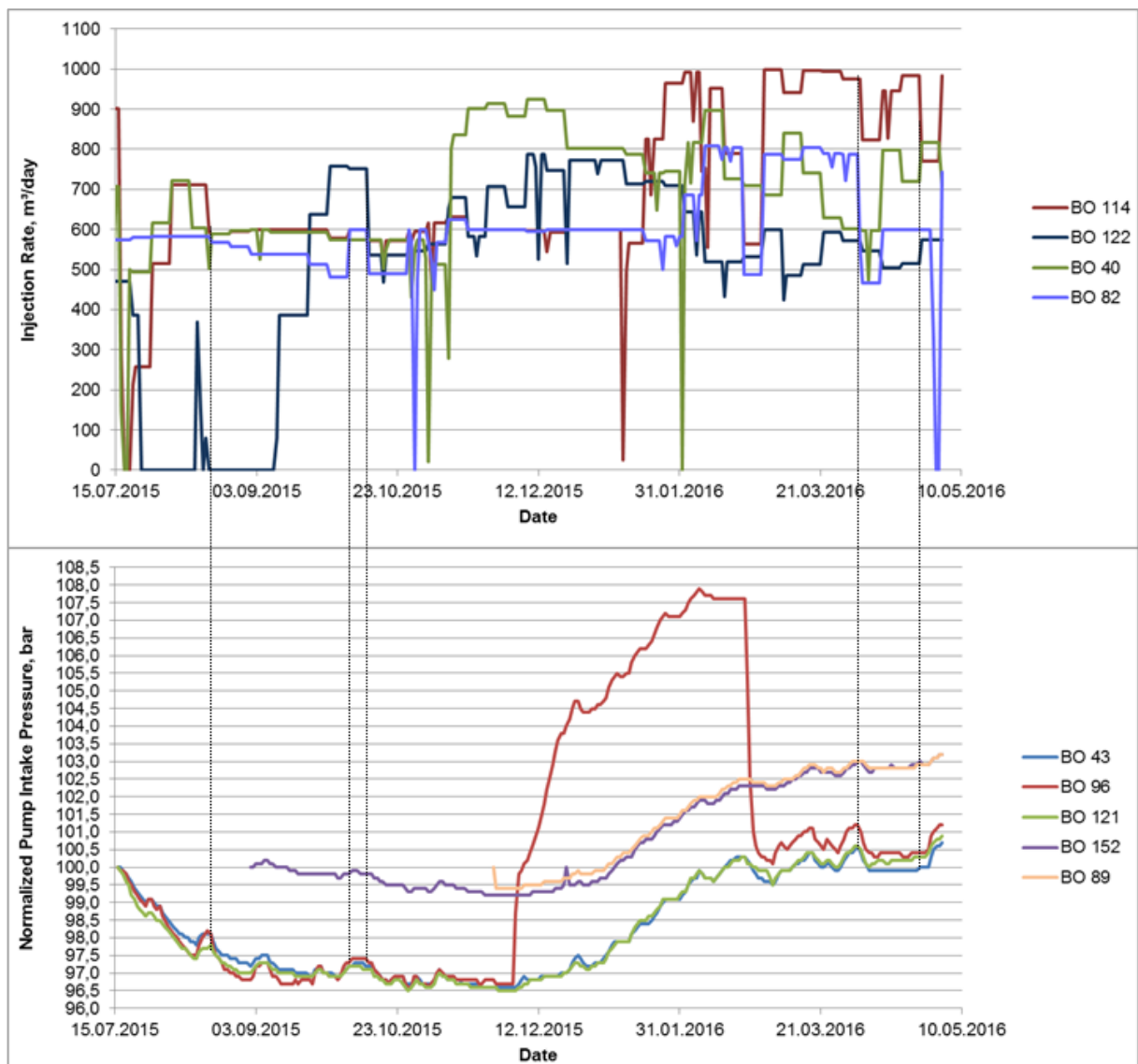
Figure 39: Influence of the most northern situated injectors and producers of cluster IV

The most influencing injection well is represented by BO 42, which is the only one that is placed in the middle of all observed producers. Due to the uselessness of the pressure data recorded at BO 96 the graph on Figure 40 cuts off the improper values, so as to achieve a closer view on the suitable information.
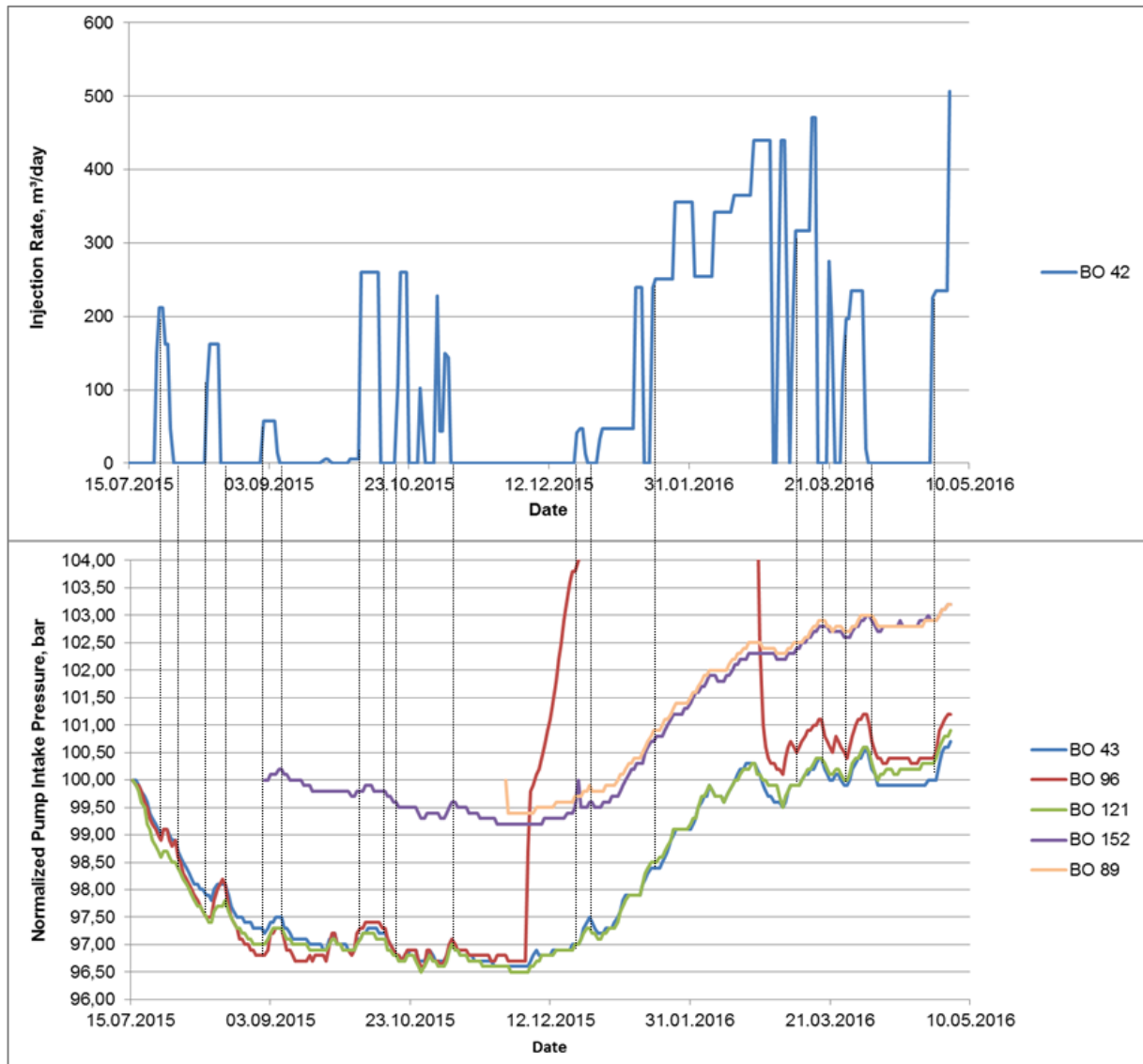
Figure 40: Influence of the centralized injector BO 42 on surrounding producers

In order to summarize the conclusion made for the fourth cluster, a map was created to show the connections together with their intensity in Figure 41. The injection wells, situated in the northern part of sector one, are influencing all wells beneath them, which makes it difficult to determine definite relations.

It is observable that the last pressure drawdown at the producing wells is of different strength. Based on the connections illustrated in Figure 39 and Figure 40, it is assumed that BO 96 and BO 43 are supported by the northern injectors BO 40 and BO 82 to a greater extent than the other three considered producers are.

Two very strong connections can be seen in Figure 41 between BO 42 and the producers BO 96 and BO 43.

Although BO 121 is located much less in distance from this specific injector, the amplitude of reaction is smaller than at the other two producers, which are assigned with a very strong connection. Different reasons might lead to this outcome. On the one hand, BO 42 is receiving support from water injectors in the north, which might boost reactions at the producers' pump intake. On the other hand, a fault is located between BO 121 and BO 42, where the water might be forced to flow around and thus a much lower impact is recorded.

Figure 41: Relations between injectors and producers in cluster IV

While most of the wells, based on the received pressure data, can be allocated to clusters, a small group of wells could not. In Appendix C.1 those unassignable pressure responses are discussed.

4.3 Pressure response time

In order to achieve an assessment for the time a pressure wave needs to travel from an injector to a producing well, three different procedures were considered. A detailed description of the applied methods is provided in the subsequent sections.
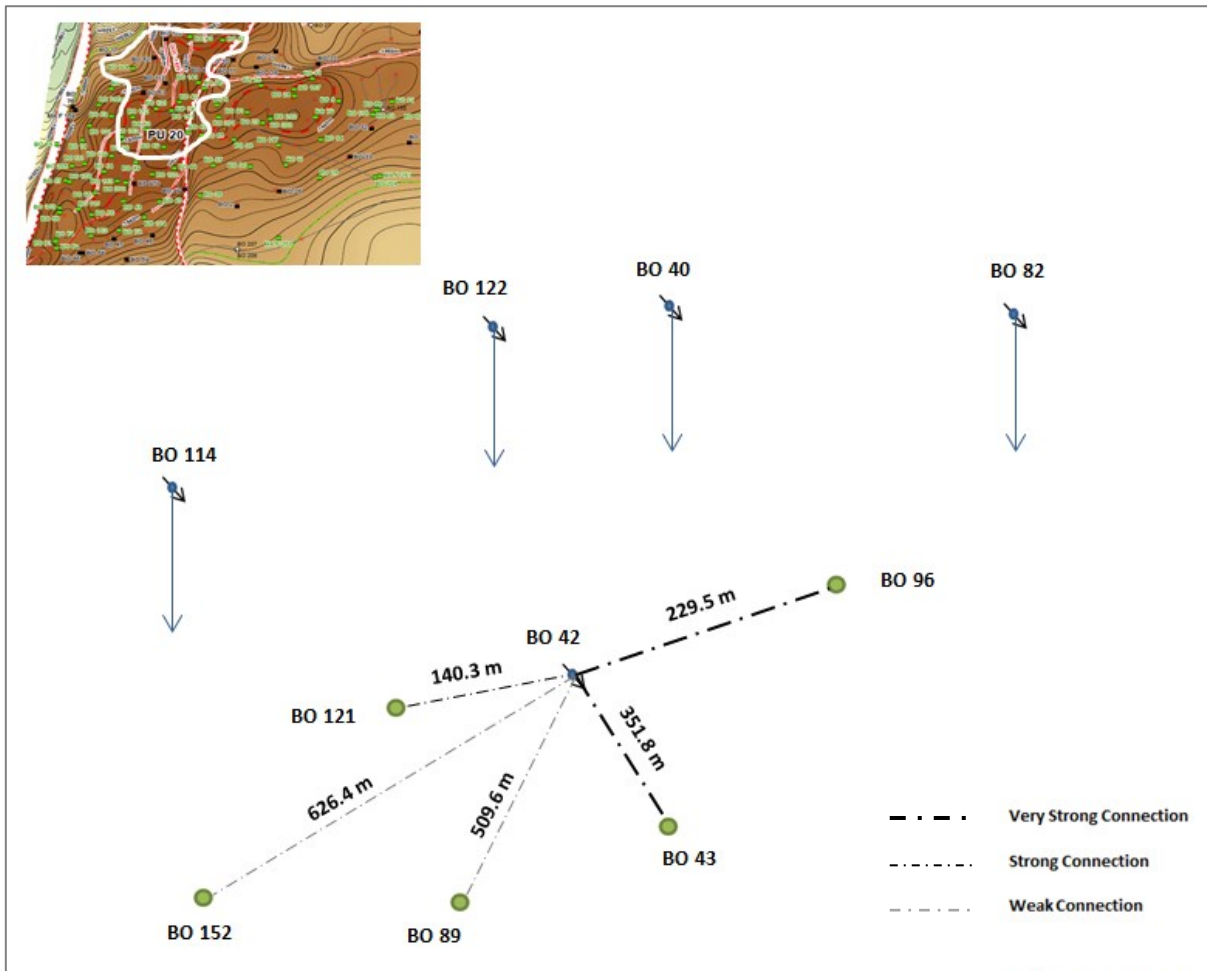
4.3.1 Analytical approach

With the purpose of an analytical determination of the pressure wave's duration, two basic formulas need to be taken into account. Equation 4.3.1 describes the hydraulic diffusivity, whereas equation 4.3.2 uses the result of the former one to eventuate in a time for the pressure wave to get transported through a distinct reservoir area, which is characterized by certain properties like permeability and porosity [6].

$$\kappa = \frac{k}{\mu \times c_t \times \phi}$$ **4.3.1**

κ diffusivity [m²/s]
k   permeability [m²]
µ   viscosity [Pas]
c_t total compressibility [Pa^{-1}]
ϕ porosity [1]

$$t = \frac{1}{4} \times \frac{r_d^2}{\kappa}$$ **4.3.2**

t   stabilization time [s]
r_d drainage radius [m]

The values used to calculate the stabilization time are discussed, together with their derivation, in the Appendix D.1. In consideration of this configuration, the pressure wave's duration was calculated, where bar charts, summarized by injection well, are illustrated in Appendix D.2. To sum up the results, a variation between approximately two hours for distances up to 150 meters and 113 hours for lengths approaching a quantity of approximately one kilometre, are observable, depending more or less exclusively on the distance the pressure wave needs to overcome.

It should be noted that those quantities are derived by using an oil viscosity of 5.19 cp. This value was derived from laboratory measurements and thus represents an accurate data for the oil's viscosity at a pressure of 113 bars. Two considerations should be taken into account concerning the viscosity information. On the one hand, oil viscosity varies strongly with applied pressure and on the other hand, the reservoir fluid consists mainly out of water. As compared with the flow behaviour of oil, water moves much easier, attributable to its lower viscosity value.

In order to illustrate the influence of viscosity on the pressure traveling time a sensitivity analysis, using a spider chart, was executed. As not only a change in viscosity can alter the result of equations 4.3.1 and 4.3.2, other variables taking active part in the mentioned equations, were also checked for their manipulation characteristics.

As observable in Figure 42 the distance between two wells is the most critical factor in the calculation of the pressure wave's traveling time followed by the formation's permeability. Those two parameters are acting vice versa, with the duration increasing with increasing distance and decreasing with increasing permeability value. The least influence on the calculation is recognizable, if a change in oil saturation is applied.
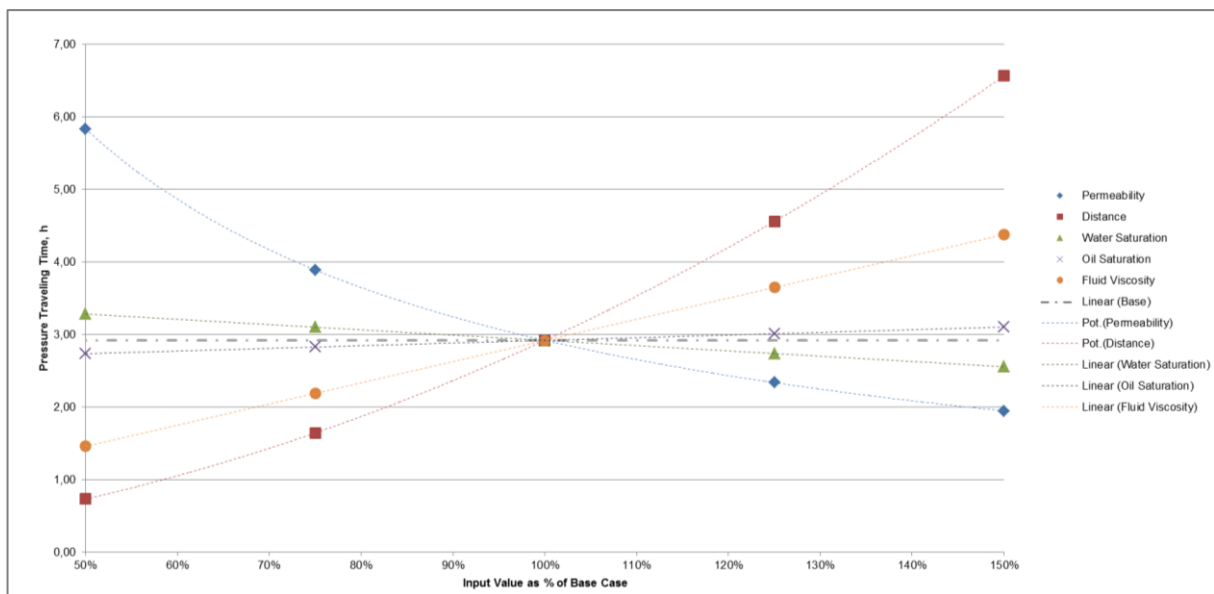
Figure 42: Sensitivity analysis based on a spider diagram accomplished by using five variables

Supplementary to the spider diagram, illustrated in Figure 42, a different method of representation was chosen. Demonstrated in Figure 43, the used variables are plotted on a radar chart, which makes an interpretation more straightforward.

As observable, the distance between two wells is characterized by the most distinctive spike, which indicates the most significant impact on the pressure wave's traveling time calculation. The blue area is shifted to the right sector of the diagram, concluding that the oil saturation barely contributes to the analysis' outcome. Basically, a radar chart graphically expresses the slopes of curves, which are plotted on the spider diagram.
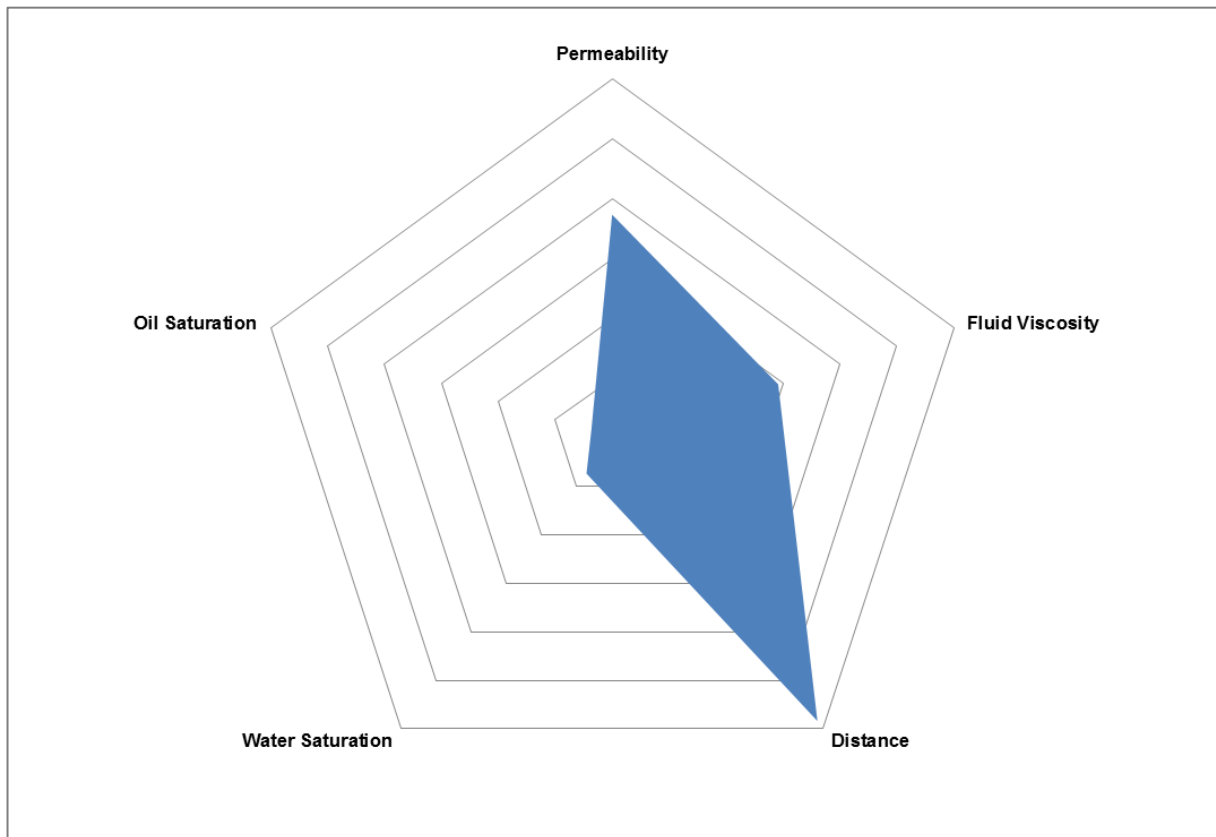
Figure 43: Sensitivity analysis based on a radar chart

4.3.2 Measured pressure approach

In section 4.2.2, the definition of clusters was described by using pump intake pressure data, gathered by the installed downhole sensor. A more detailed scope, which should have been conducted by investigations in the pressure data, is the duration between an injector shut-down and the pressure response, observable on the producer's side.

The most significant reason for the infeasibility of this approach is the fact that the pressure wave only needs a few hours for arriving at the producer well's sensor. Since the daytime, when an injector shut-in happened, is not easily comprehensible and the obtained pressure data is based on a daily average, the inaccuracy factor is substantial and cannot be neglected.

To sum up, it was not possible to figure out the pressure's traveling time based on the provided pressure data. Recommendations concerning further investigations are proposed in a later point of the thesis.

4.3.3 Well testing software approach

The software tool Pansystem, provided by the company Weatherford, was used in order to check the pressure distribution time for maintaining a reference value to the manually calculated one.

The investigation concentrates on the third cluster, which was already described in section 4.2.2.2. Injector BO 36 is performing as active well, while the three surrounding producers are considered to be observation points.

As distinguished from the approach, which was conducted in the previous chapter, a radial composite model had been used. The idea behind this assumption was that the injected fluid's viscosity differs from the viscosity of the fluid being inherent in the reservoir. Thus, a kind of permeability barrier would exist, like it is illustrated in Figure 44.
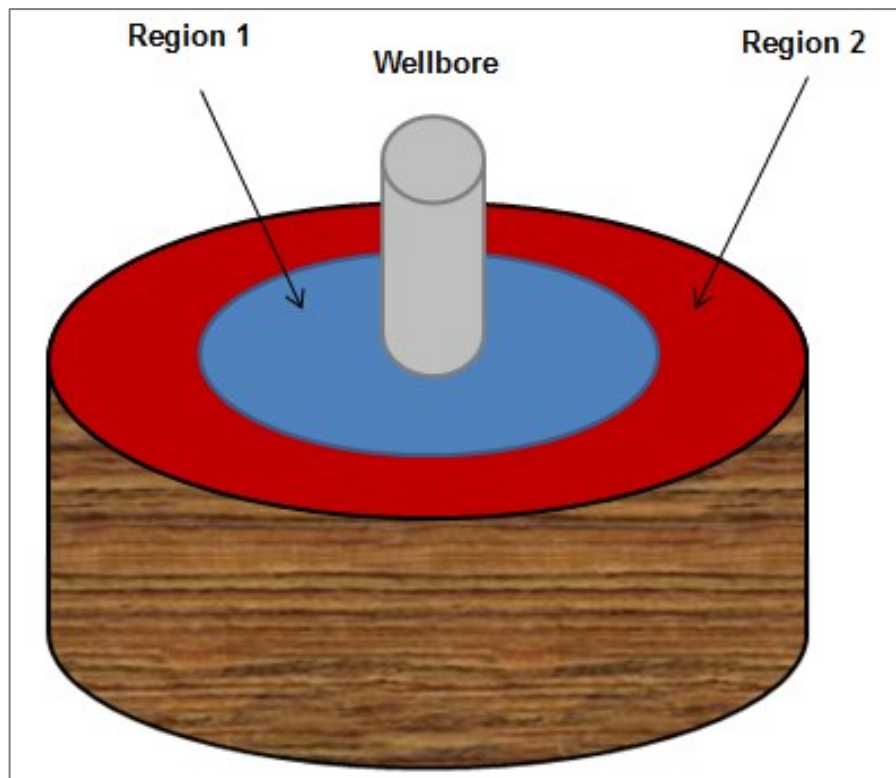
Figure 44: Radial composite model [29]

Three new parameters will have to be determined, if this model comes into use.
- Mobility ratio between the outer zone's mobility and the inner zone's mobility
- Storativity ratio
- Radial distance to discontinuity [29]

Due to the fact that the flooding activity has lasted for a long period of time, it was assumed that no such considerable barrier is in place. Rather than that, a more continuous change in properties is assumed, which led to assumed values for mobility ratio and storativity close to one. The radius to discontinuity was set to a distance, so that all observed wells are

encompassed. Unlike the strategy, performed in chapter 4.3.1, water viscosity was chosen instead of oil viscosity. This is due to the fact that different fluid saturations in combination with different viscosity values are present all the way from the injection well to the producer. As it is observable, no substantial difference in the outcome can be spotted, despite the fact that the viscosity value got changed.

The configuration for performing the illustrated interference test is based on an injection well that experienced a shut-in. Five different observation wells, located at various distances, are examined for their pressure response behavior.

As demonstrated in Figure 45, the active well's activity is parted into five sequences. The first 24 hours are characterized by a shut-down of injection, followed by 24 hours water injection. Subsequently, two days of shut-in and two days of injecting are simulated. As a last action, the active well experienced a shut-off. As soon as the active well starts injecting, the observation wells' pressures start to increase.
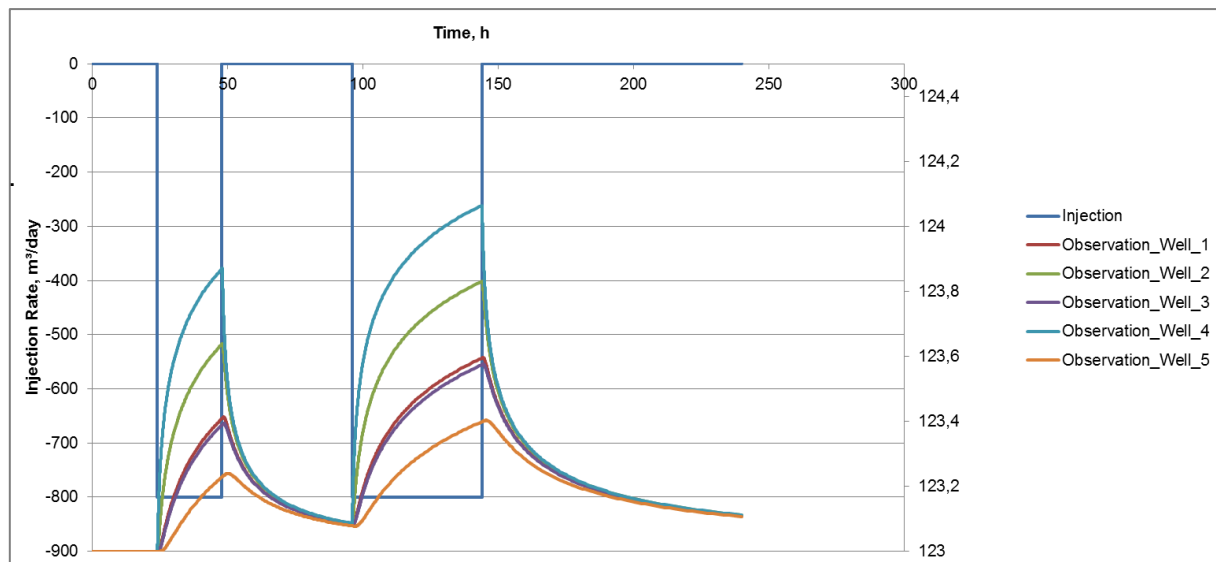
Figure 45: Overall illustration of all pressure build-up curves in combination with the applied injection scenarios

The only variation in the observation wells' setup is represented by the distance to the active well. Those distances are defined in Table 5. As it can be seen, the first three distances are represented by the distances of the three producer wells of cluster three to the injection well BO 36. The last two observation points are considered as dummy wells. Observation well 4 is located in the near vicinity of the active well, whereas the observation point 5 is described by a radius larger than that of all other wells in the analysis.

Table 5: Distances of observation wells to active well

Well identifier	Distance X, m	Distance Y, m	Response Time, h
Observation well 1, BO 35	223.34	370.81	22
Observation well 2, BO 37	222.67	103.69	7
Observation well 3, BO 85	454.16	25.09	28
Observation well 4	100	100	2.5
Observation well 5	500	500	> 2 days

In fact, two comparing scenarios have to be considered in the analysis. The first one deals with matching the radial composite model results with those outcomes gathered by applying the radial homogeneous model. Secondly, the pressure response times have to be linked with those of the analytical approach.

Considering the first injection period, which lasts 24 hours, three wells are able to reach the threshold value of 0.4 bars. One is very close to that marking line, illustrated with a black dotted line, and reaches it finally, when an injection period of two days is guaranteed. Taking a closer look at the first 60 hours of the interference test, as represented in Figure 46, the already discussed well activities are illustrated.
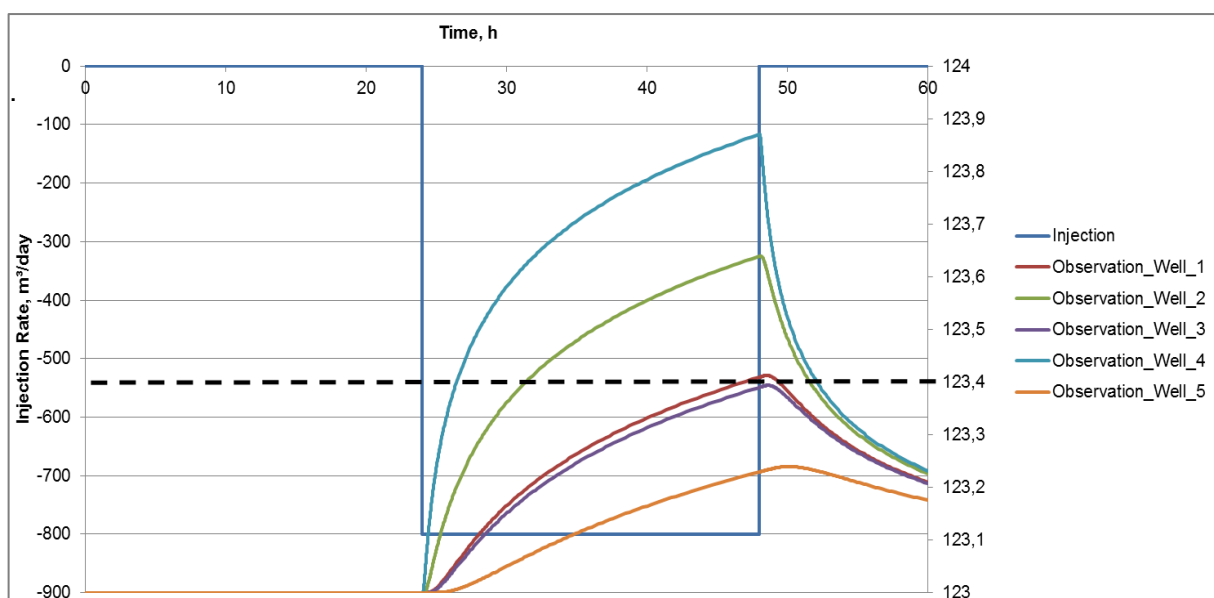
Figure 46: Zoomed view on the first 60 hours of interference testing

Furthermore, the pressure response time of every single observation well can be told, which was already listed in Table 5.

Although the assumption of water viscosity, instead of oil viscosity, should lead to lower values for the pressure stabilization time, the pressure wave needs apparently longer. However, it should be taken into consideration that a threshold value of 0.4 bars for the pressure difference was set manually, because of the downhole sensor's measuring accuracy level. The actual wave can arrive faster and, as a second explanation, the analytic solution does not reflect the magnitude of the pressure reaction.

Nevertheless, it can be concluded that it takes approximately less than two days for the reaction to show up at an observation well, when cluster three is examined.

Due to the fact that the variable "radial distance to discontinuity" was set to a value that encloses every well, also a radial homogenous model instead of a radial composite model can be applied. It is justified in the assumption that neither permeability, nor a viscosity barrier is present in the observed region.

4.4 Transport time of water

With the aim to describe the flow of water through the reservoir, the equation of Buckley and Leverett (1942) was chosen. Due to the fact that the displacement of oil in the area of interest is described by an immiscible, two-phase flow, this method has been considered. Two cases were reflected in order to achieve an appropriate representation of the true oil displacement process. Figure 47 illustrates the well pattern, the Buckley-Leverett theory was applied on.

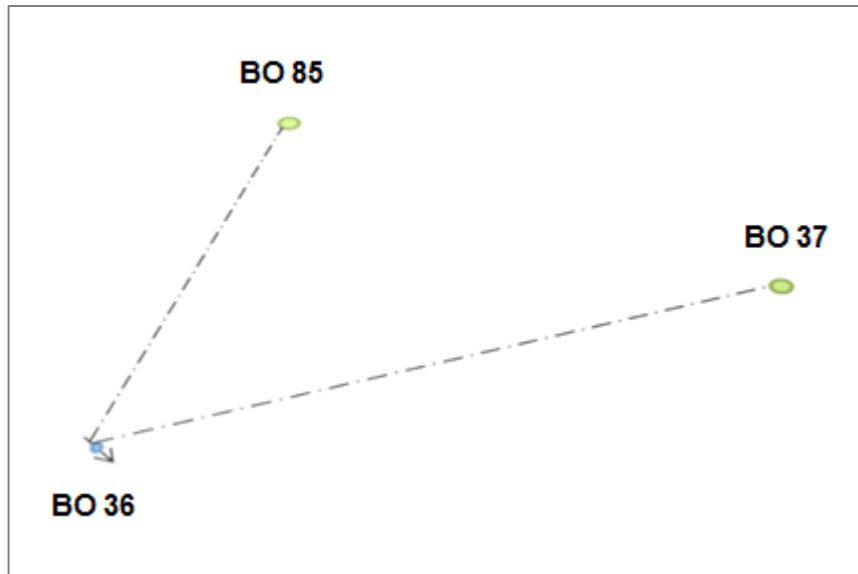**Figure 47: Well constellation for an application of Buckley-Leverett**

The very first outcome, which was concluded by looking at the relative permeability curves, was that the rock is water-wet. An illustration of the relative permeability curves of oil and water, which was gathered by special core analysis, is shown in Figure 48.
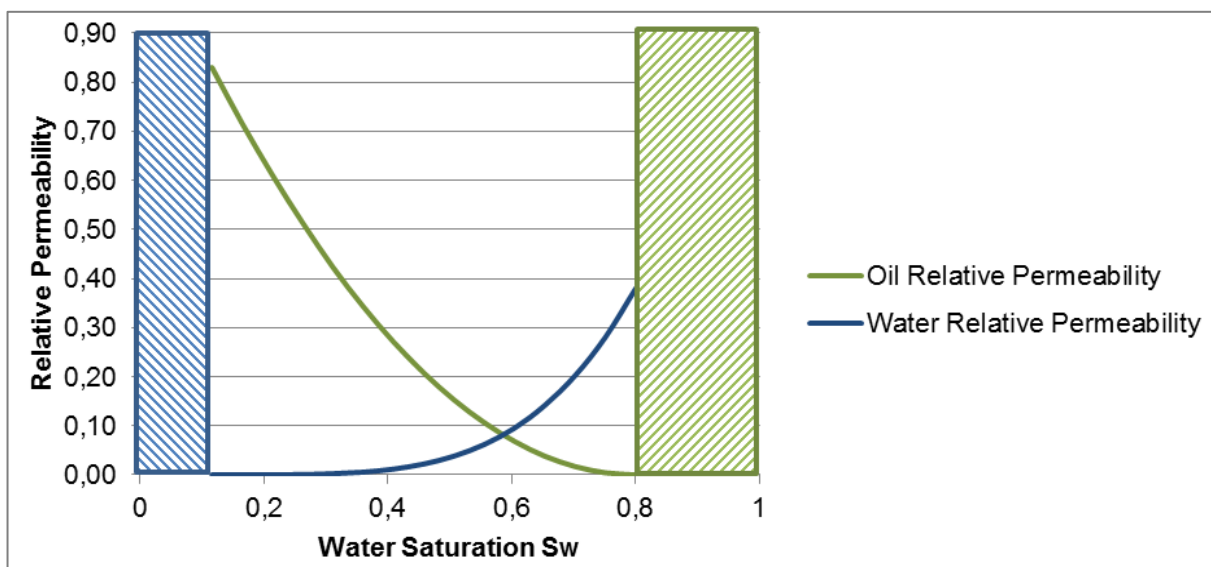
Figure 48: Relative permeability curves of the flowing system [45]

The blue shaded area represents the water saturation range at which water behaves immobile, whereas the green shaded area indicates the water saturations at which oil becomes immobile.

Appendix E.1 describes the strategy how the fractional flow curve of water, represented in Figure 49, was obtained.
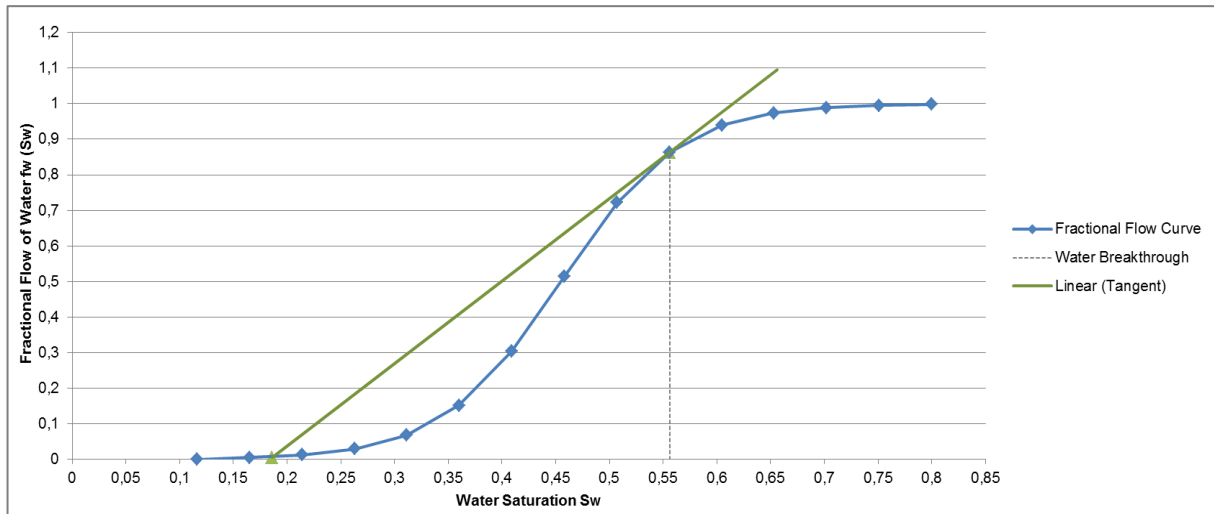
Figure 49: Fractional flow curve of water [46]

As observable in Figure 49 a tangent was drawn from the point of initial water saturation to the fractional flow curve. The crossing point of these two curves indicates the injection water's breakthrough. By using the formulas 4.4.1 and 4.4.2, a water breakthrough time of approximately 47 days in the assumed rectangular prism between BO 36, BO 37 and BO 85 is calculated [6].

$$PV = \frac{\phi \times A \times L}{5.615}$$ **4.4.1**

PV   pore volume [bbl]
A   cross sectional area [ft²]
L   distance from injector to producer [ft]

$$t_{BT} = \left[\frac{(PV)}{i_w} \right] \times \left(\frac{1}{\frac{df_w}{dS_w}} \right)_{S_{wf}}$$ **4.4.2**

t_{BT} time to breakthrough [days]
i_w injection rate [bbl/day]
f_w water fractional flow [1]
S_w water saturation [1]

However, this result assumes that the water moves exactly in the direct pathway between injection well and the producer wells. A duration of 47 days for injection water to

breakthrough at a production well BO 85 would lead to a high circulation rate. Considering the time period the injection already lasts, the water must have been circulated 22 times through the same pathway. The latter statement would cause a higher calculated water cut, which was observable at the producing wells than the prevalent water cut. So, the water does not take a direct way to the northern situated producers, but rather spreads across the area in a cone shape. This statement is also justified in the fact that the strong aquifer at the southern front manages the fluid to flow to the north direction, because of a pressure difference in that direction.
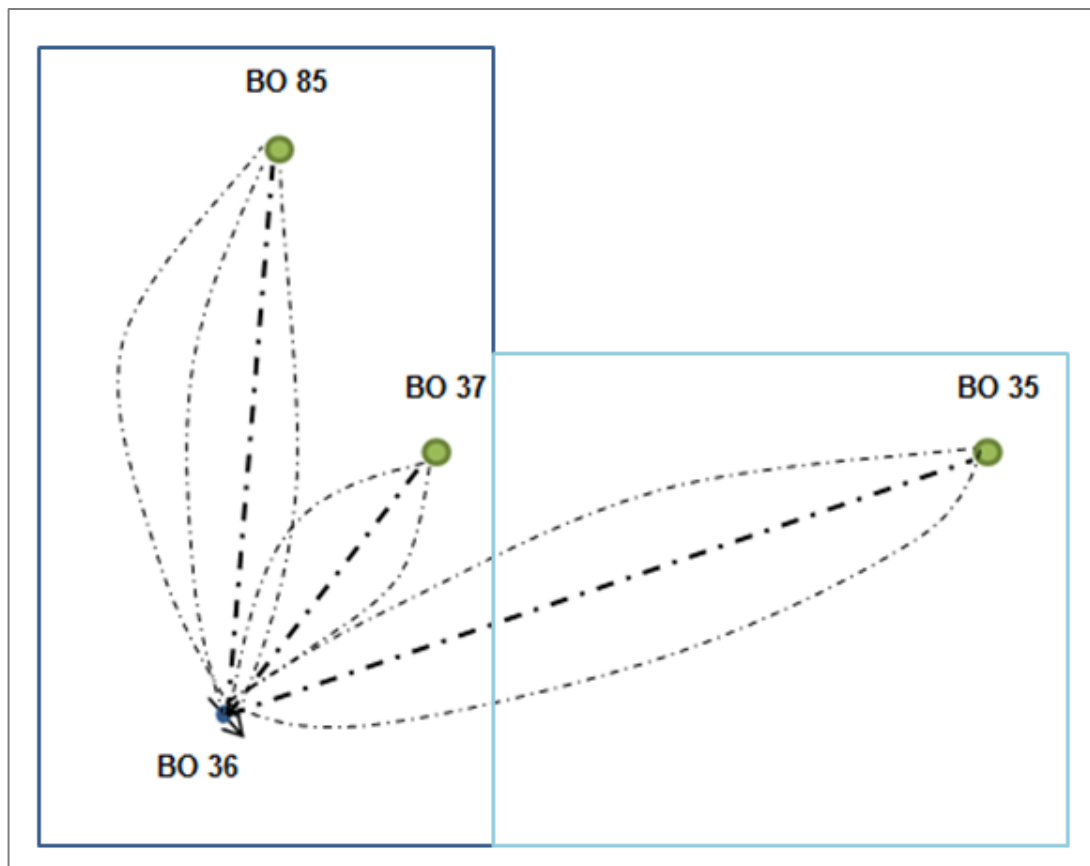
Figure 50: Possible streamline configuration between injector and producer wells

To account for the lower observed water cuts on the production wells, a larger flooding area was considered, which is illustrated in Figure 50 . Due to the fact that the pressure responses at production wells BO 37 and BO 85 are much stronger than at BO 35, two thirds of BO 36's injection water was considered to be consumed by wells in the northern direction. Only one third was assumed to be produced by wells located in the NE to NEE direction.

It is quite hard to say which pathway is more popular for the streamlines to pass through. Also, the magnitude of the injected water in a certain direction cannot be determined definitely. A reason therefore is the high prevalent conductivity in the reservoir due to the reservoir's high permeability and homogeneity. Additionally to the analytical calculation using the Buckley-Leverett approach, a streamline surveillance model has been developed in order to generate a picture of the flowing paths downhole. Chapter 4.6 describes the streamline analysis method by using the software StudioSL.

4.5 Water coning calculation

With the aim of showing practical aspects of the concept discussed in chapter 2.5, the probability of inducing a water cone in one of the field's production wells is illustrated subsequently.

Due to increased production rates applied in the AOI and the high prevalent reservoir permeability and homogeneity, it is very likely for a water cone to develop. Unfortunately, the average water cut of most of the wells was already above 90%, which makes the majority of the wells impractical for water coning calculations.

The explanation for the last statement is based on the fractional flow curve, which was already discussed in the previous chapter and shown in Figure 49. Every well that is characterized by a water fractional flow that leads to a water saturation located beyond the breakthrough line is not suitable for investigations in coning activities. Principally, the water front, triggered by flooding actions, has already reached the production wells so that a water cone cannot be identified explicitly.

As observable in Figure 51 only one well, represented by BO 89, met the requirements, showing a water saturation of less than 56%, which was found out to be the water saturation at the breakthrough point.
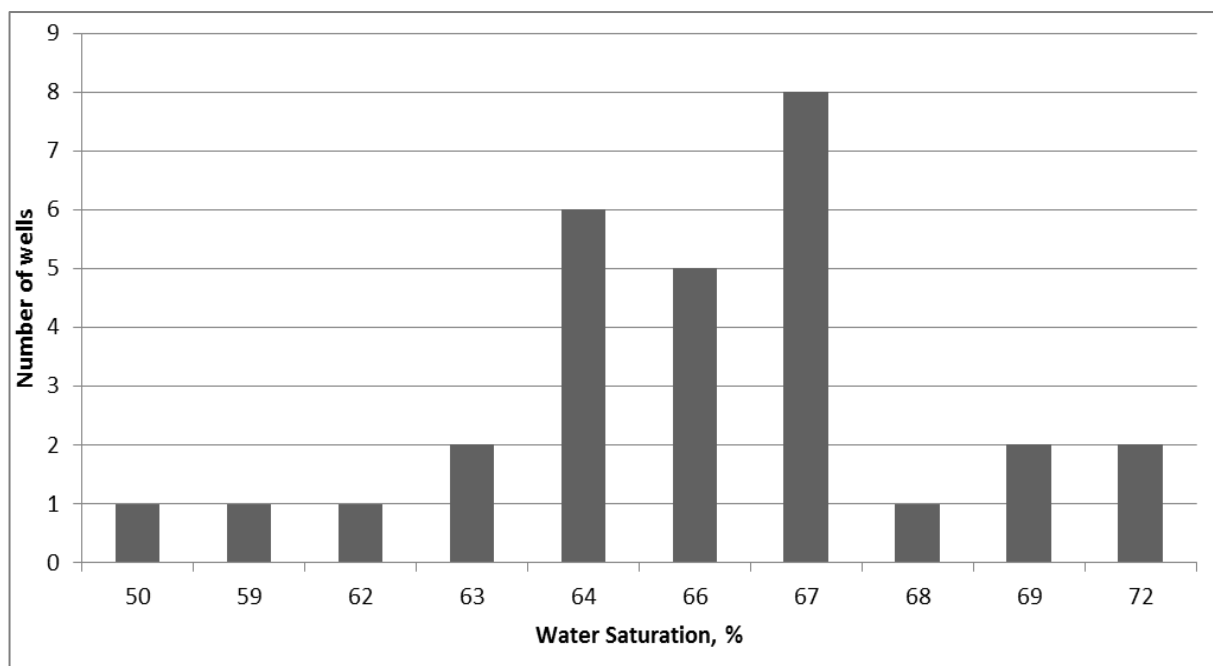
Figure 51: Number of production wells possessing certain water saturations

In order to find out the critical oil rate for a water cone to grow at well BO 89, different correlations got compared. An exclusion principle approach was applied between those different correlations to eventuate in the most probable rate for oil.

Every correlation not considering the ratio between horizontal and vertical permeability was principally excluded from the analysis. The latter is one of the most essential parameter in

determining the limiting oil rate. If the permeability in vertical direction in comparison to that in the horizontal pathway results in a high value, the likelihood for a cone build-up increases dramatically [6].

Consequently, only one strategy is discussed in order to obtain a result for the critical oil rate. All used quantities and their mode of calculation are described in Appendix F.1.

The way to define the critical oil rate is based on Chaperson's anisotropic approach, shown in equation 4.5.1. Anisotropic means that the values for horizontal and vertical permeability are not the same.

$$Q_{OC} = 0.0783 \times 10^{-4} \times \frac{k_h \times (h - h_P)^2}{\mu_O \times B_O} [\Delta\rho] \times q_c^* \qquad \textbf{4.5.1}$$

Q_{OC} critical oil rate [STB/day]
k_h horizontal permeability [mD]
Δ_ρ density difference of water and oil [lb/ft³]
h thickness of oil column [ft]
h_p perforated interval [ft]
μ_o oil viscosity [cp]
B_o oil formation volume factor [bbl/STB]

Formula 4.5.1 includes the coefficient q_c^*, illustrated in equation 4.5.2, which was investigated by Joshi (1991) via the introduced parameter α", calculated with equation 4.5.3.

$$q_c^* = 0.7311 + (1.943 \div \alpha'') \qquad \textbf{4.5.2}$$

$$\alpha'' = (r_e \div h) \times \sqrt{k_v} \div k_h \qquad \textbf{4.5.3}$$

r_e drainage radius [ft]
k_V vertical permeability [mD]
h thickness of oil column [ft]
h_p perforated interval [ft]
μ_o oil viscosity [cp]
B_o oil formation volume factor [bbl/STB]

As a result of applying the equations described above, a critical oil rate of around four to five tons per day was calculated. It must be said that the calculation is sensitive to the already mentioned ratio between vertical and horizontal permeability. Due to the fact that there could always be a local discontinuity, this ratio can only be assumed in the range between zero and one.

Anyway, the most important outcome is related to the actual daily production of the well BO 89, which is quantified by a rate of about 30 to 40 tons per day. Every correlation that was conducted, regardless of taking the permeability ratio into account or not, led to a result,

which was lower than the actual production. So, in fact, from the calculated point of view, water coning is definitely an issue, independent of the applied calculation strategy.

However, having a look on the water cut history of the well BO 89, illustrated in Figure 52, no water coning can be observed. This statement is justified in the fact that the water cut is increasing in a moderate manner. If water coning represents a problem, a sudden water cut raise will be noticeable. Though the gross production was elevated during the redevelopment project, only a creeping alteration towards a higher proportion of water was monitored over years. In the course of this year, the well reached its economical minimum and the old perforations got locked by a packer. A new perforation was opened a few meters above the old one. In consideration of this action, the remarkable drop in water cut in the year 2016 is explained.
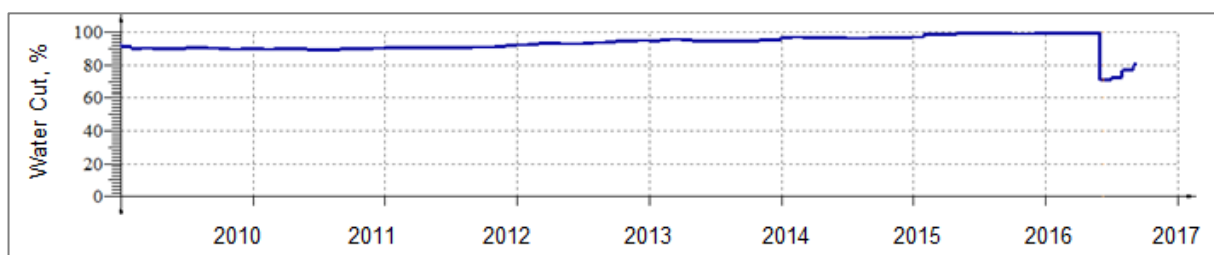

Figure 52: Water cut of BO 89 illustrated over the last seven years

It is legit to say that due to this incremental water cut increase, until only an uneconomic production was possible, an upwards shift of the WOC from the initial location to the depth of the already closed perforations happened. If the contact between water and oil is that close to the new perforation and the production rate is at the current level, the development of a water cone is very likely.

Nevertheless, Figure 52 indicates a furtherance of the creeping trend. An explanation for this behaviour is illustrated in Figure 53, which represents the well section of the well BO 89. The red frame in the right picture indicates the already closed perforations, whereas the green frame highlights the newly opened one. As the measurements of the spontaneous potential shows, a large variation between the old perforations' layer and the new perforated layer can be recognised. The last statement indicates a high deviation between the two adjacent layers' permeability.

In order to come to a conclusion, a water cone develops under the prevailing circumstances. However, because of a permeability barrier, the water cannot move upwards in a straight way, but has to follow horizontal pathways with a higher inherent permeability. The latter prevents the predestinated development of a water cone regarding the new perforation interval of the producer well BO 89.
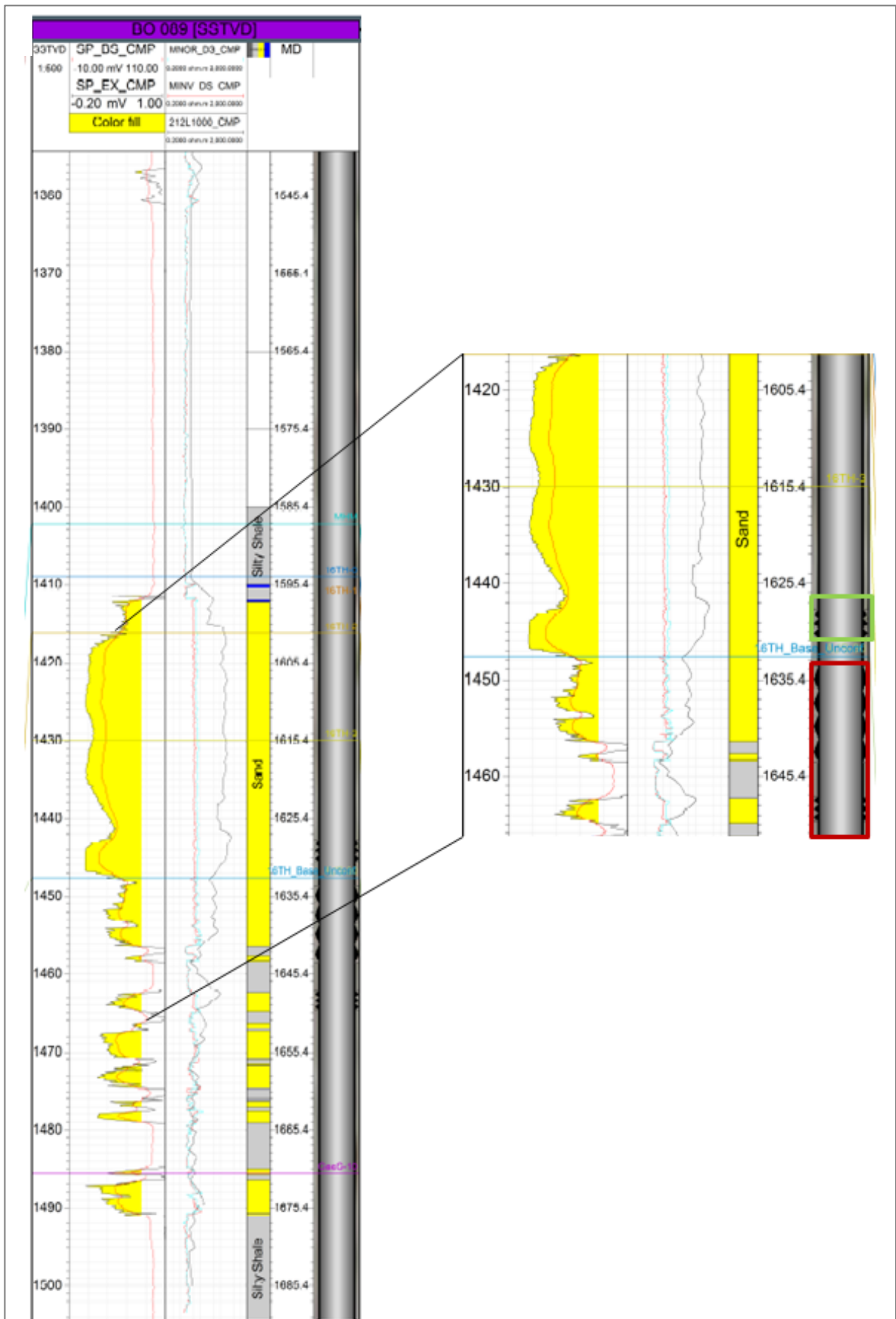
Figure 53: Well section of BO 89

4.6 Streamline model

The following subchapter describes the method of analysing the connected reservoir parts by establishing a surveillance model based on historical production- and injection data. For building the model, the wells' trajectory- and perforation coordinates were gathered by using OFM^{TM}, described in chapter 3.3.4, and subsequently entered into the software tool StudioSL.

Firstly, the connection lines, based on one injector to a number of influenced producers, were demonstrated by means of streamlines, illustrated in Figure 54. The blue dots represent injector wells, whereas the red ones are identified as producers.
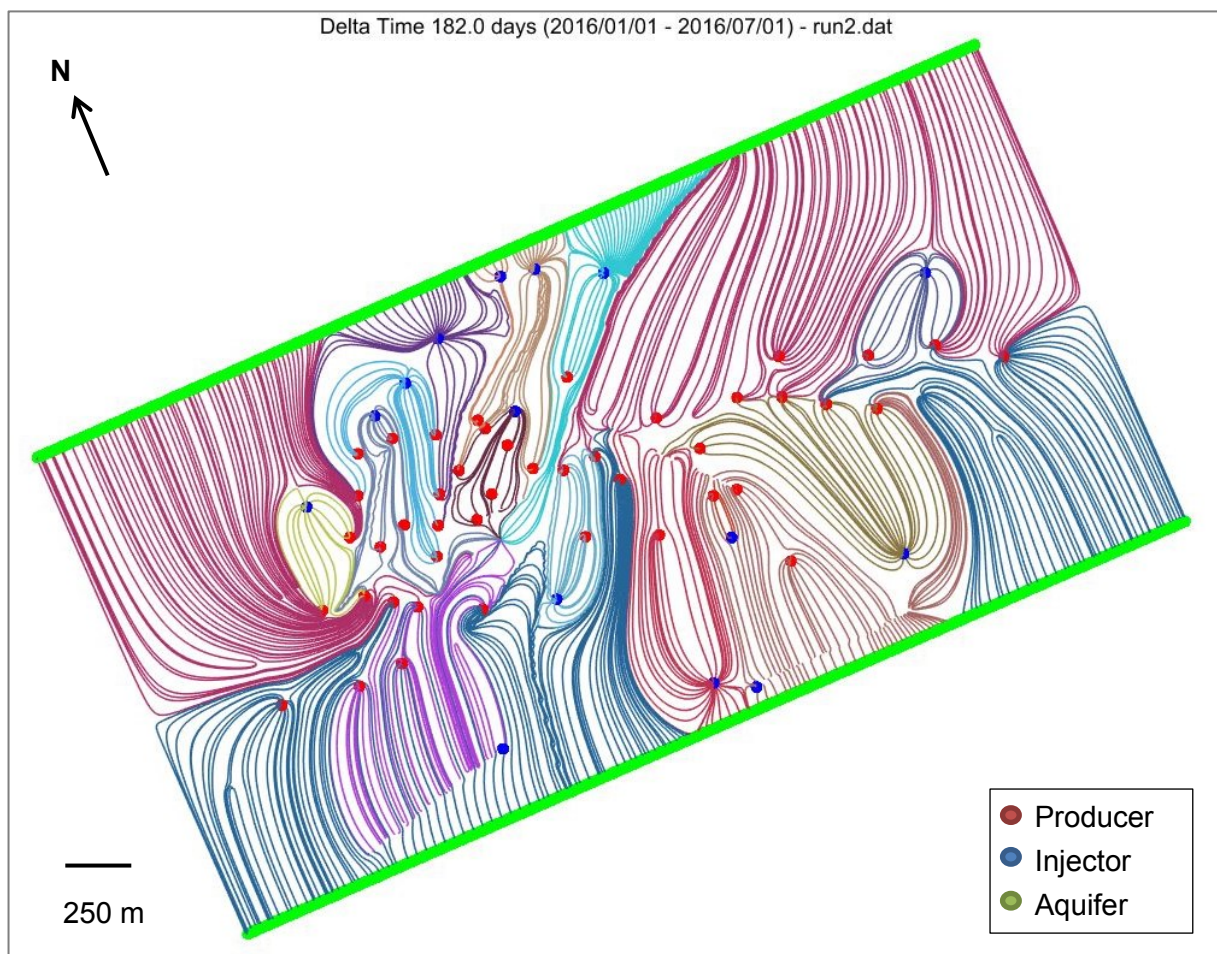
Figure 54: Streamlines from injectors to producers [42]

On the one hand, the analysis is based on the amount of water needed for a production well to produce at a certain rate and on the other hand, it depends on which injectors are most likely to support this producer with a distinct fraction of their injection water.

Principally, it should be mentioned that no geological model was loaded, which is justified in the reservoir's homogeneous behaviour. This configuration is called "shoebox model". As a result, prevalent faults needed a manual configuration. Afterwards, the analysis was continued by looking at the already mentioned WAFs (3.3.5). Furthermore, a threshold value of seven percent for a connection to be adopted was defined. This means that the producer

has to receive at least seven percent of an injector's water for considering it as influenced well. The WAFs are illustrated as FP-Map (Flux Pattern Map) in Appendix G.1. The analysis was based on the data, which was recorded in the first half of the year 2016. The reason for choosing this timeframe is that it represents the most likely reflection of recent reservoir movements. A larger time period would cause a falsification of the interpretation fundament due to, for example, conversions from producers to injectors.

For the reason that the FP-Maps showed a lot of injection water flowing directly into the existing aquifers, a configuration change was applied. Speaking with the software's key developer, only one limiting parameter allowed a change in the mentioned behaviour when the shoebox was still intended to be used. The aquifer's active cells were reduced in order to provide less activity and thus less direct inflow of injection water into the aquifer. Because the wells' connections are relatively unclear in sector one compared to the second sector, only the aquifer activity in the second sector was reduced in order to approximate the connection network resulted by the pressure analysis. The frequency of the southern aquifer was set to 25, so that every twenty-fifth cell is in an active mode, whereas the northern situated aquifer was characterized by an active frequency of 50. The latter setup is justified in the fact that the southern aquifer contributes to the reservoir's performance to a greater extent than the northern aquifer (Figure 55).
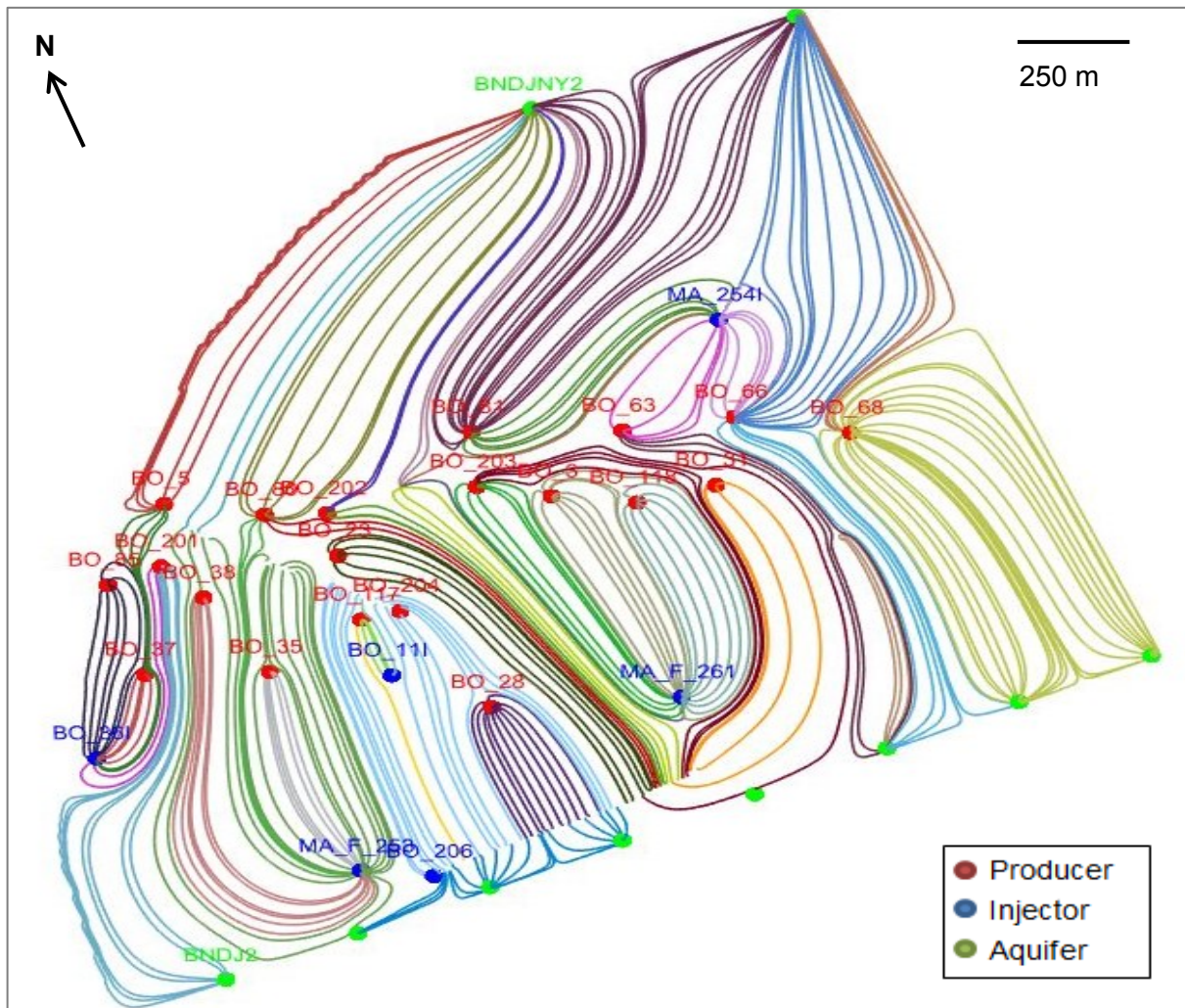

Figure 55: Second sector streamlines with well names [42]

The application of the mentioned feature gives slightly altered outcomes in the contribution of certain injectors to surrounding producers. A comparison of the unchanged and the adjusted approach is provided in Appendix G.2.

Looking at Figure 54 as well as at Figure 55, the defined boundary constraints are observable. The northern and southern flanks are identified as active water boundaries in green colour. As opposed to this, the western and eastern borders are characterised by "no-flow" boundaries. Figure 56 underpins the assumption of a "no-flow" boundary in western direction, caused by a sealing fault. The reason why the eastern side is also assumed to be sealing is that the Bockfließ area is treated as separate region. No streamline proceeds beyond the boundaries and, as Figure 55 shows, also no streamline crosses the major fault that partitions the area in two discrete sectors.
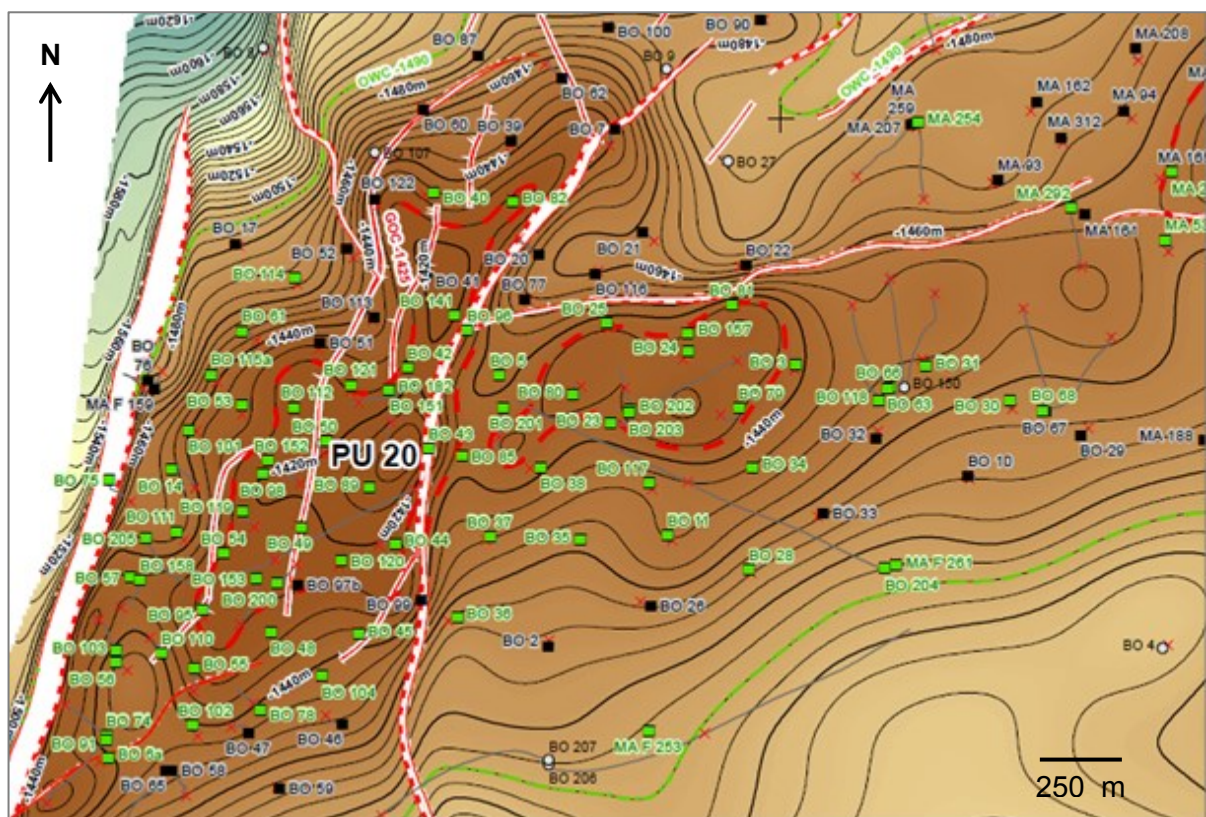
Figure 56: Bockfließ area illustrated in a geological map

Every fault, located in sector one, is taken for sealing, whereas the large fault in the second sector is assumed to be a hundred percent transmissible.

In the end, it was observable that the model reflects the pressure analysis outcomes to a certain extent. As the aquifer behaviour was altered, the connection lines much more represented the pressure analysis conclusion.

5   Optimization methods

The fifth chapter is divided in two major sections. Firstly, an approach for identifying wells with a need of improvement is conducted. As a second point, suggestions concerning the analysis procedure are made.

5.1   Well improvements

Initially, suggestions should have been considered for both, producing and injecting wells. Due to the following two reasons, only producers were considered for analysing them concerning their improvement potential:

- Primarily, the VRR (2.7) should be kept at a value of nearly 1.0, so that the pressure maintenance is guaranteed, which is achieved with the current injection rate
- The second point is that an increase in injection rate is disqualified, because otherwise a much more intense washing out of the already existing pathways is risked
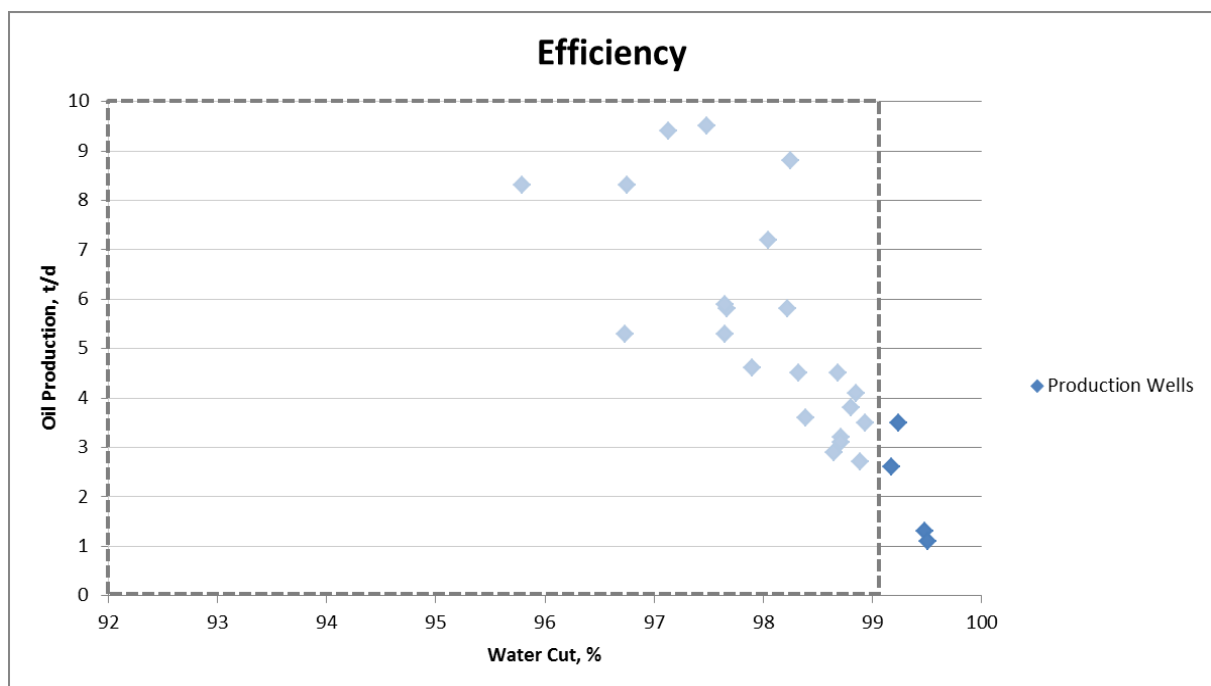

Figure 57: Efficiency plot of production wells

In order to identify wells with an upcoming need for improvement, a diagram, comparing water cut with amount of produced oil on a daily basis, was created and illustrated in Figure 57.

By giving both pictured properties a certain threshold value, four wells were able to be identified as inefficient in their current state.

Figure 58 provides a more detailed view on those four wells. As observable, the limit for an acceptable water cut was set to 99 percent, whereas the minimum oil production is characterized by a value of four tons per day.
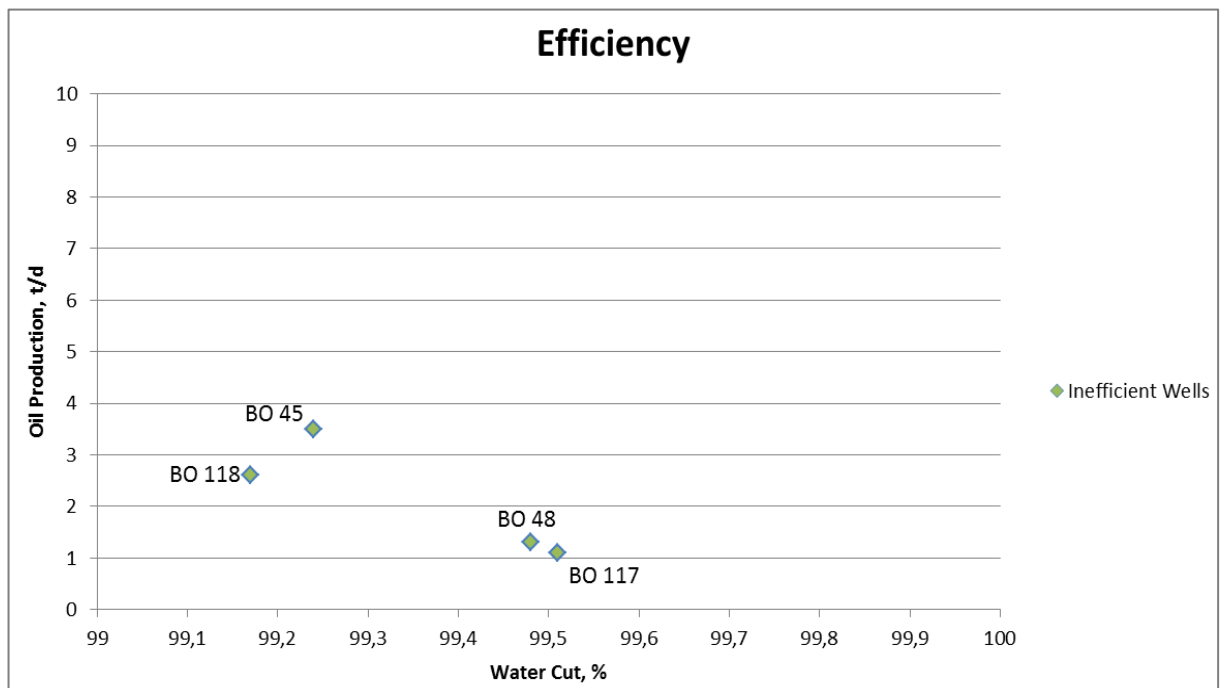

Figure 58: Closer presentation of four less efficient wells

The most inefficient well is represented by BO 117. This producing well, as already described in section 4.2.2.1, is very much dependent on injection well BO 11 and horizontal producer BO 204. Due to the fact that a highway is very likely to be already established, a shut-down action can be taken into consideration. The injection fluid might then find another pathway to travel to another producing well. In September 2015 the well was shut-in for 22 days and the water cut dropped from hundred percent to 99.5 percent. In consideration of Gabor Takacs' Electrical Submersible Pumps Manual [30], the maximum runtime of an ESP motor is guaranteed, if the ESP has once been started at the beginning of production and never gets shut down. In reference to that a frequent on-off switching action should be avoided. Thus, as financial situations recover, the already bridge plug closed perforation interval should get drilled and an additional perforation should be made between the current producing interval and the recovered one. Consequently, the whole interval is designated to be produced as one unit. As the water cut is not increasing dramatically and production remains above one ton per day, this solution is the most economic acceptable one for now.

BO 48 is located in the first sector and was also equipped with an ESP in the year 2015. As soon as the production rate was increased, the water cut raised up to a value of 100 percent. Since then, the produced fraction of water hardly diverges from one. In this case, a workover is planned in order to close the watered out perforations.

If operating conditions allow a reduction in the production rates, BO 48 and BO 45 should be lowered in rate or, as a second possible action, BO 48 should be switched off. Sooner or

later this will be achieved, when the workover is carried out on BO 48. As a consequence, the water is forced to other wells with lower water cut and new pathways might be attractive for the water to take.

In the case of BO 118, no immediate actions are necessary. With a developing trend in the lower right direction of Figure 58, it can be considered to lower the rate at BO 118 and thus promote production in direction of BO 63.

As a second feature of the program StudioSL, FloodOpt was applied. It was possible to simulate the best actions that should be considered in order to improve the field's oil production by leaving the gross production at the same level. In general it is possible to choose between an aggressive, a conservative and a neutral way of achieving a certain increase in oil production.

Different scenarios were subject to this analysis, where the observed ESPs' oil production rates were increased by 5, 10, 20 and 50 percent. A trend was observable, leading to the decision to only mention the 10 percent case for all three analysis strategies.

Firstly, the aggressive case of achieving a ten percent increased oil production by remaining gross production is demonstrated in Figure 59.
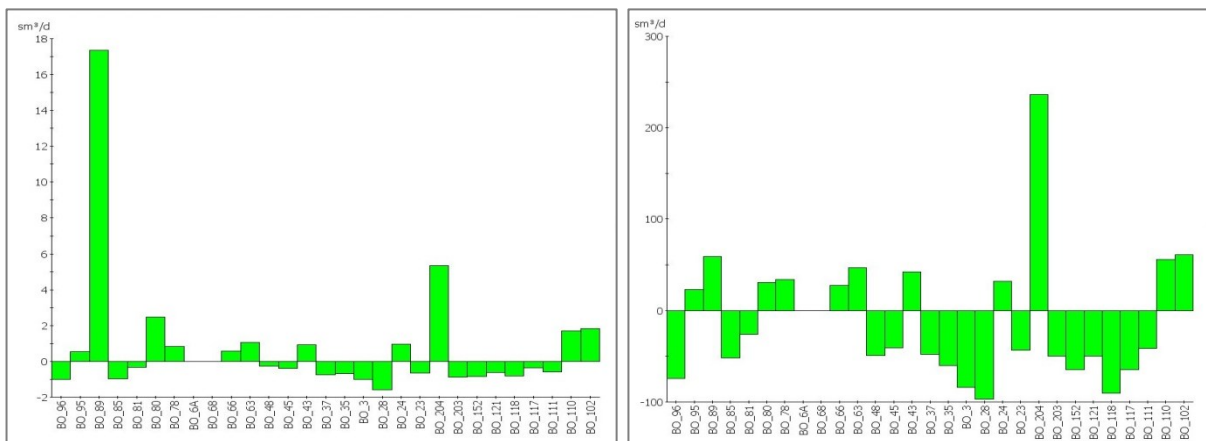
Figure 59: Aggressive case for achieving 10% more production at the observed ESP pumps a) Oil production change b) Gross production change [42]

As observable, the oil production increase is most significantly achieved by increasing the gross production at the newly perforated well BO 89. Another interesting well is represented by the horizontal producer BO 204, which also shows a potential in achieving more oil production by increasing its gross production rate. The turning down action of BO 118 and BO 28 also stands out. From an economical point of view, this step should be considered, if production rates of those two wells are lower than they are now. Having a look at the neutral and conservative analysing approach, the same wells are addressed. The only major difference is their magnitude of production change.

5.2 Analysis improvements

The second part of the improvement section deals with the process of data collection in order to achieve a better mode of operation for further investigations.

5.2.1 ESP-sensor pressure data and injection data

When analysing the pressure data of producing ESP wells, a daily average value was considered. For the approach of determining the pressure travelling time inside a homogeneous area like the Bockfließ region, a shorter time step should be considered. It is possible to extract data on a ten minutes and four hour basis. Unfortunately, due to the giant amount of data that would be produced, the pressure data's memory cache is emptied after a certain amount of time. This is done by applying the principle of first in is automatically deleted at the very beginning. If there are plans for further investigations in this area, it would be necessary to save the data over one year on, for at least, a four hours basis.

Although this would give a more detailed view on the part of production wells, the injection data is also prone to be imprecise. In case of an injection shut-in, the daytime is not registered anywhere, what makes it difficult to estimate the time, when the pressure wave was initiated. It would be favourable to take the daytime and the extent of the pressure change down in some system, so that a better reproduction of the injection events is available.

5.2.2 Chloride ion concentration

Despite the fact that the injection installation was changed, when the Bockfließ area was separated from the injection line originating from the water treatment plant Schönkirchen, it seems that injection well MA 254 is still being fed by extraction station Schönkirchen rather than by extraction station Auersthal, as the other considered injectors are. The chloride ion concentration should be measured at the production wells BO 118, BO 63 and BO 66 in order to determine their chloride ion concentration divided by m-value. The injection water delivered from the extraction station in Schönkirchen has currently a chloride ion concentration of approximately 13500 mg/l, whereas the m-value is determined at a value of 20 mmol/l. The division of both values gives 675 g/mol. Comparing this quantity with the outcomes at the three mentioned producing wells would give enough margins to interpret a possible connection across the fault, proceeding from the western to the area's eastern side, by looking at the chloride-ion concentration values.

5.2.3 Tracer test

As a third recommendation for investigations in the area's connectivity, a tracer test is suggested. For making conclusions on the injected fluid's flow behaviour, it would be appropriate to only consider a passive tracer that just follows the injected water until it is produced. However, due to the fact that OMV is planning a surfactant flooding operation in this region, it would be more advisable to use an active tracer. The reason for this is that an active tracer is able to deliver information about rock properties and fluid saturations by interacting with the rock and fluid system [31].

6 Conclusion

Recapitulating the investigations conducted in this master thesis, it was possible to find out relationships between producers and injectors. This could be achieved by comparing injection breakdowns with measured pump intake pressures at production wells. In total, four clusters of interrelated wells could be identified. Additionally, the transmissibility of the region's two major faults based on the pressure behaviour was examined. This investigation shows that one fault is completely sealing and the other one is able to allow communication between the wells lying on opposite sides of the fault. The feasibility to check on the pressure wave's travelling time on the basis of measured pressure data was not accomplished. In view of this fact, an analytical approach was realised in order to determine the pressure distribution time. The gathered outcome was later on matched with the results of an interference test. Considering the downhole sensor's accuracy, the interference test showed analogous duration results, when compared with the calculated time. It was figured out that the proposed approach of detecting injector-producer links by analysing the chloride ion concentration was no longer applicable in this reservoir region. Furthermore, a water coning activity was determined by looking at a well, where this calculation type can still be conducted. It was proven that water coning represents an issue in the observed area due to the extremely high production rates. Water coning is often prevented by the fact that permeability alterations are causing vertical flow barriers. Depending on the considered flooding area, Buckley Leverett's approach gives a time for the water to travel from injection to production well. A streamline surveillance model shows the distribution of the injected amount of water of all injecting wells to the different producers. Although no geological model was determined, the model offers a plausible reflection of the measured pressure responses. Based on this model, a flood optimization feature was applied, which gives suggestions for both, increasing certain wells' production rates and reducing rates at other producers. To sum up, it was possible to achieve an approximate representation of the wells' assignment to clusters. If a detailed reaction response of producers to injector activities was desired, more frequent data has to be considered. Another way for confirming the outcome, gained by analysing the pressure responses, would be a tracer test application.

7 References

[1] M. Gruenwalder, S. Poellitzer and T. Clemens, "Assisted and Manual History Matching of a Reservoir With 120 Wells, 58 Years Production History and Multiple Well Recompletions," in *SPE Europec/EAGE Annual Conference and Exhibition*, London, United Kingdom, 2007.

[2] G. Kienberger and R. Fuchs, "Case History of the Matzen Field - Matzen Sand (16th TH): A Story of Success; Where is The End?," in *SPE Annual Technical Conference and Exhibition*, Vienna, 2006.

[3] M. Gruenwalder, "Immiscible Gas Injection: Challenges, Example of 16th TH Horizon, Austria," in *SPE Europec/EAGE Annual Conference and Exhibition*, Rome, 2008.

[4] I. Giden, B. Kometer and M. Eschberger, "Deployment of Sensor Equipped ESPs in a Mature Oilfield – A Case Study," in *DGMK/ÖGEW-Frühjahrstagung* , Celle, 2016.

[5] Krebs, "Installations-, Betriebs- und Wartungsanleitung," FLSSmidth, Arizona, USA, 2014.

[6] T. H. Ahmed, Reservoir engineering handbook, United States of America: Elsevier Inc., 2010.

[7] H. C. Slider, "Application of Pseudo-Steady-State Flow to Pressure-Buildup Analysis," in *SPE Amarillo Regional Meeting*, Texas, 1966.

[8] M. M. Kamal, "Interference and Pulse Testing – A Review," *Journal of Petroleum Engineers,* pp. 2257-2270, 1 December 1983.

[9] J. A. Lescarboura, H. C. Walther and P. L. Wilson, "Design and Analysis of Interference Tests," in *SPE California Regional Meeting*, Texas, 1975.

[10] J. R. Jargon, "Effect of Wellbore Storage and Wellbore Damage at the Active Well on Interference Test Analysis," *Journal of Petroleum Technology,* pp. 851-858, 1 August 1976.

[11] B. Wu, C. P. Tan and N. Lu, "Effect of Water-Cut on Sand Production – An Experimental Study," *SPE Production & Operations,* pp. 349-356, 1 August 2006.

[12] A. Yang and Y. Xue, "Comparing Rigless Water-Cut Reduction Methods," in *Production and Oeprations Symposium*, Oklahoma, 2007.

[13] R. C. Kootiani and A. B. Samsuri, "Analysis Fraction Flow of Water versus Cumulative Oil Recoveries Using Buckley Leverett Method," *Proceedings of World Academy of Science,* pp. 1826-1831, 1 December 2012.

[14] "fekete.com," Fekete Associates Inc., 2012. [Online]. Available: http://fekete.com/SAN/TheoryAndEquations/HarmonyTheoryEquations/#HTML_Files/Reference_Material/Analysis_Method_Theory/Surveillance_Theory.htm. [Accessed 3 April 2016].

[15] U. E. Dickson, "Well Integrity behind casing during well operation. Alternative sealing materials to cement," Norwegian University of Science and Technology- Department of Petroleum Engineering and Applied Geophysics, Norway, 2013.

[16] C. Teodoriu, C. Kosinowski, M. Amani, J. Schubert and A. Shadravan, "Wellbore Integrity and Cement Failure at HPHT Conditions," *International Journal of Engineering and Applied Sciences,* vol. 2, no. 2, February 2013.

[17] M. R. Thiele and R. P. Batycky, "Using Streamline-Derived Injection Efficiencies for Improved Waterflood Management," *SPE Res Eval & Eng,* vol. 9, no. 2, pp. 187-196, 2006.

[18] M. Kornberger and M. R. Thiele, "Experiences With an Efficient Rate-Management Approach for the 8th Tortonian Reservoir in the Vienna Basin," *SPE Reservoir Evaluation & Engineering,* pp. 165-176, May 2014.

[19] "aqion.de," aqion, 7 July 2015. [Online]. Available: http://www.aqion.de/site/138. [Accessed 4 October 2016].

[20] E. Shevchenko, Experimental study of water coning phenomenon in perforated pipes geometry, Norwegian University of Science and Technology- Trondheim, 2013.

[21] J. Gimre, Efficiency of ICV/ICD systems, University of Stavanger, 2012.

[22] Tendeka, "tendeka.com," Tendeka, 2016. [Online]. Available: http://www.tendeka.com/product-ranges/inflow-control/. [Accessed 4 October 2016].

[23] E. Leung, "Intelligent Inflow Tracer monitoring of an Autonomous ICD Completion," in *2nd Inwell Flow Surveillance and Control Seminar*, Aberdeen, 2015.

[24] J. D. Clegg, Petroleum Engineering Handbook, Volume IV: Production Operations Engineering, Society of Petroleum, 2007.

[25] Schlumberger, *Phoenix xt150,* Schlumberger.

[26] W. International, *Life of Well Information Software- Training Manual,* Weatherford International, 2009.

[27] J. Sinner, "Practical Reservoir Performance Analysis & Review Using OFM," in *IOR/EOR Conference*, Wyoming, 2011.

[28] M. R. Thiele, "Streamline Simulation," in *6th International Forum on Reservoir Simulation*, Schloss Fuschl, Austria, 2001.

[29] H. Baarova, "Evaluation of well tests using radial composite model and dietz shape factor for irregular drainage area," Technical University in Liberec, Czech Republic, 2010.

[30] G. Takács, Electrical submersible pump manual: design, operations, and maintenance, United States of America: Elsevier Inc., 2009.

[31] S. International, "petrowiki.org," SPE International, 9 July 2015. [Online]. Available: http://petrowiki.org/Well_to_well_tracer_tests. [Accessed 4 October 2016].

[32] J. Scholz, "ingenieurkurse.de," c/o examio GmbH , [Online]. Available: https://www.ingenieurkurse.de/stroemungslehre/hydrodynamik/ reibungsbehaftete-stroemungen/verluste-in-rohrleitungen-streckenabhaengige/ moody-diagramm.html. [Accessed 9 September 2016].

[33] "fekete.com," Fekete Associates Inc., 2012. [Online]. Available: http://www.fekete.com/SAN/TheoryAndEquations/WellTestTheoryEquations/ Total_Compressibility.htm. [Accessed 5 July 2016].

[34] F. Häfner, H. D. Voigt, H. F. Bamberg and M. Lauterbach, Geohydrodynamische Erkundung von Erdöl-. Erdgas- und Grundwasserlagerstätten, Berlin: Wirtschaftlich-Technischer Informationsdienst, 1986.

[35] D. M. Oberndorfer, "Modeling of Reservoir Fluid Properties A015-216-20," Laboratory for Exploration and Production, OMV, Vienna, 2007.

[36] T. G. Farr, P. A. Rosen, E. Caro, R. Crippen, R. Duren, S. Hensley, M. Kobrick, M. Paller, E. Rodriguez, L. Roth, D. Seal, S. Shaffer, J. Shimada, J. Umland, M. Werner, M. Oskin, D. Burbank and D. Alsdorf, "The Shuttle Radar Topography Mission," *Reviews of Geophysics,* vol. 45, no. 2, 19 May 2007.

[37] J. Bovendeur and R. Mozley, "Characterisation of Polluted Material – An Environmental

Application of Mineral Processing Technology," Sydney; Australia, 1993.

[38] A. Kröll, H. Heinz, R. Jiricek, B. Meurers, W. Seiberl, P. Steinhauser, G. Wessely and D. Zych, "Wiener Becken und angrenzende Gebiete (mit Erläut., 1-22)," Geologische Bundesanstalt, Wien, 1993.

[39] J. Mach, E. Proano and K. E. Brown, "A Nodal Approach For Applying Systems Analysis To The Flowing And Artificial Lift Oil Or Gas Well," 1979.

[40] S. Beck and R. Collins, "wikipedia.org," University of Sheffield, 24 July 2008. [Online]. Available: https://en.wikipedia.org/wiki/Moody_chart. [Accessed 4 October 2016].

[41] I. Giden, B. Kometer, P. Toth, H. Geier, T. Florian and M. Sieberer, "Technology Driven Rejuvenation of a Mature Field by Doubling the Gross Production Rate," in *SPE Annual Technical Conference and Exhibition* , Dubai, 2016.

[42] Own representation based on StudioSL.

[43] Own representation based on OFM, Schlumberger.

[44] Own representation based on LOWIS.

[45] L. P. Own representation based on Dake, Fundamentals of Reservoir Engineering, Great Britain: Elsevier BV., 1978, p. 391.

[46] L. P. Own representation based on Dake, Fundamentals of Reservoir Engineering, Great Britain: Elsevier BV., 1978, p. 362.

8 Appendices

8.1 Appendix A.1

The used pressure values are illustrated in Table 6. A directly measured value was used for the wellhead pressure, whereas the hydrostatic pressure was calculated by using equation 8.1.1.

$$p_h = \rho \times g \times h = 1014 \times 9.81 \times 1655{,}8 = 164.7 \ bar \qquad \textbf{8.1.1}$$

Table 6: Pressure data

Variable	Value, bar
Wellhead pressure	30
Hydrostatic pressure	164.7
Friction pressure losses	6.45

For the friction pressure losses along the tubing string, the Moody diagram was applied, shown in Figure 60.
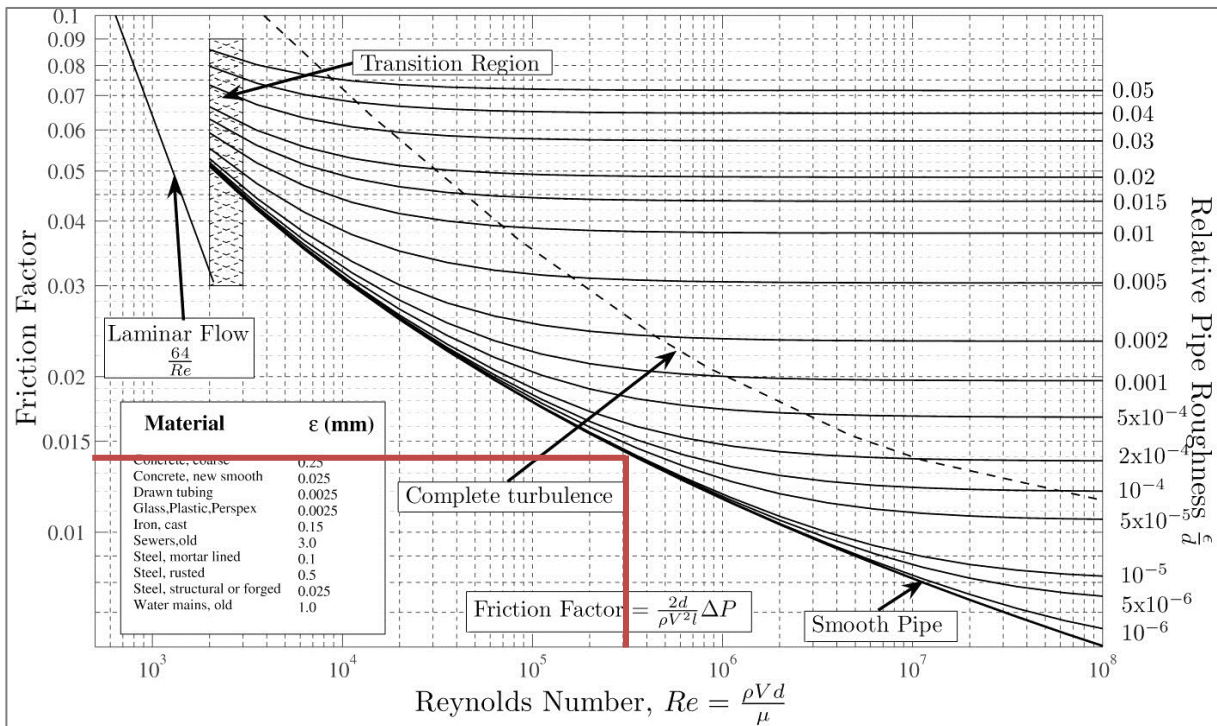
Figure 60: Moody chart [40]

In order to be able to use the diagram, the Reynolds number had to be calculated with equation 8.1.2.

$$Re = \frac{\rho \times v \times d}{\mu} = \frac{1014 \times 2.04 \times 0.076}{0,0005} = 314600.21 \qquad \textbf{8.1.2}$$

v   injection velocity [m/s]
d   characteristic length [m]
μ   dynamic viscosity [Pas]

Due to the fact that extremely smooth pipes are used for injection, with a roughness of about 1 micrometre, a hydraulically smooth behaviour was assumed [32]. This circumstance leads to the conclusion the pipe friction factor λ is only a function of the Reynolds number, which is illustrated in Figure 60 with red colour. As a result, λ was set to a value of 0.014.

$$\Delta p_f = \frac{\lambda \times L \times v^2 \times \rho}{2 \times d} = \frac{0.014 \times 1655.8 \times 2.04^2 \times 1014}{2 \times 0.076} = 6.45 \, bar \qquad \textbf{8.1.3}$$

Considering equation 8.1.3, a pressure loss due to friction in the tubing of 6.45 bars is the outcome.

8.2 Appendix A.2

For an applicability of Darcy's approach in the injectivity calculation, the values illustrated in Table 7 had to be determined.

Table 7: Injection data of BO 36

Variable	Value
Water effective permeability	95.2 mD
Injection height	42.64 ft
Water viscosity	0.5 cp
Water formation volume factor	1.02 res vol/STC vol
Drainage radius	1200 ft
Wellbore radius	0,55 ft
Skin	0

The water's effective permeability was calculated by multiplying the absolute permeability with the relative permeability, gathered from SCAL measurements. Going further on, the injection height is equivalent to the perforated interval, whereas the water viscosity and water formation volume factor are measured values from the laboratory. In order to calculate the drainage radius, formula 8.2.1 was used.

$$r_e = \sqrt{\frac{W_{inj} \times B_w}{\pi \times h \times (1-S_w) \times \Phi}} = \sqrt{\frac{662823 \times 1.02}{\pi \times 18 \times (1-0.67) \times 0.27}} = 366 \, m \qquad \textbf{8.2.1}$$

W_{inj} cumulative volume of water injected [m³]

B_W water formation volume factor [res bbl/STB]

h   formation height [m]

S_w water saturation [1]

The wellbore radius was assumed to be the casing's outside diameter and the skin, because no inflow problems are observed, was simply neglected and thus set to 0.

8.3 Appendix B.1

The second appendix section shows the pump performance curve of the installed pump type D2400N manufactured by the company REDA.
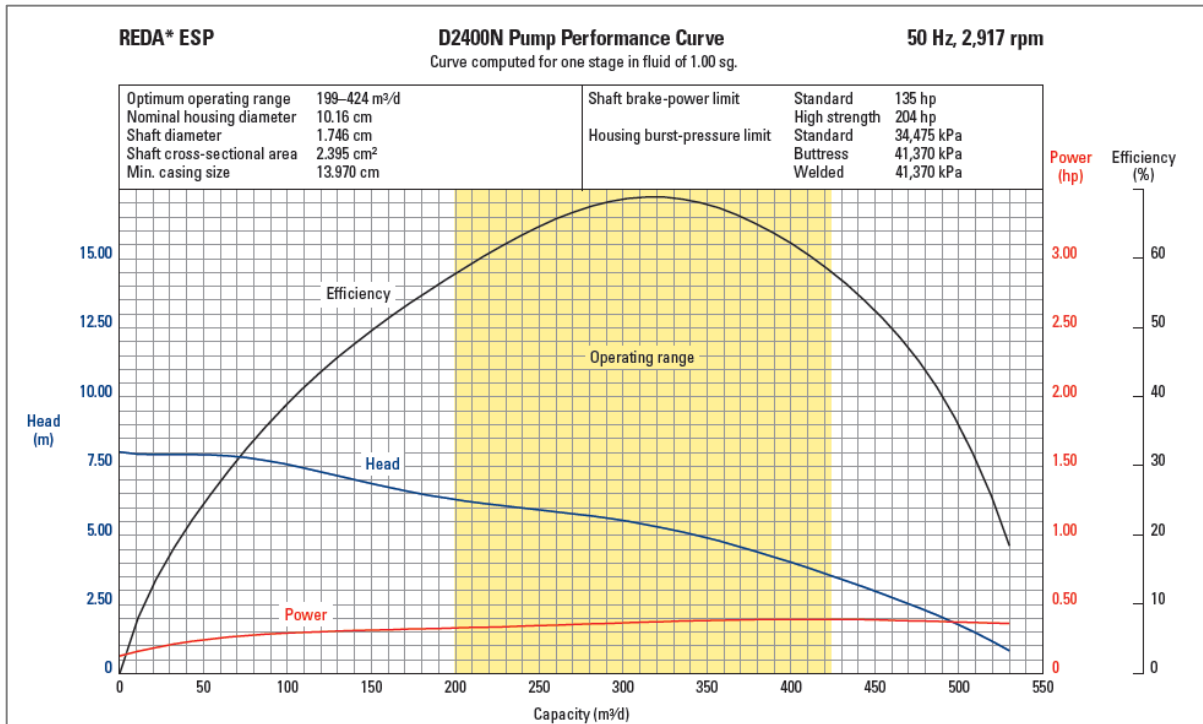

Figure 61: Pump performance curve

The pump curve is based on measurements gathered by computing one stage of the ESP-configuration while pumping water (specific gravity = 1.00).

As observable in Figure 61 the preferred operating range for avoiding up- and downthrust lies between 199 and 424 m³/d and stage.

8.4 Appendix C.1

This appendix section deals with the unanalysable sensor data and an explanation for not considering them in the investigations.

BO 204
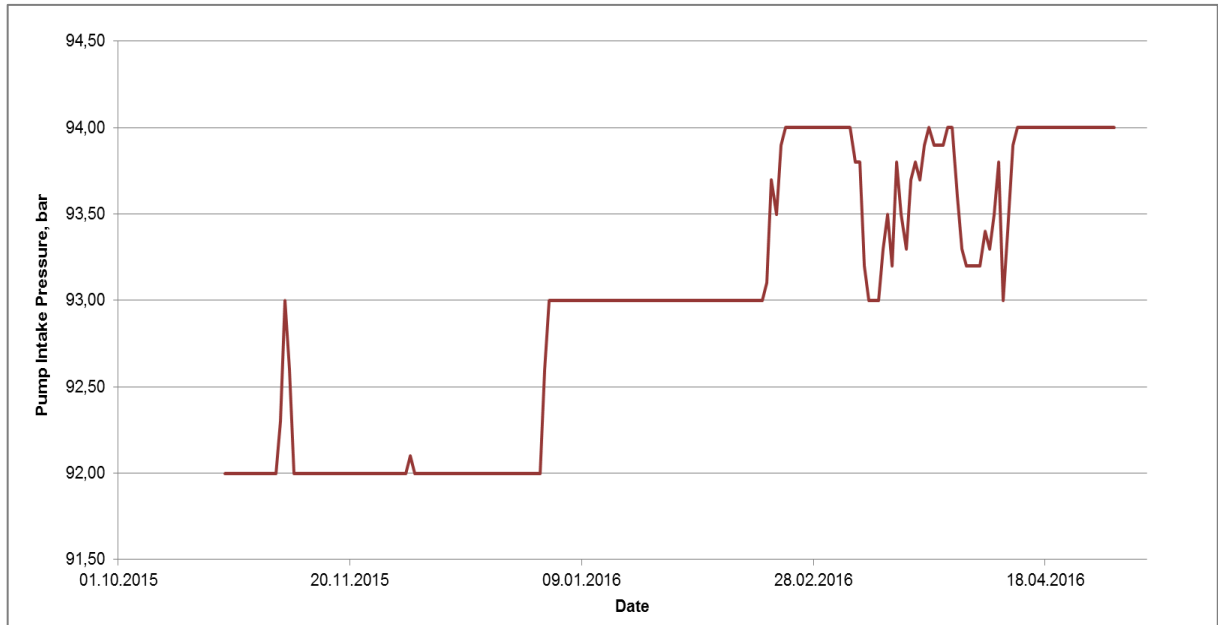
Figure 62: Pump intake pressure of BO 204

Unfortunately, no relatable trend could be observed by the pump intake pressure analysis of the horizontal well BO 204. Looking at BO 204's route, many influencing wells are in line for the unassignable pressure behaviour.

BO 28

In principle, an allocation to the combined cluster I and II would be appropriable. Due to the fact that the pressure data had a more distinctive fluctuation characteristic than the other wells of the mentioned clusters, BO 28 was regarded separately.
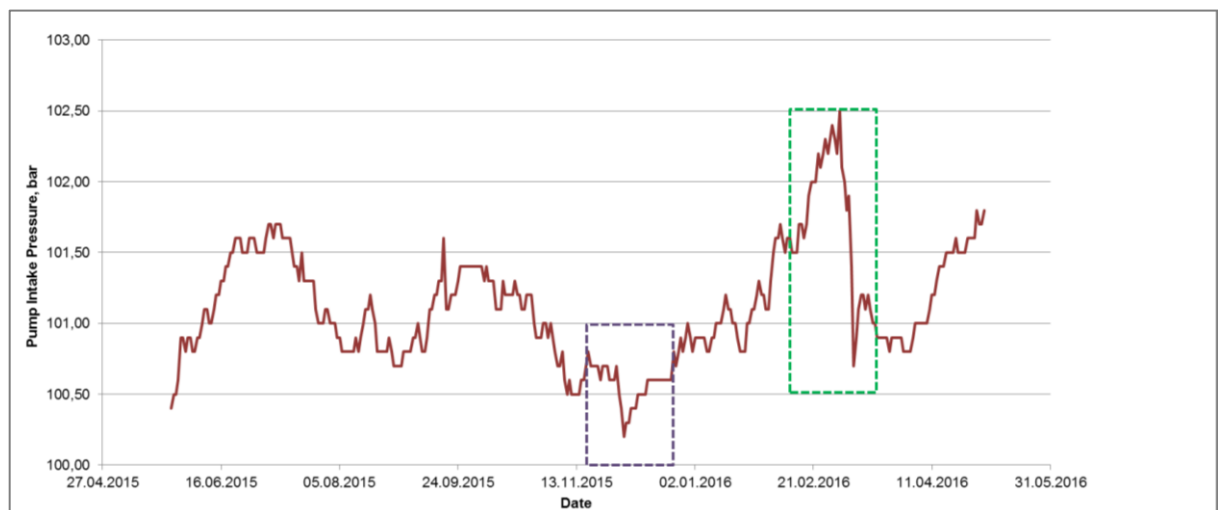
Figure 63: Pump intake pressure of BO 28

The violet marking in Figure 63 supports the conclusion that due to the position of BO 28, a more direct influence, triggered by BO 206 and MA F 253, may lead to an oscillating pressure behaviour. Also a green label can be spotted, which shows a pump intake pressure decline due to an increase in production, which makes an interpretation in this time span impossible.

BO 80

Although BO 80 is located in the near vicinity of cluster II wells, its trend differs greatly from the surrounding wells. A demonstration of the pump intake pressure response is provided in Figure 64.
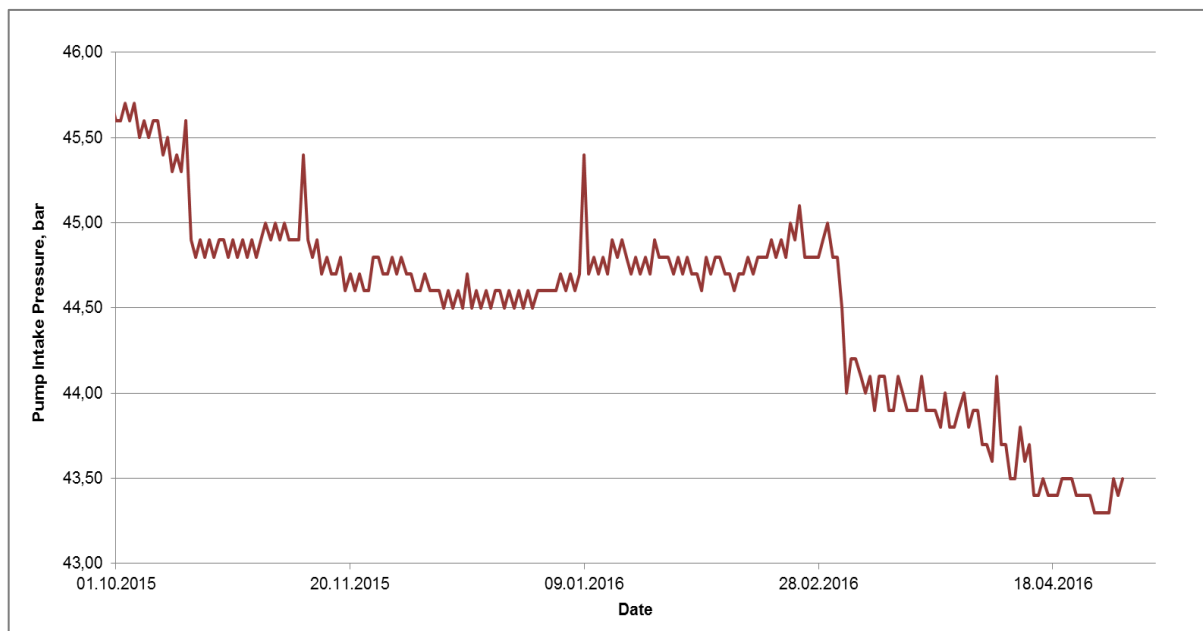
Figure 64: Pump intake pressure of BO 80

As distinguished from the other wells, BO 80 is perforated in another geological formation, the lower sands. Like the pressure response indicates, there is hardly any communication between the layers of the upper sands with those of the lower ones.

The last section dealt with unanalysable wells located in the second sector. In the next pages, uninterpretable data of first sector wells are discussed, starting with the southern situated BO 110.
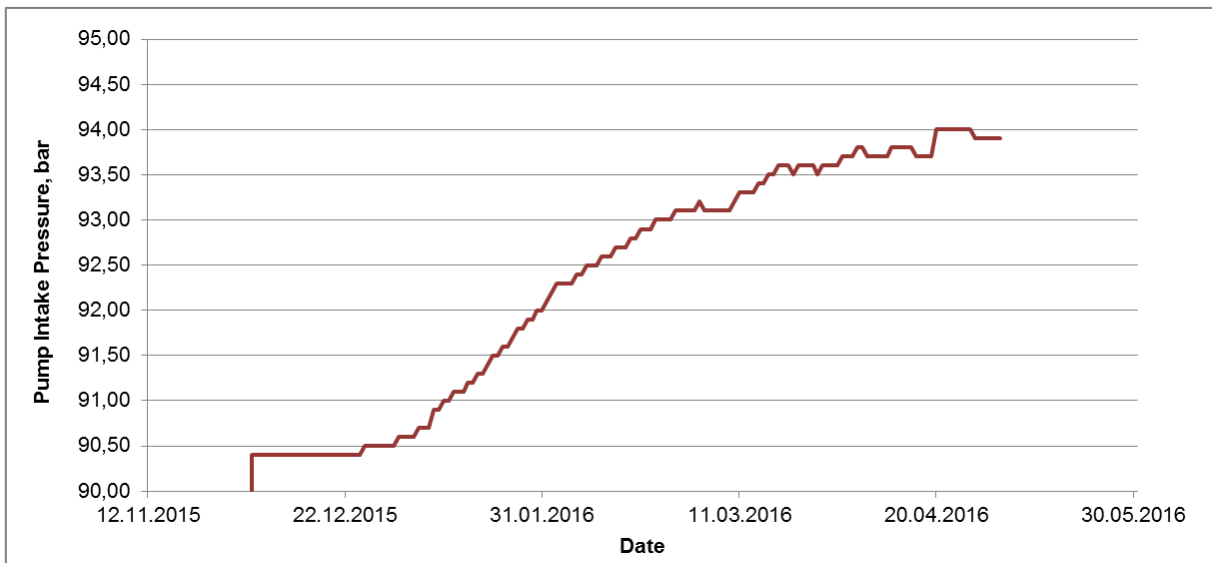
BO 110

Figure 65: Pump intake pressure of BO 110

By having a look at Figure 65, it is clear that no interpretation is possible. On the one hand the observed time span is too short for making conclusions, while on the other hand only an overall trend of increasing pressure can be noticed. No direct injector influence is reflected by the pump intake pressure response, which might lead to the assumption that this well is primarily influenced by the southern aquifer's activities.

BO 102

Due to the long shut-in period of BO 102 and the very strong fluctuations, also no conclusion about a membership to a specific cluster can be obtained. The pump intake pressure of BO 102 is illustrated in Figure 66.
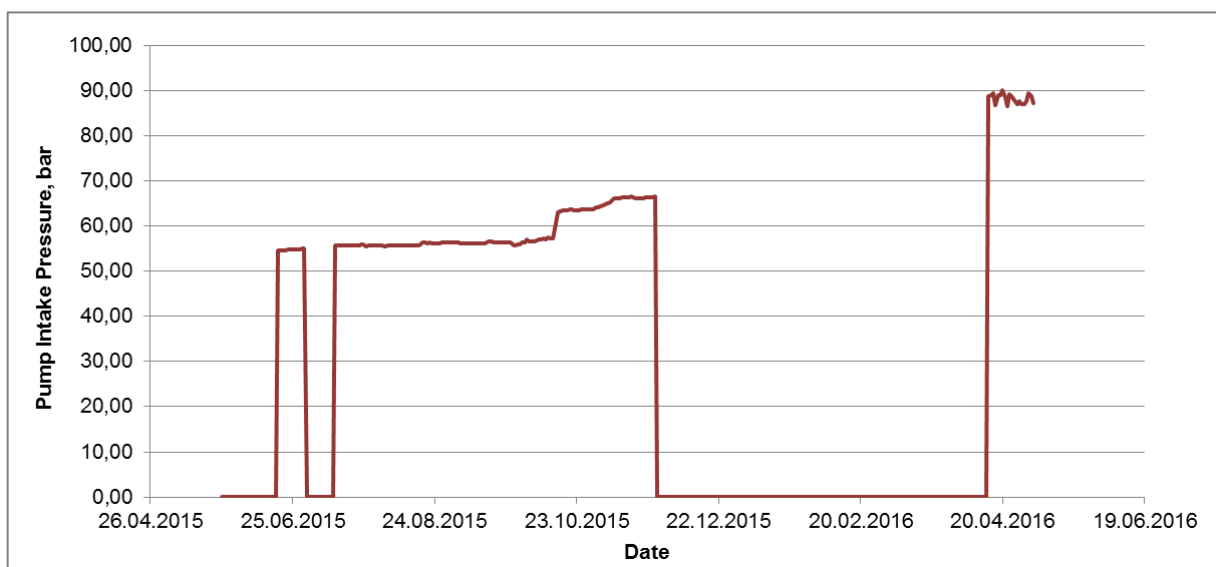

Figure 66: Pump intake pressure of BO 102

<u>BO 48, 45, 78, 95, 6a, 111</u>

The last six wells that are explained in this section would all have well-conditioned pressure data, which was recorded for a sufficient amount of time. Besides BO 78, which shows a kind of exceptional behaviour, all wells are following the same activities, which are not assignable to any injector. Also the distinguished characteristics of BO 78 cannot precisely be allocated to a certain observable behaviour of surrounding wells.
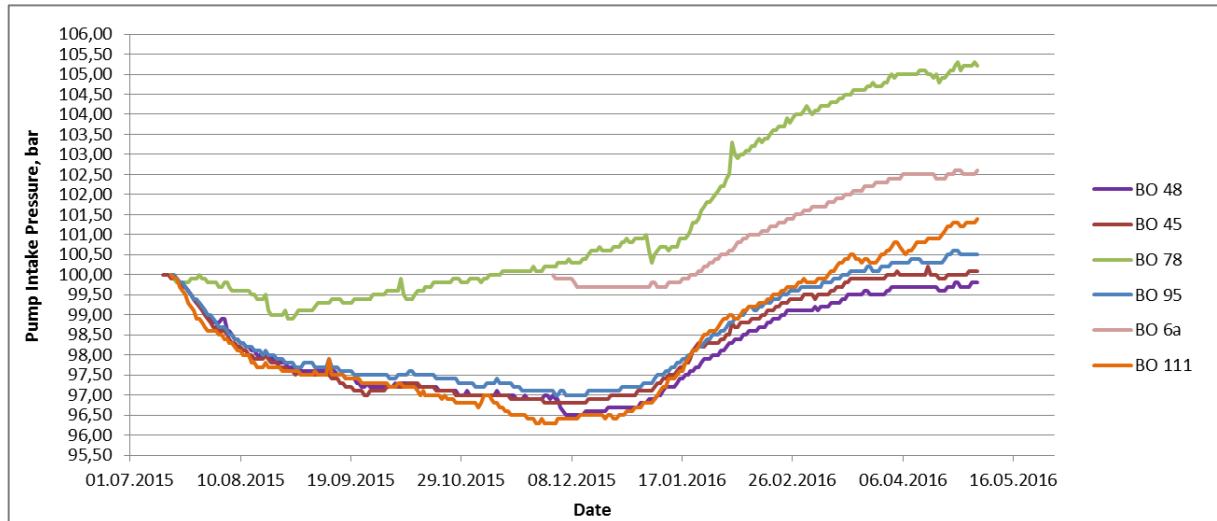

Figure 67: Combined plot of six wells with similar pressure behavior

Another small observation is noticeable at BO 111. At the pressure increase section, it increases faster than the other wells, which may lead to the assumption that this producer gets additional support from injection well BO 75, which is located next to this producing well.

It is concluded that all of the above illustrated wells are supported by the southern aquifer and the horizontal injector BO 207 to a more or less equal extent.

8.5 Appendix D.1

The pressure response time's calculation is based on parameters, whose origin is described in the next few pages.

Having a look at formulas 4.3.1 and 4.3.2, different factors needed to be derived. Three of the terms were determined by laboratory measurements:

- ⬥ Permeability: 1190 mD → 1.19 x 10^{-12} m²
- ⬥ Fluid's viscosity: 5.19 mPas → 0.00519 Pas
- ⬥ Porosity: 27 % → 0.27

The total system's compressibility was calculated by using equation 8.5.1 [33].

$$c_t = c_g \times S_g + c_O \times S_O + c_W \times S_W + c_f \qquad\qquad \textbf{8.5.1}$$

$C_{t,g,o,w,f}$ Compressibility total; gas; oil; water; formation [1/Pa]
$S_{g,o,w}$ Saturation gas; oil; water [1]

The saturations were derived from each well, respectively, in combination with the fractional flow curve. Because gas saturation is really low, it was assumed to be about 0.75 percent, for the sake of consideration. Depending on each well's water cut, the water saturation varies between 50 and 72 percent.

Considering the compressibility of each individual contributor, different strategies were applied.

Gas compressibility

For the gas compressibility a rough calculation approach was applied by just dividing one by the prevalent reservoir pressure. This approximation results in a value of 0.0816 1/MPa for the compressibility of gas by using a reservoir pressure of 123 bars.

Water compressibility

In order to obtain the compressibility for the system's water, a value of 0.000435 1/MPa was assumed. This value was acquired by the source [34] and was proved by examining the isothermal compressibility of mineralized water method by Dodson & Standing (1944).

Oil compressibility

Due to the fact that the oil compressibility is very much dependent on the prevalent pressure, laboratory measurements were considered. A value of 0.0009 1/MPa was chosen.

Formation compressibility

Dobbynin (1970) and Chierici, Ciucci u.a. (1967) suggest a value of 3 x 10^{-5} 1/MPa for sandstone reservoirs [34].

From the plausibility point of view, the applied values describe an appropriate relationship to one another. So, gas is the most compressible fluid, followed by oil, water and, as least compressible component of the system, the formation. Considering equation 8.5.1, the total compressibility results in a figure of 1.23 x 10^{-3} 1/MPa.

In alteration of the individual distances between injectors and producers, different theoretical stabilization times were calculated, which are demonstrated as bar charts in Appendix D.2.

8.6 Appendix D.2

Figure 68 represents the pressure stabilization times by demonstrating them, grouped by injectors located at sector two, in bar charts.
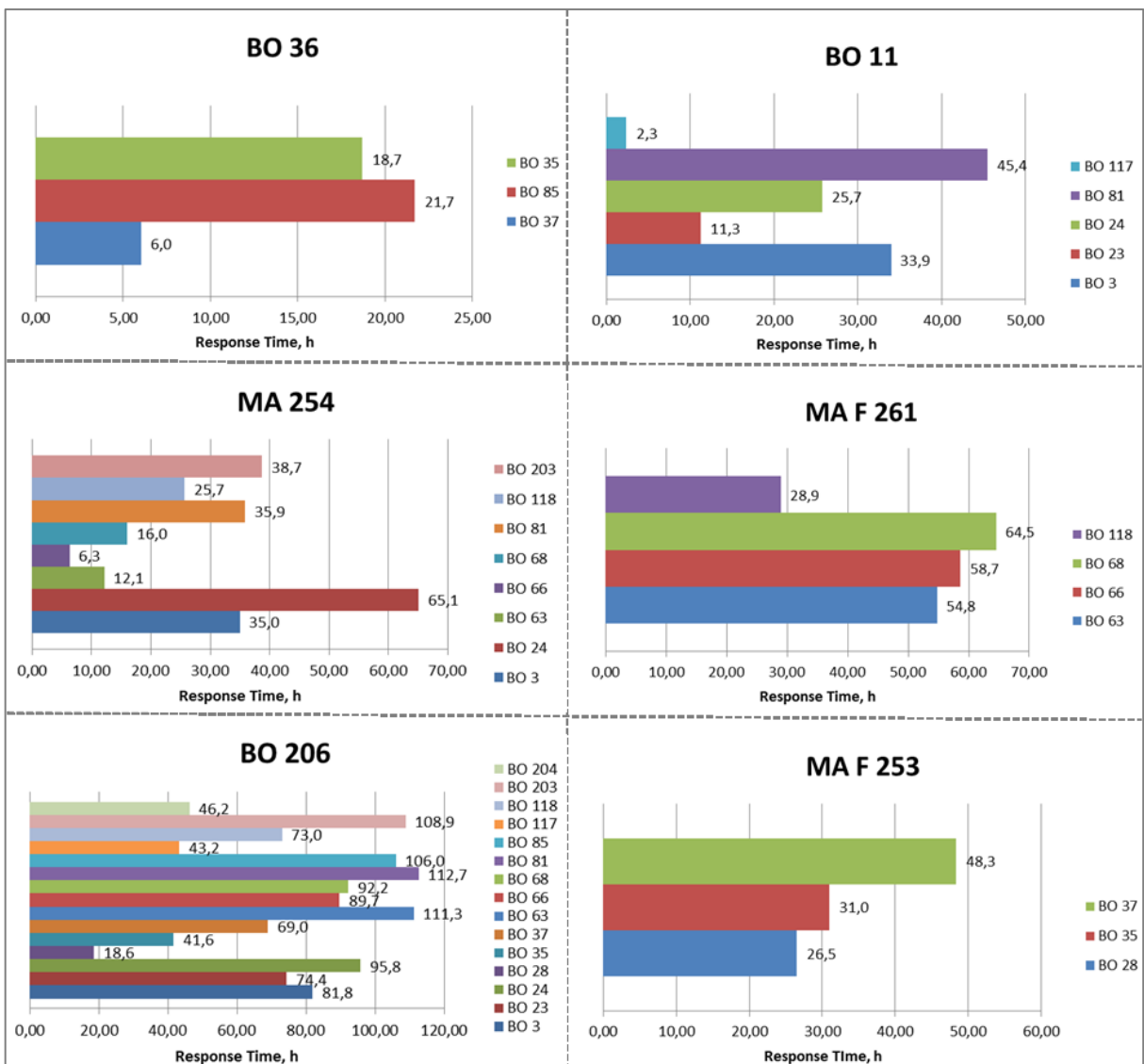

Figure 68: Pressure stabilization times of sector two

Only one cluster of sector one, regarding the pressure response time, is illustrated in Figure 69.
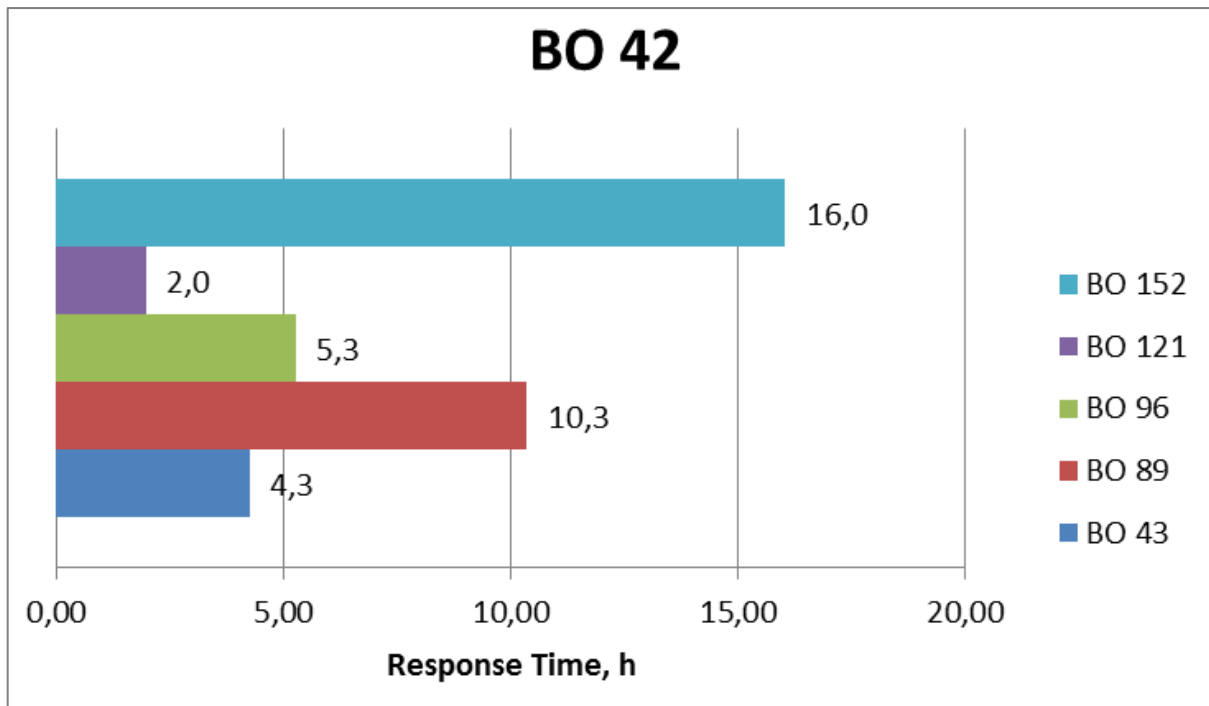

Figure 69: Pressure stabilization times of sector one

For the reason of the field's heterogeneity, the time for the pressure wave to travel from injector to the producer well is mainly dependent on the distance between the two observed wells. The distance was obtained by the program OFM.

8.7 Appendix E.1

This appendix section deals with the step-by-step explanation of deriving the fractional flow curve.

As a first point, the relative permeability values of water and oil at different water saturations were gathered from SCAL laboratory measurements. These values were plotted against the water saturation on a semi-log plot, illustrated in Figure 70. The linear part of the graph is connected with a trend line described by a slope of -18.22 and an intercept at 41119. Looking at equation 8.7.1 the slope corresponds to the variable "b" and the intercept to variable "a", respectively.

$$\frac{k_{r,o}}{k_{r,w}} = a \times e^{b \times S_w} = 41119 \times e^{-18.22x} \qquad \textbf{8.7.1}$$
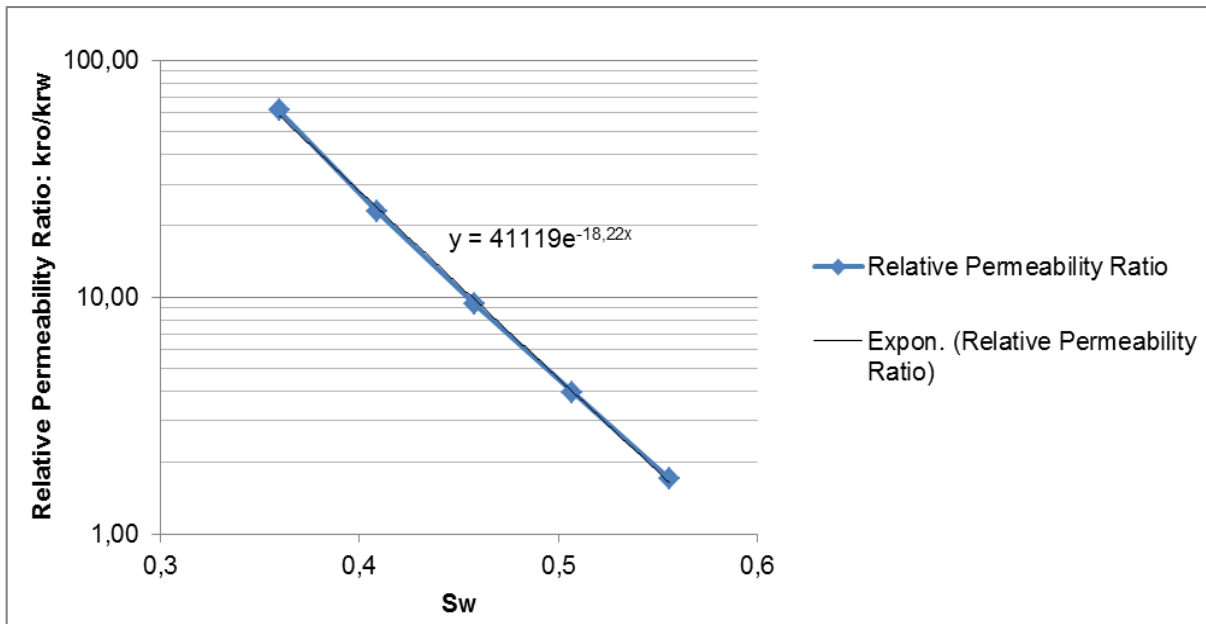

Figure 70: Relative permeability ratio versus water saturation

The fractional flow curve is further calculated by using equation 8.8.2 at different water saturation values.

$$f_w = \frac{1}{1 + \left(\frac{\mu_w}{\mu_o}\right) \times ae^{bS_w}} \qquad \textbf{8.7.2}$$

In order to derive the fractional flow curve's slope, equation 8.7.2 was differentiated with respect to the water saturation and illustrated in 8.7.3 [6].

$$\left(\frac{df_w}{dS_w}\right)_{Sw} = -\frac{\left(\frac{\mu_w}{\mu_o}\right) \times abe^{bS_w}}{\left[1 + \left(\frac{\mu_w}{\mu_o}\right) \times ae^{bS_w}\right]^2} \qquad \textbf{8.7.3}$$

8.8 Appendix F.1

The following page describes the used parameters used in Chaperson's approach to obtain the critical oil coning rate.

Table 8: Applied data for Chaperson's water coning approach

Variable	Value	Source
Density of water, ρ_w	1014 kg/m³	GDB
Density of oil, ρ_o	905 kg/m³	GDB
Effective oil permeability, $k_{e,o}$	192.19 mD	Equation 8.8.1
Drainage radius, r_e	172.9 m	Equation 8.8.2
Oil column thickness, h	17.6 m	RMDB
Distance from WOC to TOP, D_t	5.5 m	GDB
Perforated interval, h_p	4.5 m	GDB
Formation volume factor, B_o	1.1035 bbl/STB	RMDB
Viscosity oil, μ_o	5.19 cp	Laboratory Report [35]
k_v/k_h	0 – 1	Assumption

$$k_{e,o} = k_{absolut} \times k_{relative} = 1190 \, mD \times 0.1615 = 192.19 \, mD \qquad \textbf{8.8.1}$$

$$r_e = \sqrt{\frac{OIP \times B_o}{\pi \times h \times (1-S_w) \times \Phi}} = \sqrt{\frac{433467.8 \, m^3 \times 1.1035\frac{bbl}{STB}}{\pi \times 37 \, m \times (1-0.49) \times 0.27}} = 172.9 \, m \qquad \textbf{8.8.2}$$

8.9 Appendix G.1

This appendix section describes the flux pattern maps, based on injection wells. The green colour indicates the aquifer, blue reflects injectors and red dots are showing producing wells.
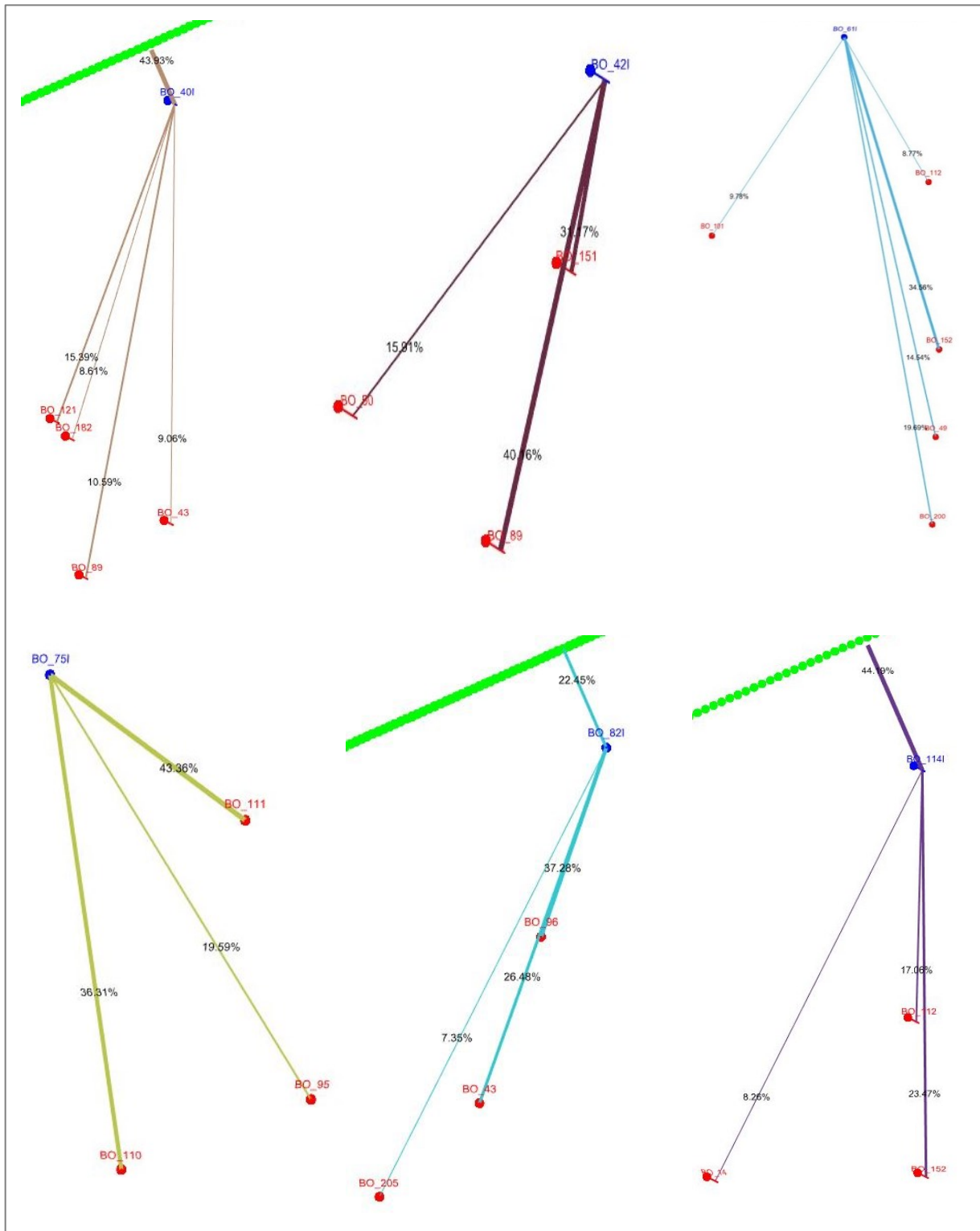
Sector 1

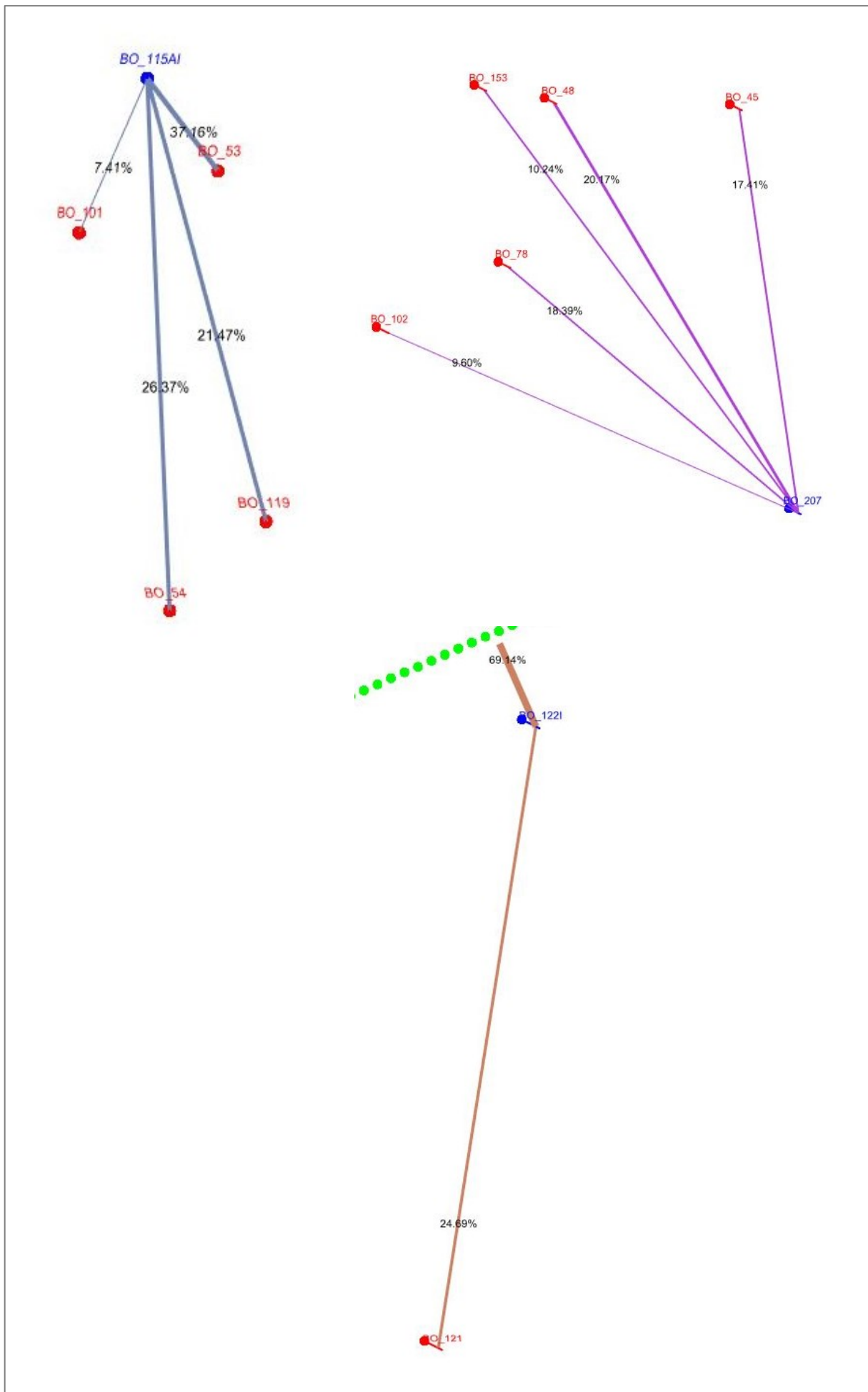**Figure 71: Flux pattern maps of six wells located at sector 1 [42]**

Figure 72: Flux pattern maps of three wells located at sector 1 [42]

8.10 Appendix G.2

In order to compare the outcomes between fully active aquifer and adjusted aquifer, the flux pattern maps of sector 2 were plotted in consideration of both cases.

In principal, the left picture always indicates a fully active aquifer and the right picture demonstrates the outcome, if the aquifer is adjusted in its activity. Due to the fact that only the second sector was adjusted concerning the aquifer, the flux pattern maps of sector 1 stayed the same.
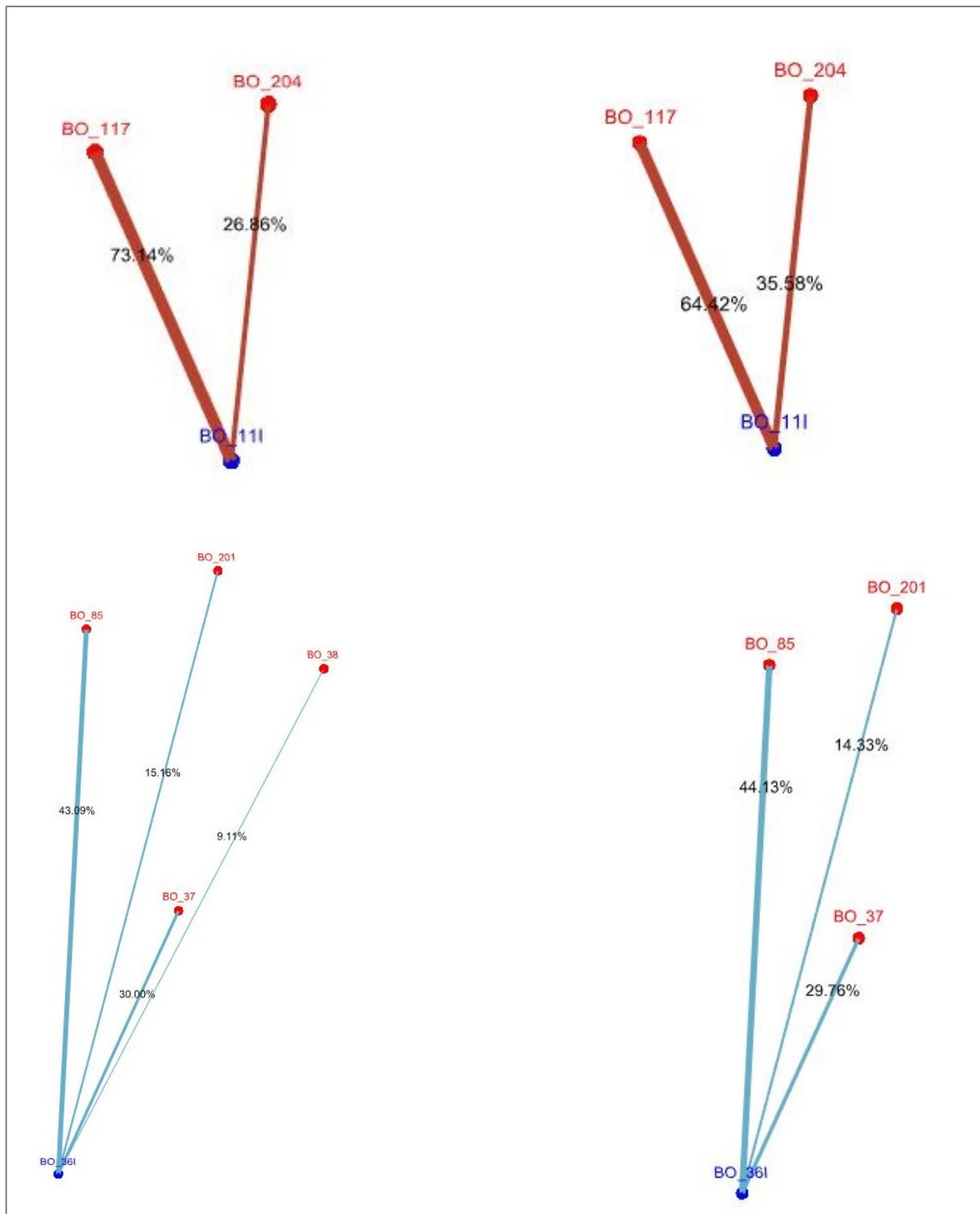

Figure 73: Flux pattern map of sector 2; BO 11 and BO 36 - fully activated aquifer (left), adjusted aquifer (right) [42]
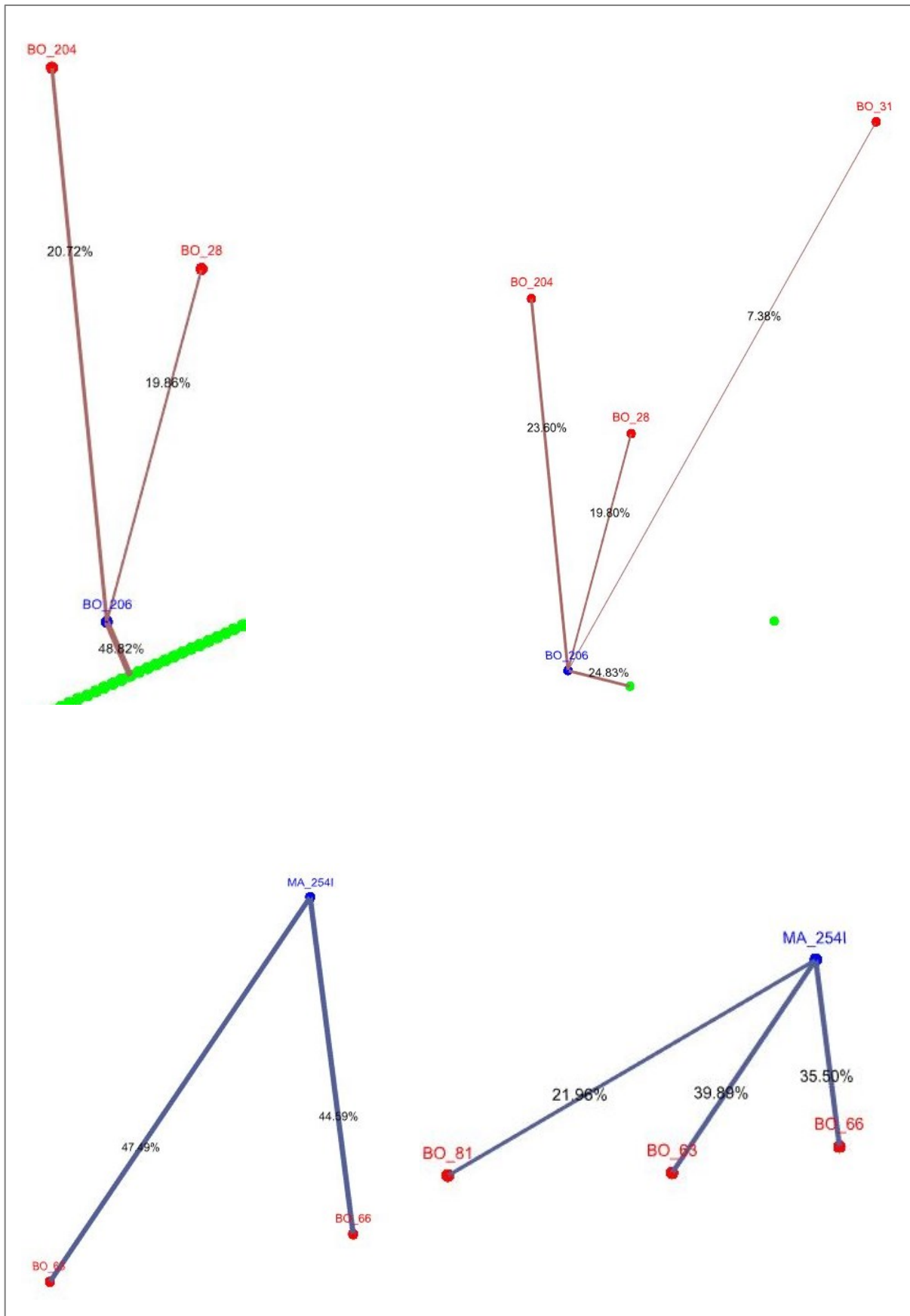
Figure 74: Flux pattern map of sector 2; BO 206 and MA 254 - fully activated aquifer (left), adjusted aquifer (right) [42]
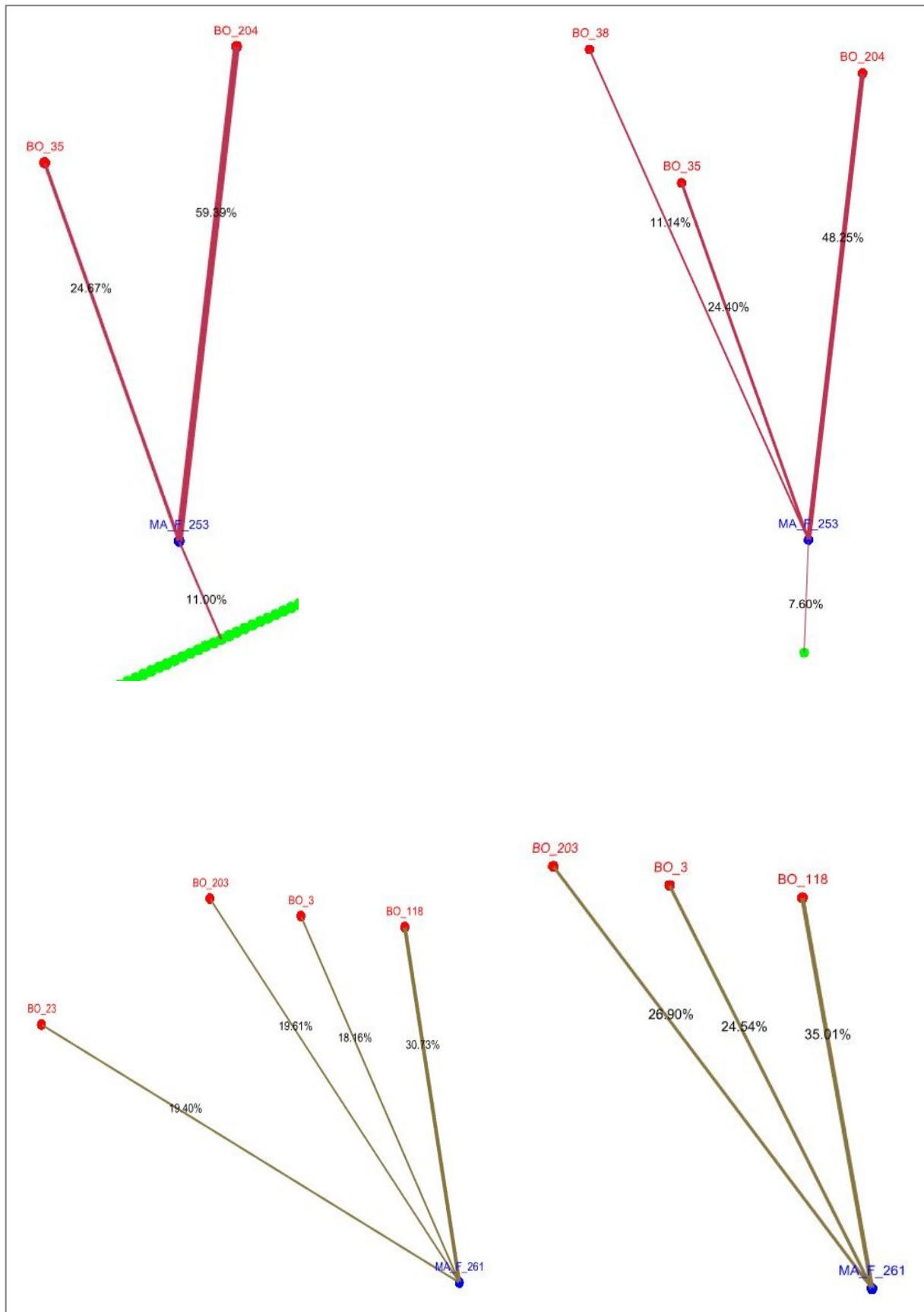
Figure 75: Flux pattern map of sector 2; MA F 253 and MA F 261 - fully activated aquifer (left), adjusted aquifer (right) [42]